1987

# Topics in chemical physics: I. Semiclassical reactive scattering theory; II. Corrected effective medium theory

Joel David Kress
*Iowa State University*

## INFORMATION TO USERS

The most advanced technology has been used to photograph and reproduce this manuscript from the microfilm master. UMI films the original text directly from the copy submitted. Thus, some dissertation copies are in typewriter face, while others may be from a computer printer.

In the unlikely event that the author did not send UMI a complete manuscript and there are missing pages, these will be noted. Also, if unauthorized copyrighted material had to be removed, a note will indicate the deletion.

Oversize materials (e.g., maps, drawings, charts) are reproduced by sectioning the original, beginning at the upper left-hand corner and continuing from left to right in equal sections with small overlaps. Each oversize page is available as one exposure on a standard 35 mm slide or as a 17″ × 23″ black and white photographic print for an additional charge.

Photographs included in the original manuscript have been reproduced xerographically in this copy. 35 mm slides or 6″ × 9″ black and white photographic prints are available for any photographs or illustrations appearing in this copy for an additional charge. Contact UMI directly to order.

UMI
Accessing the World's Information since 1938

300 North Zeeb Road, Ann Arbor, MI 48106-1346 USA

Order Number 8805098

# Topics in chemical physics: I. Semiclassical reactive scattering theory. II. Corrected effective medium theory

Kress, Joel David, Ph.D.

Iowa State University, 1987

U·M·I
300 N. Zeeb Rd.
Ann Arbor, MI 48106

# Topics in chemical physics:

# I. Semiclassical reactive scattering theory

# II. Corrected effective medium theory

by

Joel David Kress

A Dissertation Submitted to the

Graduate Faculty in Partial Fulfillment of the

Requirements for the Degree of

DOCTOR OF PHILOSOPHY

Department: Chemistry

Major: Physical Chemistry

Approved:

Signature was redacted for privacy.

In Charge of Major Work

Signature was redacted for privacy.

For the Major Department

Signature was redacted for privacy.

For the Graduate College

Iowa State University
Ames, Iowa
1987

TABLE OF CONTENTS


| | | Page |
|---|---|---|
| GENERAL INTRODUCTION | | 1 |
| PAPER I. | SEMICLASSICAL GAUSSIAN WAVEPACKET DYNAMICS FOR COLLINEAR REACTIVE SCATTERING | 15 |
| PAPER II. | CORRECTED EFFECTIVE MEDIUM METHOD. I. ONE-BODY FORMULATION WITH APPLICATIONS TO ATOMIC CHEMISORPTION AND DIATOMIC MOLECULAR POTENTIALS | 73 |
| PAPER III. | CORRECTED EFFECTIVE MEDIUM METHOD. II. N-BODY FORMULATION | 152 |
| SUMMARIES, CONCLUSIONS, AND EXTENSIONS | | 232 |
| REFERENCES | | 242 |
| ACKNOWLEDGEMENTS | | 245 |

# GENERAL INTRODUCTION

## Format of the Dissertation

Two distinct areas within theoretical chemical physics are investigated in this dissertation. First, the dynamics of collinear exchange reactions is treated within a semiclassical Gaussian wavepacket (GWP) description. Second, a corrected effective medium (CEM) theory is derived which yields: 1) a one-active-body description of the binding energy between an atom and an inhomogeneous host; and 2) an N-active-body description of the interaction energy for an N atom system.

The arrangement of this dissertation follows the alternative style format. The work describing the Gaussian wavepacket dynamics is contained in Paper I entitled "Semiclassical Gaussian wavepacket dynamics for collinear reactive scattering." The work describing the corrected effective medium theory is contained in Papers II and III, which are entitled "Corrected effective medium method. I. One-body formulation with applications to atomic chemisorption and diatomic molecular potentials" and "Corrected effective medium method. II. N-body formulation", respectively. Paper II has been accepted for publication in the Journal of Chemical Physics, to where Papers I and III have also been submitted.

## Introduction and Review

### Gaussian wavepacket dynamics

The semiclassical solution to the time-dependent Schrodinger equation (TDSE) using Gaussian wavepackets (GWPs) has been applied to many types of

atomic and molecular collision processes. As originally formulated in the pioneering work of Heller [1], the technique, which is called standard Gaussian wavepacket dynamics (GWD) herein, was initially applied to collinear inelastic atom-diatom collisions. To illustrate the standard GWD method consider the one-dimensional TDSE

$$i \frac{\partial}{\partial t} \psi(x,t) = H \psi(x,t) , \tag{1}$$

where

$$H = - \frac{1}{2M} \frac{\partial^2}{\partial x^2} + V(x) \tag{2}$$

A solution to Eq. (1) is constructed by expanding the wavefunction in terms of time-dependent GWPs

$$\psi(x,t) = \sum_j c_j G_j(x,t) , \tag{3}$$

where the expansion coefficients $c_j$ are forced to be independent of time and

$$G_j(x,t) = \exp[ia_j(x-x_j)^2 + ip_j(x-x_j) + if_j] . \tag{4}$$

Upon substitution of Eq. (3) into the TDSE, equations of motion for the

time-dependent parameters $a_j$, $x_j$, $p_j$, and $f_j$ are obtained by equating terms in powers of $(x-x_j)$ on both sides of Eq. (1). The coordinate and momentum (phase space) parameters, $x_j$ and $p_j$, evolve according to Hamilton's equations. Each GWP travels through phase space "riding" on a classical trajectory, thus providing an intuitive picture of the dynamics. The phase parameter, $f_j$, evolves as the classical action (the time integral of the classical Lagrangian). This dependence of phase upon the classical action is fundamental to semiclassical scattering theory [2]. The width of the GWP, $a_j$, evolves according to an equation of motion which is dependent on the order of truncation for the Taylor series for $V(x)$ expanded about $x_j$. For example, upon first order truncation the width parameter evolves as a particle of mass M in free space.

The solution to the TDSE, $\psi(x,t)$, is generated by explicitly integrating the equations of motion for the GWP parameters. The initial values of the GWP parameters are chosen such that $\psi(x,t_0)$ represents the initial scattering state. Upon integration, the resulting parameters at time = t are substituted into Eq. (3) and $\psi(x,t)$ is constructed. Note that each GWP remains Gaussian throughout the entire wavefunction propagation and propagates independently of the others, thus allowing for a strict adherence to Hamilton's equations for each GWP phase space trajectory. These two properties are extremely important in terms of the computational effort needed to numerically propagate the GWP equations of motion. By propagating the GWPs independently, the equations of motion for the phase space parameters can be decoupled from those for the width and phase parameters. This implies that wavefunctions with various initial values of

$a_j$ and $f_j$ can be generated from a single run of classical trajectories, thus providing a tremendous savings in terms of computational effort.

To implement the standard GWD method for a potential V(x,y) with two degrees of freedom, such as for the collinear inelastic atom-diatom scattering problem [1], the wavefunction is given the form

$$\psi(x,y,t) = G(x,t) \sum_j c_j g_j(y,t) . \qquad (5)$$

The initial vibrational state of the diatom is expanded in a set of GWPs, $\{g_j(y,t)\}$, and the initial translational state is represented as a single GWP, G(x,t). Upon substitution of Eq. (5) into the TDSE, equations of motion for the GWP parameters in G(x,t) and $\{g_j(y,t)\}$ are obtained. Besides treating the inelastic scattering problem in this manner, Heller and coworkers have also successfully applied the standard GWD method to the processes of photodissociation [3], Raman scattering [4], and atom-surface diffraction [5].

Many extensions to the standard GWD method have been proposed and implemented. Coalson and Karplus [6] considered the collinear inelastic atom-diatom scattering problem and constructed the wavefunction as a product of a single GWP times an expansion in Hermite polynomials for x and y. They derived equations of motion for both the GWP parameters and time-dependent expansion coefficients. Although this method provided the exact converged quantum results for the transition probabilities, the desirable property of semiclassically and independently propagated GWPs was removed from their formalism.

Other approaches to GWD have been based upon the Dirac-Frenkel-McLachlan time-dependent variational principle [7]. These yielded a method to minimize the global least squares error for the TDSE. By inserting the GWP expansion into an expression for the error, equations were derived which couple the motion between the GWPs. In an extensive study of the collinear inelastic atom-diatom scattering problem, Skodje and Truhlar [8] considered both the standard GWD method and a variational principle method. The diatom was treated both as a harmonic and a Morse (anharmonic) oscillator. Even for a Morse oscillator by itself (i.e., without any colliding atom), they found that the standard GWD representation of the vibrational eigenstate breaks down after a short interval of integration time. The use of the variational principle method improved the stationary state representation and provided reasonable results for the transition probabilities. But, within this method the GWPs were coupled and the equations of motion for the phase space parameters obeyed an Ehrenfest average of the potential and not Hamilton's equations.

Another approach based on the time-dependent variational principle is the Minimum Error Method (MEM) as developed by Sawada et al. [9] By minimizing an error functional, which is a least squares estimate for the TDSE, MEM equations of motion were obtained. As in the method of Skodje and Truhlar, the MEM equations of motion for the phase space parameters were coupled, thus each GWP did not evolve independently. The MEM formalism has been applied to atom-surface scattering [10], molecule-surface scattering [11], and curve crossing problems involving two potential energy curves [12].

Another variational principle approach, proposed by Mukamel [13a], yields a set of "reduced" equations of motion (REM). The REM formalism also provides a set of coupled GWP equations of motion. Still another approach has been formulated by Muckerman et al. [13b], where the GWPs serve as basis functions in a classical path approximation to the quantum dynamics.

A comprehensive review of GWP methods as applied to molecular scattering from surfaces [14] has been provided by Gerber et al. Not only are semiclassical methods reviewed, but methods based on a time step propagation using fast Fourier transforms are also discussed. These time step methods are exact and not semiclassical wavepacket methods, and have been applied to the $H + H_2$ collinear exchange reaction [15].

In Paper I, the application of GWD to the collinear reactive scattering problem, $AB + C \rightarrow A + BC$, is considered. The major complexity which differentiates this problem from the other problems previously reviewed in this Introduction is the existence of two arrangements: the reactant's channel (AB,C) and the product's channel (A,BC). The scattering wavefunction must be adequately represented in both channels; it is within this context that the standard GWD method fails as applied to reactive scattering.

The treatment of the collinear exchange reaction using standard GWD has been reported in only two instances, with both studies examining the $H + F_2$ reaction. In the first case, Zuhrt [16] stated "We found that the dynamics is strongly dependent on the initial conditions ... The (GWD) method therefore is not adequate ... and the questionable results will not

be given here." The specific transition probabilities were not presented in that paper. In the other investigation of the F + $H_2$ reaction, a study by Skodje [17], it was found that the application of the standard GWD method yielded a final scattering wavefunction which did not conserve spatial normalization. The transition probabilities summed to less than 0.1.

In an attempt to provide a semiclassical GWP method which can adequately treat collinear reactive scattering, two extensions to the standard GWD are proposed and implemented in Paper I. The two extensions are: 1) the interaction picture representation in each arrangement channel of the wavefunction is evaluated explicitly by numerical integration of the appropriate differential equations corresponding to the GWP equations of motion; 2) the initial translational wavefunction is expanded over a finite spatial interval as a linear combination of GWPs (as opposed to the single GWP expansion of Eq. (5) in this Introduction). Even with these extensions, two desirable properties present in the standard GWD method remain: 1) the GWPs remain Gaussian upon propagation; and 2) the GWPs evolve independently, thus strictly obeying classical mechanics. This extended GWD approach (interaction picture propagation plus multiple translational GWPs) is then applied to the collinear exchange reaction of H + $H_2$ and the results are reported.

Effective medium theories

The prediction of spectroscopic and dynamical properties for a many-body atomic system requires an accurate estimate of the adiabatic potential energy surface (PES) governing the interaction among the various

bodies. Many-body systems of interest include that of atomic chemisorption, molecular chemisorption, and clusters of metal atoms. When each atom of the system contains many electrons and the system possesses low spatial symmetry, calculations of the PES which treat all of the electrons are rather difficult. Application of either the Hartree-Fock [18] or Kohn-Sham local density (LD) [19] method becomes complicated in terms of computational requirements and convergence criteria. A promising alternative is embodied in an effective medium (EM) [20] or quasi-atom [21] scheme whereby the many-body system is modeled by a system which consists of each atom interacting with a homogeneous electron gas.

Based upon density functional theory [22], the EM theory replaces, to zeroth order, the (low symmetry) self-consistent solution of an atom interacting with a many-body electron density, by the (high symmetry) self-consistent Kohn-Sham LD solution [23] of an atom interacting with an extended system of constant electron density and constant positive background charge (i.e., jellium). As an illustration of the general EM approach, consider atom A interacting with a many-atom, many-electron host B (e.g., a metal surface or a cluster of metal atoms). Formally, the interaction energy is expressed as

$$\Delta E = E[AB] - E[A] - E[B] \quad . \tag{6}$$

The zeroth order EM approximation [20, 21] to Eq. (1) is

$$\Delta E = \Delta E_A(n_H) \quad , \tag{7}$$

which represents the self-consistently calculated embedding energy of an atom of chemical identity A into jellium of unpolarized electron density $n_H$. The jellium density is obtained by evaluating the electron density of the host at the position of atom A in space.

Corrections to the zeroth order description of the EM interaction have been developed by Norskov and Lang [20, 24] by considering the first-order perturbation theory contribution with the ion-cores of the host system included as weak pseudopotentials. To first order, the EM interaction is

$$\Delta E = \Delta E_A(n_H) - \alpha_A n_H + \Delta E^{hyb} \quad . \tag{8}$$

The jellium density is provided by averaging the host electron density over the electrostatic potential of atom A. The second term in Eq. (8), the polarizability of atom A times the jellium density, accounts for the electrostatic Coulomb interaction under the following assumption: within a given radius about atom A the density of the host is nearly constant and void of any host ion cores. The last term of Eq. (8) describes covalent binding effects (resonances) between the atomic states of atom A and any localized electronic states of the host (such as occupied d bands in a metal).

A new approach to calculating the interaction energies within an EM formalism, which is called the corrected effective medium theory (CEM), is presented in Papers II and III. Specifically, the approach derived in Paper II is limited to that of one-active-body systems (atom A embedded

into host B), and is denoted CEM-1. Within the CEM-1 theory, a correction to the zeroth order EM embedding energy is provided by using a spin-polarized analog of the Gordon-Kim electron gas [25] approximation. The CEM-1 interaction energy thus becomes

$$\Delta E = \Delta E_A(n_H) + \Delta V_{AB} + \Delta G_{AB} \quad . \tag{9}$$

$\Delta V_{AB}$ is the Coulomb interaction between the total charge distributions on atom A and B, and is explicitly evaluated within the superposition of atomic charge density approximation. $\Delta G_{AB}$ is the difference in the kinetic-exchange-correlation energy between the atom A/host B system and the atom A/jellium system. The jellium density $n_H$ is chosen such that the dominant contribution to $\Delta G_{AB}$, (i.e., the local kinetic-exchange energy), is set to zero, since $\Delta G_{AB}$ is the only non-self-consistently calculated term in Eq. (9) which depends on $n_H$. An analytic expression for $n_H$ is obtained if an (excellent) quadratic approximation to the local kinetic-exchange energy density is used for $\Delta G_{AB}$. This yields a $n_H$ which is a weighted average of the pairwise overlap of electron density between atom A and the atoms in host B.

In contrast to the EM method, the CEM-1 method can be formulated to treat host bodies which are localized in terms of electron density, thus the treatment of AB diatomic molecules is possible. Within Paper II, three types of chemically interesting systems are considered: 1) H atom embedded into spin-polarized jellium; 2) H atom containing diatomic molecules; and 3) H atom chemisorption on the transition metal surfaces, Ni(100), Cu(100),

and Fe(110).

Another method similar in spirit to the EM method is the embedded atom (EA) method [26] as developed by Baskes and Daw. The EA energy for an atom A interacting with a collection of atoms representing host B is expressed as

$$\Delta E = \sum_j \Delta F_j(n_{Hj}) + \sum_{i<j} \sum \Phi_{ij} \ , \tag{10}$$

where both atom A and the atoms in host B are included in the sums. $\Delta F_j$ is a semi-empirically determined embedding energy for an atom of chemical identity j into jellium of electron density $n_{Hj}$. The $n_{Hj}$ are obtained by summing the electron densities due to each atom (not including j) evaluated at the position of atom j in space. The $\Phi_{ij}$ are empirical short range two-body potentials which represent ion core-ion core repulsions. The exact forms of $\Delta F_j$ and $\Phi_{ij}$ are obtained by fitting to experimental information (bulk metal binding potentials, elastic constants, atomic surface and bulk diffusion potentials, etc.) The EA method has the desirable property of simultaneously embedding atom A into the host atoms as well as the host atoms into atom A, thus allowing the embedding atom A to perturb the host. The inclusion into the CEM formalism of the host backbinding to the embedded atom is possible by considering an N-active-body theory. The initial development of this approach, the CEM-N theory, is the subject of Paper III.

Two major difficulties associated with the CEM-1 theory are removed by considering the CEM-N formalism. The first problem involves the lack of

symmetry which restricts the results of the CEM-1 method to the interaction energy of a single atom with a host. For an N-body system, the CEM-1 method can be applied sequentially to each body in the system. This yields an overall interaction energy which partially removes the asymmetry problem. However, such a scheme lacks uniqueness with respect to the physical order from which the embedding atoms are chosen. The second problem is more subtle. The division into an active atom and a host assumes that the active atom has a negligible influence on the bonding in the host system. Such an approximation will be adequate for weak chemical bonding, but will become increasingly poor as the atom-host interaction becomes as strong as the interaction among the host atoms.

As derived in Paper III, the CEM-N interaction energy within the approximation of superposition of atomic charge densities is expressed as

$$\Delta E = \sum_j \Delta E_j(n_{Hj}) + \sum_{i<j} \sum \Delta V_{ij} + \Delta G \ . \tag{11}$$

The first term is the embedding energy contribution, where each atom in the N-body system where is embedded into jellium of electron density $n_{Hj}$. The second term in Eq. (11) is the pairwise sum of the Coulombic interactions between the charge distributions on atom i and j, which is evaluated explicitly. $\Delta G$ is similar to $\Delta G_{AB}$ in the CEM-1 expression of Eq. (4) and provides the difference in kinetic-exchange-correlation energy between the real and effective systems. As in CEM-1, the choice of the jellium densities $n_{Hj}$ are determined by setting to zero the local kinetic-exchange

energy contribution to $\Delta G$. The $n_{Hj}$ are found to be weighted sums of the overlap of electron density between atom j and the other (N-1) atoms pairwise. A physical interpretation of binding is provided by this overlap of electron density between pairs of atoms. This picture has a parallel interpretation within a molecular orbital scheme [27], where it is argued that binding results from the constructive interference (overlap) between orbitals on each center.

The binding for homonuclear diatomic molecules up to $F_2$ are examined within the CEM-N formalism in Paper III. Differences are found between the experimental (Morse) potentials and the predicted CEM-N potentials generated by using the self-consistently calculated embedding functions [23] of Puska et al. These differences illustrate the need for a new set of "covalent" embedding energies, which are constructed semi-empirically for the elements considered in Paper III.

An expression has been derived within the CEM-N theory which yields the cohesive energy of a homogeneous infinite solid [28], although it has not been included in this dissertation. Likewise, expressions for the cohesive energy of bulk solids have been derived recently within the EM theory by Manninen [29] and Jacobsen et al. [30] Preliminary results for various properties of Al metal were reported in both studies. A project is underway to treat the relaxation of metal surfaces [28], as well as the interactions in metal clusters [31], using the CEM-N method.

Another topic, which is discussed briefly in the Summary, Conclusions and Extensions section, is the calculation of a PES for dissociative molecular chemisorption using the CEM-N method. The

calculation of a PES of quantitative accuracy for the $H_2$/Mg(0001) and $H_2$/Ni(100) systems provided the original impetus for deriving an N-active-body CEM theory. Many PESs have been generated by this author for these systems using various options (e.g., the choice of embedding function) within the CEM-N method, but none are presented in this dissertation since they provide only a qualitative description. In this author's opinion, all other methods (the Hartree-Fock-ECP-CI cluster model [32] and Local Density semi-infinite jellium model [33]) also provide a qualitative description for $H_2$ dissociative chemisorption. An attempt to improve upon the CEM-N description of the PESs for these systems is presently underway.

PAPER I.

# SEMICLASSICAL GAUSSIAN WAVEPACKET DYNAMICS FOR COLLINEAR REACTIVE SCATTERING

# SEMICLASSICAL GAUSSIAN WAVEPACKET DYNAMICS FOR COLLINEAR REACTIVE SCATTERING

Joel D. Kress and Andrew E. DePristo

Ames Laboratory-USDOE and Department of Chemistry
Iowa State University
Ames, Iowa 50011

## ABSTRACT

The dynamics of collinear exchange reactions is treated within a semiclassical Gaussian wavepacket (GWP) description. Two extensions to the previous methodology of GWP dynamics are presented. The first involves the evaluation of the interaction picture wavefunction propagators directly via the GWP solution to the time-dependent Schrodinger equation. The second involves use of a sum of GWPs to represent the initial translational plane wave on a finite interval. As usual, the vibrational wavefunction is also represented as a sum of GWPs, where the expansion coefficients are chosen to yield the desired initial vibrational state.

The details for constructing analytically the $N_x$ (translational) by $N_y$ (vibrational) grid of GWP parameter trajectories from the numerical integration of only $N_y$ sets of GWP equations of motion is outlined. The limitations of the previous GWP dynamical methods as applied to the reactive scattering problem are pointed out and the solutions provided by the present extensions are discussed. Results for the $H + H_2$ collinear exchange reaction using the Porter-Karplus II potential energy surface are shown.

# INTRODUCTION

The semiclassical solution to the time-dependent Schrodinger equation (TDSE) for molecular collisions using Gaussian wavepackets (GWPs) has met with considerable success. Among the types of processes treated with some accuracy are vibrational inelastic scattering [1], atomic and molecular diffraction from solid surfaces [2], and photodissociation [3]. Similar success has not been reported for reactive events, in which there exists more than one arrangement channel for the products.

In the approach developed by Heller [1a], which we call Gaussian wavepacket dynamics (GWD), the solution to the TDSE is expanded in a basis of time-dependent GWPs. Each GWP is centered on a point in phase space, and the TDSE is propagated by integrating the equations of motion for each GWP independently. The resulting equations of motion for the position and momentum of each GWP consist of Hamilton's equations, which provides a convenient picture of the dynamics as each GWP follows a classical trajectory through phase space.

In this paper, we show how GWD can be applied to the collinear exchange reaction of $H + H_2$. Two new features are crucial for this application: 1) the interaction picture representation in each arrangement channel of the wavefunction is evaluated explicitly by numerical integration of the appropriate differential equations corresponding to the GWP equations of motion; 2) the initial translational wavefunction is expanded over a finite interval as a linear combination of GWPs.

We should note that methods to improve GWD have been derived [1c,4] based upon the Dirac-Frenkel-McLachlan time-dependent variational principle [5], where the TDSE is minimized in a least squares average over time. Application of these approaches couples the equations of motion for each GWP in the wavefunction expansion, and therefore the desirable property of independently propagating GWPs (i.e., strictly adhering to Hamilton's equations) is lost. In our application of GWD we retain the exact classical trajectory description of the GWP parameters and allow each GWP to propagate independently.

We note that in contrast to the semiclassical GWD method, where the GWPs remain Gaussian throughout the duration of the propagation, there exist grid methods where only the initial wavefunction is expanded in GWPs. The TDSE is integrated by either a time step differencing scheme [6] or a Chebyshev polynomial expansion of the propagator [7]. In either case, the GWPs of the basis do not remain Gaussian upon propagation. These grid methods are exact and not semiclassical wavepacket methods, and have been applied to the H + $H_2$ collinear exchange reaction [8], as well as to other scattering problems [9].

# THEORY

We wish to solve the TDSE which governs the collinear reactive scattering problem, AB + C $\longrightarrow$ A + BC. The major complexity is the existence of two arrangements: the reactant's channel (AB,C) and the product's channel (A,BC). Mass-weighted Jacobi coordinates are defined in both channels, and are constructed from the internuclear distances $r_{AB}$ and $r_{BC}$ as follows. We define the reactant's channel coordinates as

$$\begin{pmatrix} \tilde{y} \\ \tilde{x} \end{pmatrix} = \begin{pmatrix} 1 & 0 \\ \gamma_{AB} & 1 \end{pmatrix} \begin{pmatrix} r_{AB} \\ r_{BC} \end{pmatrix} \tag{1}$$

and the product's channel coordinates as

$$\begin{pmatrix} \tilde{y}' \\ \tilde{x}' \end{pmatrix} = \begin{pmatrix} 0 & 1 \\ 1 & \gamma_{BC} \end{pmatrix} \begin{pmatrix} r_{AB} \\ r_{BC} \end{pmatrix} . \tag{2}$$

The transformation between the two sets of channel coordinates is

$$\begin{pmatrix} \tilde{y}' \\ \tilde{x}' \end{pmatrix} = \begin{pmatrix} -\gamma_{AB} & 1 \\ \gamma & \gamma_{BC} \end{pmatrix} \begin{pmatrix} \tilde{y} \\ \tilde{x} \end{pmatrix} . \tag{3}$$

The $\gamma$ factors which appear in the above transformation matrices (and in subsequent transformations appearing later) depend on the mass of atoms A, B, and C and are defined in the Appendix. Using the coordinate system defined by Clark and Dickinson [10], we scaled the coordinates in both arrangement channels by the quantity $s = (\mu_{AB}\omega_{AB}/\hbar)^{1/2}$ where $\mu_{AB}$ is the reduced mass of the AB molecule and $\omega_{AB}$ is the angular frequency of the AB binding potential. The dimensionless reactant's and product's channel coordinates are then defined as $(x,y) = (s\tilde{x},s\tilde{y})$ and $(x',y') = (s\tilde{x}',s\tilde{y}')$, respectively.

The Hamiltonian for the ABC system can be expressed in two equivalent forms using either set of channel coordinates:

$$H = -\frac{1}{2M_R}\frac{\partial^2}{\partial x^2} - \frac{1}{2\mu_R}\frac{\partial^2}{\partial y^2} + V(x,y) \qquad \text{(Reactant's)} \qquad (4a)$$

or

$$H = -\frac{1}{2M_P}\frac{\partial^2}{\partial x'^2} - \frac{1}{2\mu_P}\frac{\partial^2}{\partial y'^2} + V(x',y') \qquad \text{(Product's)} \; . \qquad (4b)$$

The masses appearing in each H are defined in the Appendix. The energy of the resulting dimensionless Hamiltonian is measured in units of the AB molecular vibrational quanta, $\hbar\omega_{AB}$. The interaction potential for the

ABC system is written as $V(x,y)$ (or equivalently as $V(x',y')$). The TDSE, which we can formulate with either set of coordinates, is expressed in the dimensionless reactant's channel coordinates as

$$i \frac{\partial}{\partial t} \psi(x,y,t) = H \psi(x,y,t) \ . \tag{5}$$

The behavior of H in the asymptotic limits $x \longrightarrow \infty$ and $x' \longrightarrow \infty$ allows us to set the boundary conditions upon the solution of the TDSE. In this limit we define the channel Hamiltonians

$$H^R = - \frac{1}{2M_R} \frac{\partial^2}{\partial x^2} - \frac{1}{2\mu_R} \frac{\partial^2}{\partial y^2} + V^R(y) \qquad \text{(Reactant's)} \tag{6a}$$

$$H^P = - \frac{1}{2M_P} \frac{\partial^2}{\partial x'^2} - \frac{1}{2\mu_P} \frac{\partial^2}{\partial y'^2} + V^P(y') \qquad \text{(Product's)} \ . \tag{6b}$$

The asymptotic limits of the full interaction potential define the binding potentials of the AB and BC molecules, respectively, via

$$V^R(y) = \lim_{x \to \infty} V(x,y) \tag{7a}$$

and

$$V^P(y') = \lim_{x' \to \infty} V(x',y') \ . \tag{7b}$$

## Interaction Picture Quantum Mechanics

Before expressing the solution to the TDSE in terms of GWD, we review the formal treatment of the quantum mechanical solution to the reactive scattering problem [11,12]. From this analysis we derive the interaction picture propagation method. The solution to the scattering problem is provided by the S operator which relates the initial and final wavefunctions,

$$|\psi_{out}\rangle = S|\psi_{in}\rangle \, . \tag{8}$$

For the reactive scattering problem, $|\psi_{out}\rangle$ and $|\psi_{in}\rangle$ are vectors with components in both the reactant's channel (space) and the product's channel (space). The two components are rigorously orthogonal to each other in the asymptotic limit of $x \longrightarrow \infty$, $x' \longrightarrow \infty$. Choosing the initial scattering wavefunction completely in the reactant's space yields

$$|\psi_{in}\rangle = \{\psi^R_{in}, 0\} \, , \tag{9a}$$

whereas the final wavefunction may have components in both spaces

$$|\psi_{out}\rangle = \{\psi^R_{out}, \psi^P_{out}\} \, . \tag{9b}$$

With this choice of $|\psi_{in}\rangle$ the S operator is expressed as a 2 x 2 matrix of wavefunction propagators

$$\underline{S} = \lim_{t\to\infty} \begin{pmatrix} U^R(t)^\dagger U(t) & U^R(t)^\dagger U(t) \\ U^P(t)^\dagger U(t) & U^P(t)^\dagger U(t) \end{pmatrix}, \tag{10}$$

where $\underline{S}$ relates Eqs. (9a) and (9b) by

$$|\psi_{out}\rangle = \underline{S} \cdot |\psi_{in}\rangle . \tag{11}$$

Note that t = 0 is defined as the infinite past for the scattering event. The propagators are defined by

$$U(t) = \exp[-iHt] \tag{12a}$$

$$U^C(t) = \exp[-iH^C t] \qquad C = R,P . \tag{12b}$$

In general,

$$U(t - t_0) = \exp[-iH(t - t_0)] \tag{13}$$

relates the solution of the TDSE at time t to the initial wavefunction $\psi(t_0)$ upon integration (in time) of the TDSE using the Hamiltonian H. In this paper, the wavefunction propagator will represent the explicit time integration using the GWD propagation procedure.

## Gaussian Wavepacket Dynamics

In previous applications of GWD, the translational wavefunction, in x, was represented by a single GWP. Here, we expand the total scattering wavefunction in terms of multiple GWPs for both the translational and vibrational coordinates

$$\psi(x,y,t) = \sum_{i}^{N_x} \sum_{j}^{N_y} c_{ij}\, G_{ij}(x,t)\, g_{ij}(y,t) \ , \tag{14}$$

where the $c_{ij}$'s are <u>time-independent</u> and

$$G_{ij}(x,t) = \exp[i\alpha_{ij}^{x}(x-x_{ij})^{2} + ip_{ij}^{x}(x-x_{ij})] \tag{15a}$$

$$g_{ij}(y,t) = \exp[i\alpha_{ij}^{y}(y-y_{ij})^{2} + ip_{ij}^{y}(y-y_{ij}) + if_{ij}] \ . \tag{15b}$$

(Confusion between $i = (-1)^{1/2}$ and the subscript i should not occur.) All the subscripted parameters in the exponentials are time dependent. Specifically, $\alpha_{ij}^{x}$ and $\alpha_{ij}^{y}$ are width parameters; $x_{ij}$, $y_{ij}$, $p_{ij}^{x}$, and $p_{ij}^{y}$ are the centers of the GWPs in phase space; and the $f_{ij}$ are phase parameters. To determine the time evolution of $\psi(x,y,t)$ using the GWP basis, V(x,y) is expanded in a Taylor series about $x_{ij}$ and $y_{ij}$. If the expansion of V(x,y) is truncated at first order, substitution of the GWP expansion into the TDSE yields the following GWD equations of motion [1a]

$$\dot{\alpha}^x_{ij} = -2(\alpha^x_{ij})^2/M \quad ; \quad \dot{\alpha}^y_{ij} = -2(\alpha^y_{ij})^2/\mu \tag{16a,b}$$

$$\dot{p}^x_{ij} = \frac{-\partial V(x_{ij},y_{ij})}{\partial x_{ij}} \quad ; \quad \dot{p}^y_{ij} = \frac{-\partial V(x_{ij},y_{ij})}{\partial y_{ij}} \tag{16c,d}$$

$$\dot{x}_{ij} = p^x_{ij}/M \quad ; \quad \dot{y}_{ij} = p^y_{ij}/\mu \tag{16e,f}$$

$$\dot{f}_{ij} = i\alpha^x_{ij}/M + i\alpha^y_{ij}/\mu + L(x_{ij},p^x_{ij},y_{ij},p^y_{ij}) \, . \tag{16g}$$

The classical Lagrangian in Eq. (16g) is given by

$$L = (p^x_{ij})^2/2M + (p^y_{ij})^2/2\mu - V(x_{ij},y_{ij}) \, , \tag{17}$$

where M and $\mu$ are the reduced masses appropriate for the arrangement channel under consideration. The coordinate parameters $(x_{ij}, y_{ij})$ and the momentum parameters $(p^x_{ij}, p^y_{ij})$ of the individual GWPs evolve according to classical mechanics.

Specification of an initial wavefunction $\psi(x,y,t_0)$ determines the initial set of GWP parameters. This set of GWP parameters is used as the initial conditions when solving the differential equations obeyed by the GWP equations of motion. Eqs. (16) are integrated either numerically or analytically until a desired time t. The resulting set of GWP parameters are then substituted into the GWP expansion to construct the wavefunction at time t, $\psi(x,y,t)$.

Truncating the Taylor series for V(x,y) beyond first order yields terms in the width parameter equations of motion which depend on the second partial derivatives of V(x,y) with respect to $x_{ij}$ and $y_{ij}$. Using the first order truncation, the width parameter equations of motion are decoupled from V(x,y) and are solvable analytically, yielding

$$\alpha^x_{ij}(t) = M\,[\alpha^x_{ij}(t_0)] \,/\, [2\,\alpha^x_{ij}(t_0)\,(t - t_0) + M] \tag{18a}$$

$$\alpha^y_{ij}(t) = \mu\,[\alpha^y_{ij}(t_0)] \,/\, [2\,\alpha^y_{ij}(t_0)\,(t - t_0) + \mu]\,. \tag{18b}$$

These describe two particles of mass M and $\mu$ propagating uncoupled through free space. Given a reasonable size for the values of the width parameters at $t_0$, Eqs. (18) predict that the values of the widths decrease rapidly. Thus an initially narrow GWP (large $\alpha$) decays rapidly in time to a very diffuse GWP (small $\alpha$) in coordinate space. This decay of the width parameters presents difficulties in applying the standard GWD method to scattering problems as the initial values for the translational width parameters must be carefully chosen to focus the GWP as it approaches the interaction region [1c]. We show later in this paper how the IPGWD propagation scheme circumvents this problem of spreading GWPs.

## Construction of the Initial Wavefunction

Here we consider the construction of $|\psi_{in}>$, which is of a separable form in the reactant's channel

$$\psi^R_{in}(x,y,t=0) = X(x)\ \phi_n(y)\ . \tag{19}$$

The initial vibrational wavefunction satisfies

$$\left(\frac{-1}{2\mu_R}\ \frac{d^2}{dy^2} + V^R(y) - \varepsilon_n\right)\ \phi_n(y) = 0\ . \tag{20}$$

where $\varepsilon_n$ is the vibrational eigenvalue of the $n^{th}$ quantum vibrational state. This initial vibrational state is expanded in terms of the vibrational GWPs as

$$\phi_n(y) = \sum_j^{N_y}\ c_j^y\ g_{ij}(y,0)\ . \tag{21}$$

Since this expansion is independent of the translational index i, the total GWP expansion can be separated. We define the initial vibrational GWP parameters as

$$\mathrm{Im}\{\alpha^y_{ij}(0)\} = \beta^y \quad ; \quad \mathrm{Re}\{\alpha^y_{ij}(0)\} = 0 \tag{22a,b}$$

$$y_{ij}(0) = y_j^0 \quad ; \quad p^y_{ij}(0) = p_j^{y0} \tag{22c,d}$$

$$f_{ij}(0) = 0 \tag{22e}$$

for all $i=1,N_x$ and $j=1,N_y$. As suggested by Davis and Heller [13], the set

of vibrational basis parameters, $\{y_j^0, p_j^{y\,0}\}$, are chosen equally spaced in time for the periodic motion fixed by $V^R(y)$ and classical energy $\varepsilon_n$. Two of the vibrational basis parameters are placed at the inner and outer turning points of the oscillator where $p_j^{y\,0} = 0$. The set of coefficients, $\{c_j^y\}$, are determined by a linear least squares fit to $\phi_n(y)$ obtained from an accurate numerical solution to Eq. (20).

The initial translational wavefunction is expanded in translational GWPs as

$$X(x) = \sum_i^{N_x} c_i^x \, G_{ij}(x,0) \quad . \tag{23}$$

Since this expansion is independent of the vibrational index j, we complete the separation of the total GWP expansion by defining the initial translational GWP parameters as

$$\mathrm{Im}\{\alpha_{ij}^x(0)\} = \beta^x \quad ; \quad \mathrm{Re}\{\alpha_{ij}^x(0)\} = 0 \tag{24a,b}$$

$$x_{ij}(0) = x_0 + (i-1)\,(\tau_y/N_y)\,(p_0^x/M_R) \tag{24c}$$

$$p_{ij}^x(0) = -p_0^x \tag{24d}$$

for all $i=1,N_x$ and $j=1,N_y$. Every initial translational GWP is assigned a classical momentum of $-p_0^x$, and travels at a classical velocity of $(-p_0^x/M_R)$.

$x_0$ is chosen as the boundary in coordinate space where the full Hamiltonian H reduces to $H^R$ to within a given tolerance of the total classical energy.

The initial coordinate parameters of each translational GWP, $x_{ij}(0)$, are chosen equally spaced in x where the spacing is determined by the fractional vibrational period $(\tau_y/N_y)$ with $\tau_y = 2\pi$ (in units of $1/\omega_{AB}$). The fractional vibrational period is the amount of time the vibrational trajectories must be integrated to replicate the initial set of vibrational trajectories, $\{y_j^0, p_j^{y\,0}\}$. Since we have specified the vibrational GWP parameters equally spaced in time on a constant energy orbit in phase space, the set $\{y_j^0, p_j^{y\,0}\}$ possesses the following special property. Each pair of phase points $(y_j^0, p_j^{y\,0})$ evolves into another pair $(y_{j'}^0, p_{j'}^{y\,0})$ upon integration of the vibrational equations of motion over a time interval equal to integral amounts of $(\tau_y/N_y)$. This mapping of j onto j' we define in general using

$$j' = M(j, \delta t) ,$$

where j is the phase point pair of the vibrational basis which evolves into the j' phase point pair upon integration of the vibrational equations of motion for an interval $\delta t$. The M map holds true <u>only</u> if $\delta t = n \cdot (\tau_y/N_y)$ where n is an integer. In this case, each j' is mapped onto a unique j at time $\delta t$. While the actual form of the map is dependent on how we arrange the vibrational basis parameter set in phase space, this special choice of the time interval allows us to generate all $N_x \times N_y$ sets of trajectory parameters by only numerically integrating $N_y$ sets of GWP parameters. From

this ($i=1$, $j=1,N_y$) subset of parameters, we can construct the solutions to the equations of motion for the other $(N_x - 1) \times N_y$ sets analytically.

Using the above choice of initial translational GWP parameters in Eqs. (22), the set of coefficients, $\{c_i^x\}$, are determined by a linear least squares fit of Eq. (23) to an incoming plane wave

$$X(x) = (2\pi)^{-1/2} \exp[-ip_0^x x] . \tag{25}$$

over the <u>finite</u> interval $[x_0, x_0 + \delta x_0]$. Here

$$\delta x_0 = (N_x - 1)\ (\tau_y/N_y)\ (p_0^x/M_R)$$

and $x_0 + \delta x_0$ is the initial translational coordinate parameter of the $(i = N_x, j)^{th}$ translational GWP.

With these choices of the initial GWP parameters for $|\psi_{in}>$, the total classical energy of the system is fixed as

$$E_{sys} = \varepsilon_n + (p_0^x)^2/2M_R \tag{26}$$

and the time-independent expansion coefficients are given as

$$c_{ij} = c_i^x\ c_j^y . \tag{27}$$

With the representation for $|\psi_{in}>$ at hand, we are now ready to discuss the

time-dependent propagation using IPGWD.

## The IPGWD Propagation Procedure

### Forward propagation with the full Hamiltonian

The IPGWD propagation of $|\psi_{in}>$ corresponds to integrating the equations of motion for the GWP parameters using the appropriate propagators as dictated by the operation of $\underline{S}$ upon the initial wavefunction. At t = 0, the wavefunction consists of a single component residing completely in the reactant's channel. Each element of $\underline{S}$ is composed of two successive applications of two different wavefunction propagators. The first propagator integrates the GWP equations of motion forwards in time using the full interaction Hamiltonian. The parameter equations of motion are defined by Eqs. (16) where the reactant's channel reduced masses $M_R$ and $\mu_R$ are substituted for M and $\mu$, respectively. The full interaction potential V(x,y) is used wherever $V(x_{ij},y_{ij})$ is specified. The classical trajectory equations of motion as well as the Lagrangian contribution to the phase parameter equations of motion are integrated numerically using a fifth-order Hamming predictor-corrector scheme [14]. As mentioned earlier, only the $(i=1,\ j=1,N_y)$ set of parameters are explicitly integrated. The other $(i=2,N_x,\ j=1,N_y)$ sets of parameters are constructed analytically from the $(i=1,\ j=1,N_y)$ set after the full IPGWD propagation is completed.

After starting the numerical integration using the full Hamiltonian, we follow the progress of each translational coordinate, $x_{1j}$, and continue

integrating until every $x_{1j}$ resides asymptotically either in the entrance of the reactant's channel or in the exit of the product's channel. The measure of this asymptote is provided by a cutoff value $x_{asp}$ (usually set equal to $x_0$) which is chosen so that the final value of $x_{1j}$ is large enough to reduce H to either $H^R$ or $H^P$ for each and every GWP. Upon detection of the last $x_{1j}$ satisfying the asymptotic criteria, the forward integration with the full Hamiltonian is terminated at time $t_{asp}$.

In terms of a two component state vector, we have now formed the wavefunction

$$|\psi_{asp}\rangle = \exp[-iHt_{asp}]\ |\psi_{in}\rangle\ , \tag{28}$$

where the initial wavefunction has <u>bifurcated</u> into <u>both</u> arrangement channels

$$|\psi_{asp}\rangle = \{\psi^R_{asp},\ \psi^P_{asp}\}\ . \tag{29}$$

The component in the reactant's channel consists of all the GWPs whose centers followed classical trajectories that underwent inelastic scattering, returning back to the reactant's channel. In terms of the GWPs, the i=1 component of $\psi^R_{asp}$ becomes

$$\psi^R_{asp,1} = \sum_j^{N_y} c_{1j}\ \delta^R_{1j}\ G_{1j}(x,t_{asp})\ g_{1j}(y,t_{asp})\ , \tag{30}$$

where $\delta^R_{1j}$ is the reactant's channel index which equals unity if $x_{1j}$ is in the reactant's channel and equals zero if $x_{1j}$ is in the product's channel.

An analogous definition is made for the product's channel component of $|\psi_{asp}>$, but here the reactant's channel coordinates, momenta and width parameters must be transformed to an equivalent set of parameters in product's space. Here we use the transformation of Eq. (3) for the coordinates and a similar transformation for the momenta and widths. The resulting wavefunction for the i=1 component of $\psi^P_{asp}$ is

$$\psi^P_{asp,1} = \sum_j^{N_y} c_{1j}\ \delta^P_{1j}\ G_{1j}(x',t_{asp})\ g_{1j}(y',t_{asp})\ , \qquad (31)$$

where the $G_{1j}(x',t)$ and the $g_{1j}(y',t)$ are exactly the form of Eqs. (15) <u>except</u> that x' and y' are substituted for x and y and the transformed parameters appearing in the GWPs are denoted with a prime (i.e., $x_{1j} \rightarrow x'_{1j}$, etc.) The phase parameters, $f_{ij}$, remain invariant under the arrangement channel transformation.

Eq. (31) is not the most general result. Upon transformation from the GWP pair $G_{ij}(x,t)\cdot g_{ij}(y,t)$ to the pair $G_{ij}(x',t)\cdot g_{ij}(y',t)$ crossterms of the form $i\lambda'_{ij}\cdot(x'-x'_{ij})\cdot(y'-y'_{ij})$ will appear in the argument of the exponential. Specifically, this transformation yields for the product's channel parameters

$$\alpha^{y'}_{1j} = (\gamma_{BC})^2\ \alpha^{y}_{1j} + (\gamma)^2\ \alpha^{x}_{1j} \qquad (32a)$$

$$\alpha^{x'}_{1j} = \alpha^{y}_{1j} + (\gamma_{AB})^2 \alpha^{x}_{1j} \tag{32b}$$

$$\lambda'_{1j} = -2\gamma_{BC} \alpha^{y}_{1j} + 2\gamma_{AB}\gamma \alpha^{x}_{1j} . \tag{32c}$$

Since we intend to propagate $|\psi_{asp}>$ using the channel wavefunction propagators to complete the second step of the S operation, propagation of the GWPs in the product's channel would require the integration of this equation of motion

$$\dot{\lambda}'_{ij} = -2(\alpha^{x'}_{ij}/M_p + \alpha^{y'}_{ij}/\mu_p)\, \lambda'_{ij} \tag{33}$$

as well as integration of Eqs. (16a) and (16b) with the addition of the coupling terms [1a], $-(\lambda'_{ij})^2/2\mu_p$ and $-(\lambda'_{ij})^2/2M_p$, respectively. (Again, the potential does not appear since a first order truncation of the Taylor expansion has been used.) Integration of these coupled differential equations can be accomplished by integrating Eqs. (16a) and (16b) in the reactant's channel for all the GWPs back to t = 0, and then performing the transformations of Eqs. (32) to yield GWPs in the product's channel. As pointed out by Heller [1a], these crossterms, $\lambda'_{ij}$, provide x', y' correlation which could improve the GWP expansion in the product's channel when attempting to approximate the superposition of final quantum scattering states which evolve from the dynamics.

At this point in the analysis, two parameters, $\beta^y$ and $\beta^x$, are yet to be specified. With the last paragraph in mind, one could arrive at final values for $\beta^y$ and $\beta^x$ through a variational procedure (e.g., by requiring

the final wavefunction to satisfy some criteria such as constant norm, cf. Eq. (47) later). To avoid such a two parameter variation in this work, we will relate the values of $\alpha^x_{1j}$ and $\alpha^y_{1j}$ at $t = t_{asp}$ such that $\lambda'_{ij}$ becomes identically zero upon the channel transformation. Setting Eq. (32c) equal to zero and using Eqs. (22a) and (24a) yields

$$\beta^x = (1 / \gamma) (\gamma_{BC} / \gamma_{AB}) \beta^y . \tag{34}$$

The identity is <u>independent</u> of $t_{asp}$ since we could also enforce $\lambda'_{ij} = 0$ at $t = 0$ after backward propagation in the reactant's channel. The relationships between the initial translational and vibrational width parameters then become

$$\alpha^{y'}_{1j}(t) = \frac{\gamma_{BC}}{\gamma_{AB}} \alpha^y_{1j}(t) \quad ; \quad \alpha^{x'}_{1j}(t) = \frac{\gamma_{AB}}{\gamma_{BC}} \alpha^x_{1j}(t) , \tag{35a,b}$$

where we have used the additional fact that the identities hold for arbitrary t. In a mass symmetric ABC system ($m_A = m_B = m_C$) the coefficients scaling the widths are unity. A vibrational GWP in reactant's space transforms to a vibrational GWP in product's space with <u>only</u> a change in the GWP coordinate and momentum parameters with the same holding true for the translational GWP. This property provides an <u>a posteriori</u> justification for the one parameter search in terms of describing the final vibrational wavefunction in the product's channel. From experience we have found that a good representation of a vibrational wavefunction exists for

only a limited range of values for $\beta^y$. By relating the $\beta^x$ and $\beta^y$ as above, we can expect to construct a $|\psi_{out}>$ which will provide an adequate representation of the various superimposed quantum vibrational states resulting from the dynamics. We will use $\beta^y$ as a variational parameter when determining scattering information from the IPGWD wavefunction defined later in the paper.

Backward propagation with the channel Hamiltonians

The next step in the wavefunction propagation scheme involves operation on $|\psi_{asp}>$ with the channel wavefunction propagators $U^R$ and $U^P$, thus completing the second step of the S operation. Addressing the reactant's component first, we must evaluate formally

$$\psi^R_{out,1} = \exp[iH^R t_{asp}]\ \psi^R_{asp,1} \cdot \tag{36}$$

This corresponds to integrating the parameter equations of motion using $H^R$, and thus propagating the GWPs which remain in the reactant's channel at time $t_{asp}$. The value of the GWP parameters at $t_{asp}$ are used as the initial conditions; the equations of motion are integrated backwards until t = 0; and the values at t = 0 are substituted into Eq. (30) to form $\psi^R_{out,1}$. Similarly, the i=1 component in the product's channel is integrated backwards in time using $H^P$

$$\psi^P_{out,1} = \exp[iH^P t_{asp}]\ \psi^P_{asp,1} \cdot \tag{37}$$

The equations of motion for the GWP parameters which cross over into the product's channel are derived from $H^P$ and integrated backwards in time over the interval $[t_{asp},0]$. Upon substitution of the resulting GWP parameters into Eq. (31), $\psi^P_{out,1}$ is formed.

Only the classical equations of motion and the Lagrangian contribution to the phase parameters are integrated numerically. The analytic solution to the equations of motion for the width parameters show that the final width parameters equal the initial width parameters upon forward and backward integration on the interval $[0,t_{asp}]$. This equality bypasses the problem of the spreading GWPs. The IPGWD procedure also provides a formal justification for the use of time-independent width parameters as defined in the frozen Gaussian approximation (FGA) [15]. Within the FGA, the equations of motion for the width parameters are neglected, and the final values of the width parameters are set equal to the initial values. The IPGWD procedure yields the FGA result for the final width parameters provided that the Taylor expansion for the potential which appears in the TDSE is truncated at first order. Truncation at second order yields the equations of motion for the width parameters [1a] which depend explicitly on the instantaneous second derivatives of the potential with respect to the coordinate parameters. Except for the trivial case of a harmonic potential where an analytical solution can be found, the equations of motion for the widths must be integrated numerically. The numerical integration of the width equations of motion, which are highly non-linear, becomes unstable after only a very few time steps. Although a method, the P-Z transform [16], has been developed to handle this problem we choose to

use the first order truncation of the potential so we can obtain analytic orbits for the width parameters.

Using the same arguments, we can show that the width dependence in the equations of motion for the phase parameters provides a zero contribution to the phase. The remaining contribution to the final phase parameters is

$$f_{1j} = A^F(y_{1j},p^y_{1j},x_{1j},p^x_{1j},t_{asp}) - A^C(y_{1j},p^y_{1j},x_{1j},p^x_{1j},t_{asp}) , \qquad (38)$$

where A represents the classical action integral

$$A(y,p^y,x,p^x,t-t_0) = \int_{t_0}^{t} L(y,p^y,x,p^x)\, dt' . \qquad (39)$$

The first term of $f_{1j}$ arises from the forward integration and is evaluated with the classical Lagrangian defined by Eq. (17), with F denoting the full interaction Hamiltonian. The second term of $f_{1j}$ arises from the backward integration and is evaluated with the channel classical Lagrangian

$$L^C = (p^x)^2/2M_C + (p^y)^2/2\mu_C - V^C(y) , \qquad (40)$$

where the reduced masses, momenta and coordinates for the appropriate channel (C = R or P) are used.

The final phase parameter is the difference between the classical action of the full Hamiltonian minus the classical action of the appropriate channel Hamiltonian. Such a dependence on the classical action is fundamental to semiclassical scattering theory [17]. The appearance of

this feature within GWD was first pointed out by Heller [16]. These action integrals lead to a unique phase parameter for each GWP in the final scattering wavefunction and each of these phases in turn critically influences the constructive and destructive interference effects in $|\psi_{out}\rangle$ upon summation of the GWPs.

Backward integration of the trajectory and phase parameters is possible using analytical methods. The channel Lagrangian is the sum of a free particle and a bound oscillator Lagrangian. The analytic solution to the free particle equations of motion is trivial. In the Results section of this paper, we model the oscillator with a Morse potential for which the analytic solution to the equations of motion is known [18]. Upon knowledge of the equations of motion we can construct the channel Lagrangians.

Another convenient feature of the IPGWD procedure is that it provides a final wavefunction independent of the stopping time for the forward integration, $t_{asp}$. Let us represent the IPGWD time propagation of a single GWP in Fig. 1. Motion along the line corresponds to following what we will define as the GWP time trajectory. The integration is started on the upper branch of the time trajectory at $t = 0$ and position $x_0$ in the reactant's channel. In Fig. 1, the progress of the time trajectory is expressed in a time domain and not in coordinate space. (Use the $i = 1$ time domain and neglect the trajectory on $[-\delta t_i, 0]$, which is used later.) The integration of the equations of motion proceeds forward in time until $t_{asp}$ (traveling to the right) with the full Hamiltonian. Switching to the lower time trajectory, we proceed to integrate the equations of motion backwards in time until $t = 0$ (traveling left) with $H^C$. To illustrate the independence

Figure 1. Time trajectory for the interaction picture propagation of a GWP. The elapsed time of the trajectory is referenced to both the i=1 and the $i^{th}$ time domains. The appropriate Hamiltonian which governs the equations of motion over a given interval is also provided

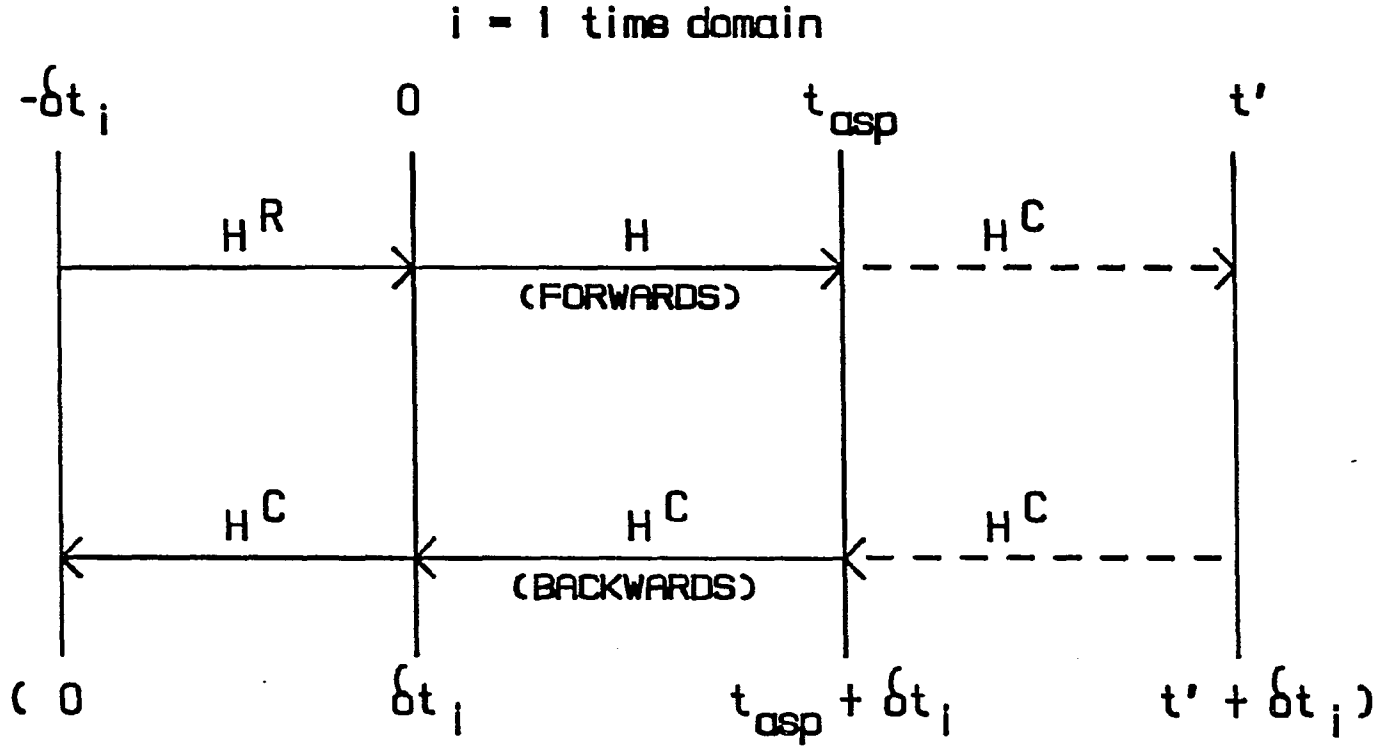


$$\delta t_i = (i - 1)\,\frac{\tau_y}{N_y}$$

of the IPGWD with respect to stopping time, consider continuing the forward integration from $t_{asp}$ to t' before switching to the lower branch. In the region $[t_{asp}, t']$ on the upper branch, H reduces to $H^C$ by definition since the trajectory has passed the asymptotic boundary. Thus, forward integration with $H^C$ from $t_{asp}$ to t' on the upper branch, followed by the backward integration with $H^C$ from t' to $t_{asp}$ on the lower branch is equivalent to <u>not</u> traveling at all on $[t_{asp}, t']$. This proves that the final IPGWD scattering wavefunction is <u>independent</u> of stopping time provided that the translational coordinate parameter is outside of the interaction region of V(x,y).

In general, the independence with respect to stopping time is <u>not</u> true for the final scattering wavefunction determined by the previous applications of GWD. The time trajectory for a single GWP started at t = 0 and propagated using "standard" GWD is represented by the upper branch of Fig. 1. The equations of motion are integrated forward in time <u>only</u>, with the final scattering wavefunction determined from the GWP parameters obtained at $t_{asp}$. If the forward integration is continued onto t', the final wavefunction constructed from the parameters at t' does <u>not</u> have to correspond to the wavefunction at $t_{asp}$. Previous work on inelastic scattering [1] mentions little on how to determine t'. In those examples, the stopping time was determined by monitoring the scattering information (S matrix transition elements) generated from the final scattering wavefunction. After each and every translational coordinate parameter passed $x_{asp}$, the propagation was terminated when the scattering information became "pseudo-stationary" with respect to further integration over an

additional finite time interval. However, as we showed above, the forward-only propagated wavefunction is not time-invariant and thus cannot provide stationary scattering information if integrated to $t \to \infty$ as required formally by the S operation.

It could be argued that the backward integration step merely adds a constant phase shift of $\exp[iE_{sys}t_{asp}]$. This is only true if $|\psi_{asp}>$ is an eigenfunction of the channel time-independent Schroedinger equation. Even though $|\psi_{out}> = \{U^R(t_{asp})^\dagger, U^P(t_{asp})^\dagger\}\cdot|\psi_{asp}>$, both $H^R\psi^R_{out} \neq E_{sys}\psi^R_{asp}$ and $H^P\psi^P_{out} \neq E_{sys}\psi^P_{out}$, which is required for addition of the constant phase. For example, even a single GWP evolving under the influence of a free particle H within GWD does not allow for this addition of constant phase.

Constructing the $i=2,N_x$ Components of the Final Wavefunction

Only the i=1 contribution to the overall expansion in translational GWPs is defined by Eqs. (36) and (37). Given the initial and final sets of the i=1 GWP trajectory parameters from the IPGWD procedure, we can construct the other $i=2,N_x$ sets of final parameters analytically. This is important since the numerical integration of the equations of motion is the most demanding step of the IPGWD procedure in terms of computational effort. We integrate only $N_y$ sets of parameter equations of motion instead of $(N_x \times N_y)$ sets.

The initial GWP parameters are given in Eqs. (22) and (24). Let us define the sets of GWP parameters obtained after applying IPGWD to the i=1 initial sets of parameters as $\{y^f_{1j}, p^{yf}_{1j}, x^f_{1j}, p^{xf}_{1j}, f^f_{1j}\}$. The arrangement channel dependence of the $1j^{th}$ set is implictly contained in these

parameters. If the $1j^{th}$ trajectory crosses over to the product's channel, we then apply the appropriate transformations to obtain the final parameters in terms of the product's channel coordinate system (unprimed $\rightarrow$ primed). To aid in the assignment of the final $i=2,N_x$ sets of final parameters, we will examine the time trajectory for a single GWP as displayed in Fig. 1. The i=1 trajectories correspond to the IPGWD propagation over the interval $[0,t_{asp}]$. We construct the $i=2,N_x$ sets by taking advantage of the spacing of the initial translational GWPs in time. As an example we will explicity construct the i=2 set, and then generalize the procedure to obtain all $i=2,N_x$ sets.

Recall that the initial i=2 translational coordinate parameters were determined by pulling the initial i=1 translational coordinate parameters backwards in time from 0 to $-\delta t_2 = -(\tau_y/N_y)$. Returning back to Fig. 1, let us start the forward time trajectory for the i=2 parameters, but now reference our measure of time such that the i=2 parameter integration is started at t = 0 in what we will refer to as the i=2 time domain. In the i=1 time domain, the i=2 trajectories start at $-\delta t_2$. The values of pertinent points along the time trajectory are provided in terms of both the i=1 and general $i^{th}$ time domain in Fig. 1. This shift in time allows us to construct the i=2 parameters from the i=1 parameters. Following the time trajectory on $[0,\delta t_2]$ in the i=2 time domain requires integrating the equations of motion using $H^R$. The values of the parameters at time $\delta t_2$ become

$$y_{2j}(\delta t_2) = y_j^0, \qquad ; \qquad p^y_{2j}(\delta t_2) = p_j^{y0} \qquad (41a,b)$$

$$x_{2j}(\delta t_2) = x_0 \quad ; \quad p^x_{2j}(\delta t_2) = -p^{x^0} \tag{41c,d}$$

$$f_{2j}(\delta t_2) = A^R(y_{2j}(0), p^y_{2j}(0), x_{2j}(0), p^x_{2j}(0), \delta t_2) \ , \tag{41e}$$

where $j' = M(j, \delta t_2)$ .

Forward integration for the (i=2,j) parameters from time $\delta t_2$ in the i=2 time domain is identical to integrating (i=1,j') parameters from t=0 in the i=1 time domain. We can match the j trajectories onto the j' trajectories and follow the j' trajectories forwards in time up to $t_{asp}$. Within the i=2 time domain, the $j^{th}$ trajectory is terminated at $t = t_{asp} + \delta t_2$. Since the IPGWD final wavefunction is independent of stopping time, integration beyond $t_{asp}$ is acceptable. Switching onto the lower branch of the time trajectory in Fig. 1, we now back integrate the i=2 parameters using the appropriate $H^C$. Here the backward integration of the (i=1,j') parameters on $[t_{asp},0]$ in the i=1 time domain corresponds to a backward integration of the (i=2,j) parameters on $[t_{asp}+\delta t_2, \delta t_2]$ in the i=2 time domain. Therefore to construct the final (i=2,j) parameters we must integrate the (i=1,j') parameters over the interval $[0,-\delta t_2]$ in the i=2 time domain so to complete the backward integration to t = 0. Since $H^C$ governs the propagation over this additional time interval, (see Fig. 1), we can analytically construct the i=2 parameters. This assumes knowledge of the analytic solution for the equations of motion for an oscillator of total classical energy

$$\varepsilon = (p^{yf}_{1j'})^2/2\mu_C + V^C(y^f_{1j'}) . \tag{42}$$

The translational equations of motion are trivial to extend since the interaction potential is independent of x (or x') in the asymptotic region. The final i=2 parameters become

$$y^f_{2j} = y^f_{1j'} + F_y(y^f_{1j'},p^{yf}_{1j'},-\delta t_2) \tag{43a}$$

$$p^{yf}_{2j} = p^{yf}_{1j'} + F_{py}(y^f_{1j'},p^{yf}_{1j'},-\delta t_2) \tag{43b}$$

$$x^f_{2j} = x^f_{1j'} - (p^{xf}_{1j'}/M_C)\delta t_2 \tag{43c}$$

$$p^{xf}_{2j} = p^{xf}_{1j'} \tag{43d}$$

$$f^f_{2j} = f^f_{1j'} + A^R(y_{2j}(0),p^y_{2j}(0),x_{2j}(0),p^x_{2j}(0),\delta t_2) + A^C(y^f_{1j'},p^{yf}_{1j'},x^f_{1j'},p^{xf}_{1j'},-\delta t_2) \tag{43e}$$

where $j' = M(j,\delta t_2)$. The appropriate channel reduced masses and channel Lagrangian for the arrangement of the (i=1,j') trajectory are used. $F_y$ and $F_{py}$ represent the analytic solutions for the oscillator classical trajectories where the first two arguments are the initial conditions and the last argument is the amount of time the trajectory is propagated.

We now generalize the above procedures to construct the other sets of

GWP parameters. We start by initializing the $i^{th}$ translational coordinate parameters by pulling the initial i=1 translational coordinate parameters backwards in time by an amount $\delta t_i = (i - 1)\ (\tau_y/N_y)$. Referring to the upper branch of the time trajectory in Fig. 1, we perform the same transformation of the time domain as before and set t = 0 in the $i^{th}$ time domain. Upon integrating forwards in time an amount $\delta t_i$ using $H^R$, a set of equations identical to Eqs. (41) are obtained for the $i^{th}$ parameters at $\delta t_i$ except now the subscript 2 is replaced by the subscript i throughout. Also, $j' = M(j,\delta t_i)$. Continuing the forward integration on $[\delta t_i, t_{asp} + \delta t_i]$ and subsequently back integrating with $H^C$ over the interval $[t_{asp} + \delta t_i, \delta t_i]$ in the $i^{th}$ time domain, the $i=2,N_x$ trajectories match onto the i=1 trajectories integrated over $[0,t_{asp}]$ and back. The final i=1 parameters are extended in the same manner as before to give the final $i=2,N_x$ parameters. The final parameters are defined identical to Eqs. (43) except that the subscript 2 is replaced by the subscript i (e.g., 2j -> ij, $\delta t_2$ -> $\delta t_i$).

We started this section by mentioning the implicit dependence of the arrangement channel on the i=1 final parameters. If a given set of $1j'^{th}$ trajectory parameters cross over to the product's channel, then the $ij^{th}$ set constructed from the $1j'^{th}$ set also crosses over. Therefore this $ij^{th}$ set of final trajectory parameters must be transformed to the product's channel coordinates system.

The determination of the channel indices $\delta^R_{ij}$ and $\delta^P_{ij}$ is related to a given $ij^{th}$ set of translational and vibrational classical trajectory

parameters. The outcome of the final $ij^{th}$ classical trajectory parameters depends solely on the value of the phase space parameters as they reach the point in phase space where the numerically integrated i=1 set of equations of motion were initiated at t = 0. Thus, the $i=2,N_x$ channel indices in terms of the i=1 channel indices are

$$\delta_{ij}^{C} = \delta_{1j'}^{C} \qquad \text{for } C = R \text{ or } P \ , \tag{44}$$

where $j' = M(j,\delta t_i)$. C represents the channel that the $(i=1,j')^{th}$ classical trajectory ended in asymptotically.

Before assigning the final values to the width parameters, let us emphasize that all $(N_x \times N_y)$ sets of parameter equations of motion are integrated formally over the interval $[0,t_{asp}]$ both forwards and backwards. The determination of the $i=2,N_x$ sets of GWP parameters by a backward integration in time over increments of $(\tau_y/N_y)$ is a technique to obtain the classical trajectory information for all $(N_x \times N_y)$ trajectory parameters from a given set of $N_y$ classical trajectories. Therefore, coupled with the fact that the final width parameters are time-independent with respect to IPGWD propagation, we obtain

$$\alpha_{ij}^{xf} = \beta^{x} \quad ; \quad \alpha_{ij}^{yf} = \beta^{y} \ . \tag{45a,b}$$

At this point we can construct the final scattering wavefunction

$$|\psi_{out}\rangle = \sum_{i}^{N_x} \sum_{j}^{N_y} c_{ij}\, \delta_{ij}^{C}\, G_{ij}(x,t_{out})\, g_{ij}(y,t_{out}) \,, \tag{46}$$

where $t_{out}$ signifies that each GWP is constructed from the parameters determined by the IPGWD propagation. Strictly speaking $t_{out} = 0$. The value of $\beta^y$, our one remaining unspecified parameter, is determined by requiring conservation of norm:

$$\langle\psi_{out}|\psi_{out}\rangle \,/\, \langle\psi_{in}|\psi_{in}\rangle = 1 \,. \tag{47}$$

Due to the truncation of the Taylor series for the potential in the GWD formalism, the wavefunction propagators are non-unitary, and a normed wavefunction is not guaranteed for all values of $\beta^y$. We determined numerically the values of $\beta^y$ which satisfied Eq. (47).

Using the normed $|\psi_{out}\rangle$, we construct reaction probabilities by taking the norm in each <u>arrangement channel</u> as

$$P(GWP,R) = \int |\psi_{out}^{R}|^2 \, dx\, dy \tag{48a}$$

$$P(GWP,P) = \int |\psi_{out}^{P}|^2 \, dx'dy' \,. \tag{48b}$$

The values of these norms are identified as the non-reactive and reactive scattering probabilities, respectively. If vibrational state-to-state reaction probabilities are desired then we must project a basis of a plane wave times a vibrational eigenfunction onto $|\psi_{out}\rangle$ [1a]. By such a

procedure, reaction probabilities and S-matrix transition elements for total quantum energies different from the total classical energy could also be predicted.

## A SAMPLE ($N_x$=4, $N_y$=4) IPGWD SCATTERING SOLUTION

To illustrate the advantages of using the IPGWD coupled with the use of the multiple GWP expansion for X(x) (which we denote IPGWD-M), we will examine the dynamics exhibited by a prototype $N_x$=4, $N_y$=4 GWP wavefunction applied to a collinear exchange reaction on an unspecified potential. We will contrast the results obtained for IPGWD-M with the results obtained for IPGWD using a single GWP expansion for X(x) (which we denote IPGWD-1). The IPGWD-1 wavefunction expansion is a subset of the IPGWD-M wavefunction corresponding to $N_x = 1$.

We let the total classical energy be $E_{tot} = E_{trans} + \varepsilon_n$ where $E_{trans}$ is sufficiently large so that the classical trajectory possesses enough translation kinetic energy to overcome any barriers on the potential. The GWP vibrational wavefunction is linear least squares fit to $\phi_n(y)$ yielding the set of coefficients $\{c_j^y\}$. The M map function which describes the evolution of the vibrational classical trajectories governed by $H^R$ is provided in Table I. The initial translational wavefunction is linear least squares fit to a plane wave of momentum $p_0^x = (2\, E_{trans} \cdot M_R)^{1/2}$, and the initial translational coordinate parameters are spaced in time by the interval $\delta t = (\tau_y/4)$.

Next, we apply the IPGWD propagation procedure to the initial

Table I. M mapping function for the sample 4 x 4 GWP scattering problem

| | | $j' = M(j, \delta t)$ | | | |
|---|---|---|---|---|---|
| j | $\delta t =$ (i=) | 0 (1) | $\delta\tau_y$[a] (2) | $2\delta\tau_y$ (3) | $3\delta\tau_y$ (4) |
| 1 | | 1 | 2 | 3 | 4 |
| 2 | | 2 | 3 | 4 | 1 |
| 3 | | 3 | 4 | 1 | 2 |
| 4 | | 4 | 1 | 2 | 3 |

[a] $\delta\tau_y = (\tau_y/4)$.

wavefunction. We represent each GWP in the expansion of both $|\psi_{in}\rangle$ and $|\psi_{out}\rangle$ in Fig. 2. Each X represents an individual GWP pair, $G_{ij}g_{ij}$. On the left hand side of Fig. 2, all 16 pairs of GWPs are present in the reactant's channel. The spacing between each GWP pair, both horizontally and vertically, is arbitrary and does not reflect the actual spacing in terms of the translational and vibrational coordinate system. The results of the trajectory propagation is presented in the right hand side of the Fig. 2. Note that $|\psi_{out}\rangle$ spans both arrangement channels. The trajectories which are actually integrated numerically correspond to the i=1 column of GWPs. Quasi-classical Trajectory (QCT) reaction probabilities [19] are constructed from this column of i=1 GWPs. For the given initial conditions represented in Fig. 2, we obtain the QCT reaction and non-reaction probabilities of P(QCT,P) = 1/4 and P(QCT,R) = 3/4, respectively. We can also assign the i=1 channel indices as $\delta^R_{11} = \delta^R_{12} = \delta^R_{13} = \delta^P_{14} = 1$, and $\delta^P_{11} = \delta^P_{12} = \delta^P_{13} = \delta^R_{14} = 0$. The i=2,3,4 channel indices and GWP parameters are constructed from the i=1 results by using the M map function defined in Table I. For example, the initial (i=2,j=1) GWP pair evolves into the (i=1,j=2) pair if integrated for a time $\delta t = (\tau_y/4)$. The (i=1,j=2) pair, upon IPGWD propagtion, remains in the reactant's channel asymptotically. Therefore, the (i=2,j=1) pair is also found in the reactant's channel. Repeating the above procedure, all of the GWP points in Fig. 2 are assigned. One important observation is that the QCT reaction probabilities are <u>independent</u> of the value we choose for $N_x$: 75% of the trajectories end in the reactant's channel and 25% end in the product's channel. This independence is due to the fact that the translational GWPs

Figure 2. The initial and final GWP distributions for a sample 4x4 GWP scattering problem. For a given arrangement channel: X = $(i,j)^{th}$ GWP pair is present; 0 = $(i,j)^{th}$ GWP pair is absent. Initially the product's channel is empty

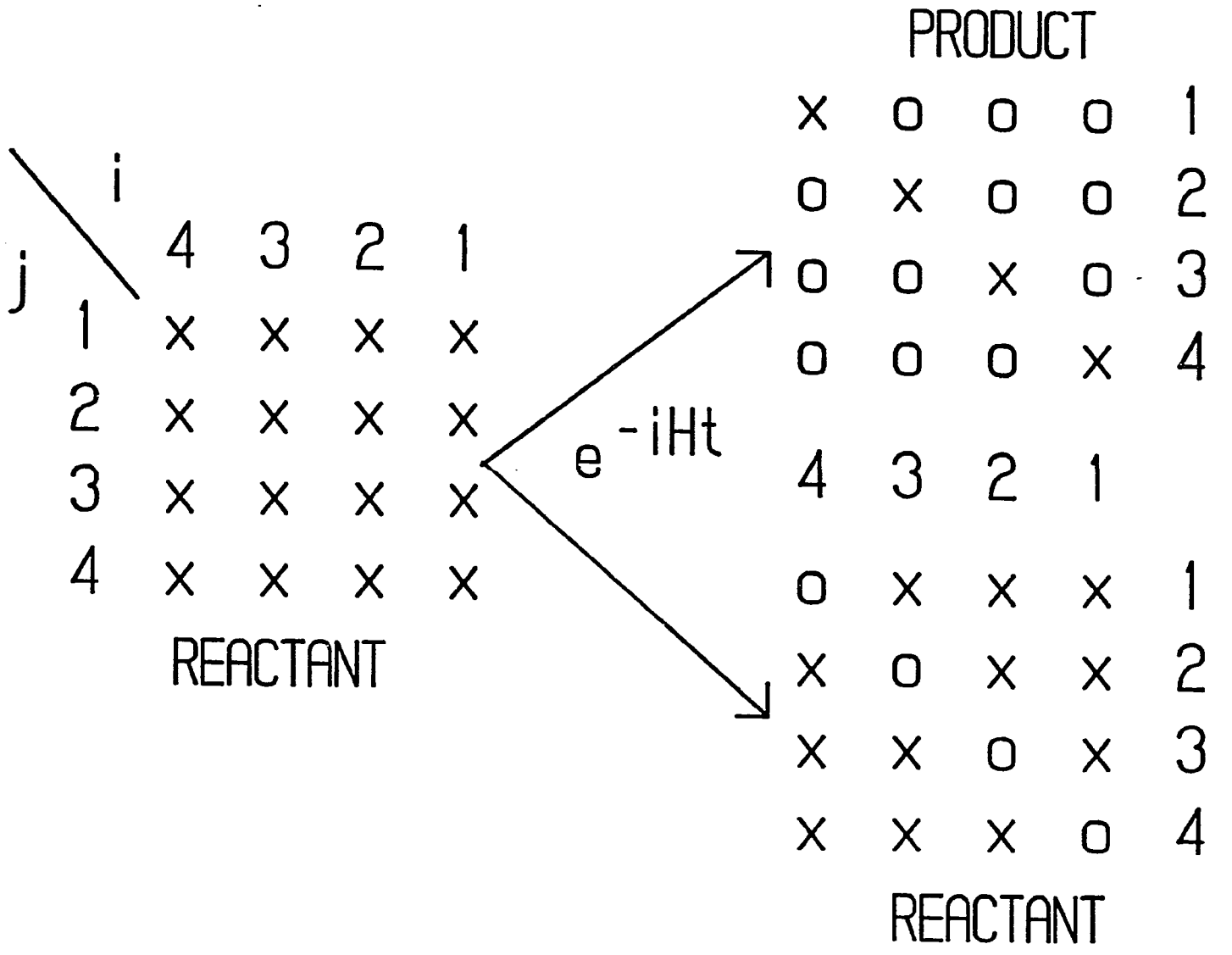
PRODUCT
x o o o 1
o x o o 2
o o x o 3
o o o x 4
4 3 2 1
o x x x 1
x o x x 2
x x o x 3
x x x o 4
REACTANT
i
j
4 3 2 1
1 x x x x
2 x x x x
3 x x x x
4 x x x x
REACTANT
e -iHt

are initialized as specified by Eq. (24c), thus taking advantage of the periodic spacing of the vibrational GWPs.

Whereas the GWP parameters are time-dependent and transform according to the M mapping, the GWP expansion coefficients are time-independent. Since they do not evolve in time, they are independent of the M map. This independence leads to the major difference between the IPGWD-M and IPGWD-1 determined reaction probabilities. The IPGWD-1 scattering wavefunction corresponds to using a given $i^{th}$ column of GWPs from Fig. 2. Since each $i^{th}$column of GWPs is initialized in the asymptotic region of the reactant's channel, ($x_{ij}(0) > x_0$, for all j), each and every $i^{th}$ column is an adequate representation for $|\psi_{in}>$ in terms of satisfying the asymptotic criteria. To illustrate the weakness of the IPGWD-1 wavefunctions, let us construct each $i^{th}$ IPGWD-1 final wavefunction in the product's channel explicitly as

$$\psi_1^P = c_1^x c_4^y G_{14} g_{14} \tag{49a}$$

$$\psi_2^P = c_2^x c_3^y G_{23} g_{23} \tag{49b}$$

$$\psi_3^P = c_3^x c_2^y G_{32} g_{32} \tag{49c}$$

$$\psi_4^P = c_4^x c_1^y G_{41} g_{41} \, . \tag{49d}$$

The final IPGWD-M wavefunction is the sum of all four IPGWD-1 wavefunctions

$$\psi^P_{out} = \psi^P_1 + \psi^P_2 + \psi^P_3 + \psi^P_4 . \qquad (50)$$

Each $G_{ij}$ and $g_{ij}$ are individually normalized to the same values, a norm which depends on the values of $\beta^x$ and $\beta^y$, respectively. Upon fitting the vibrational GWP expansion to $\phi_n(y)$, the relative values of each and every $c^y_j$ in $\{c^y_j\}$ are not necessarily equal. The identical argument applies to the translational GWP expansion, also. Thus when we determine P(GWP,P) and P(GWP,R), the product $c^y_j\ c^x_i$ for a particular j and i leads to differences in the computed IPGWD-1 reaction probabilities. Therefore, the GWP probabilities constructed from each $\psi^P_i$ and $\psi^R_i$ are implicitly dependent on the $x_{ij}(0)$ since the $x_{ij}(0)$ govern which trajectories pass into a given channel asymptotically. This in turn determines which coefficient from $\{c^y_j\}$ and which from $\{c^x_i\}$ contribute to a given channel wavefunction. Since the coefficients contribute unequally to each $\psi^P_i$ and $\psi^R_i$, the reaction probabilities determined from each will not be identical.

Use of the IPGWD-M wavefunction removes this dependence on the initial representation of $\phi_n(y)$ and X(x) since each $c^y_j$ and $c^x_i$ occurs once in $\psi^P_{out}$, as we have shown specifically for our sample scattering problem. Although the IPGWD-M wavefunction is asymptotically correct for any value of $N_x$, the independence of the IPGWD-M $|\psi_{out}\rangle$ with respect to the representation of $\phi_n(y)$ only holds true for $N_x$ equal to an integer multiple of $N_y$.

A weakness of the IPGWD-M procedure is the dependence of $|\psi_{out}\rangle$ on the QCT generated from a given set of initial conditions. The standard error associated with P(QCT,R) and P(QCT,P) is estimated as $[P(1-P)/N_y]^{1/2}$. In

practice, the number of trajectories which enter into a given channel varies by ±1 depending on the exact value chosen for $x_0$. For the 4 x 4 sample problem, there may exist a region in the initial x,y phase space, (corresponding to an initial $x_{1j}(0)$ within the interval $[x_0, x_0+\delta x_1]$, $-p_0^x$, and $\{y_j^0, p_j^{y0}\}$), which leads to a final trajectory distribution different from the distribution obtained in our sample problem (i.e., a 100%/0% or a 50%/50% distribution). A change in the number of trajectories entering the respective channels leads to a change in the number of GWPs in each channel. This in turn leads to large variations in the calculated P(GWP,R) and P(GWP,P). However, this dependence of the IPGWD-M wavefunction on the QCT is restricted to a small region in the initial translational interval since the vibrational trajectories are periodic. Theoretically, one can remedy this problem by choosing $N_y$ large enough, (i.e., $\delta x_0$ small enough), although a maximum value of $N_y$ is constrained by considering other properties of the wavefunction such as the goodness of fit to X(x) and $\phi_n(y)$.

# RESULTS

The $H-H_2$ collinear exchange reaction was studied using the Porter-Karplus II potential energy surface (PES) [20]. The initial vibrational wavefunction representing the n=0 state of $H_2$ was expanded in sets of $N_y$ = 10, 12, 14, and 20 trial GWPs. All the GWPs were centered between the two classical turning points on the phase space orbit with energy $\varepsilon_0$ = 0.273 eV. These initial vibrational wavefunctions were linear least squares fit to the exact n=0 quantum state derived from a 20 GWP numerical basis expansion which diagonalized the vibrational Hamiltonian using the symmetric orthogonalization approach [14]. The width of each numerical basis GWP was set equal to the width of the n=0 state within the harmonic oscillator approximation. This value, $\beta^y_{har}$ = 1/2 (in dimensionless units), was found optimal when diagonalizing the Morse oscillator. We will reference our trial basis GWP widths to $\beta^y_{har}$. The IPGWD propagation was applied to the trial sets of GWPs where $x_0$ = 10 A was found to place the initial translational GWP asymptotically in the reactant's channel. $x_{asp}$ was set equal to $x_0$ for consistency.

The QCT reaction threshold on this PES is $E_{sys}$ = 0.49 eV [21]. For the limited number of trajectories we propagated, a practical reaction threshold of $E_{sys}$ = 0.51 eV was found. For each $N_y$ value, we propagated trajectories on the $E_{sys}$ interval [0.51 eV, 0.99 eV] in steps of 0.01 except in the reaction threshold region where we placed trajectories every 0.005 eV. Over the interval [0.58 eV, 0.72 eV], P(QCT,P) equals unity therefore propagation on this range was not necessary.

We then obtained the value(s) of $\beta^y$ which normed $|\psi_{out}\rangle$ for each combination of $N_y$ and $E_{sys}$, and constructed the GWP reaction probabilities. With this $\beta^y$, we examined each $|\psi_{in}\rangle$ for the goodness of the least squares fit to the initial states $\phi_0(y)$ and $X(x)$. The goodness of fit was measured by calculating the overlap between the GWP expansion and exact wavefunctions, $\langle\phi_0(\text{exact})|\phi_0(\text{GWP})\rangle$ and $\langle X(\text{exact})|X(\text{GWP})\rangle$. The results of these overlaps and the value (or range of values) of $\beta^y$ which normed $|\psi_{out}\rangle$ are provided in Table II, with $N_x$ set equal to $N_y$. The entries presented for $\beta^y$ and the vibrational overlaps were obtained by constructing the norm for each scattering wavefunction on the full $E_{sys}$ interval. When $\beta^y$ varies only slightly as a function of $E_{sys}$, we present the average of the values, which occurred for $N_y$ = 10 and 12. For a large spread in $\beta^y$, we give the range of values obtained over the $E_{sys}$ interval, which occurred for $N_y$ = 14 and 20. The translational overlap, determined from $X(x)$, is dependent on $E_{sys}$ since $E_{sys}$ determines the momentum of the plane wave. As $E_{sys}$ increases, the wavelength of $X(x)$ decreases which in turn causes $X(x)$ to oscillate more frequently over the finite fitting interval. The increased oscillation degrades the fit as more GWPs are needed to reproduce the oscillations. The entries in Table II correspond to $X(x)$ for $E_{sys}$ = 0.51 eV.

Using Table II, we arrived at an optimal number of GWPs to represent $|\psi_{in}\rangle$ and $|\psi_{out}\rangle$. For $N_y$ = 10 and 12, the $\beta^y$ values (measured in units of $\beta^y_{har}$) which normed $|\psi_{out}\rangle$ provided an unsatisfactory representation for $|\psi_{in}\rangle$. A range of $\beta^y$ was found (= 4 to 5) where excellent representations

Table II. Measure of the goodness of fit for the GWP initial vibrational and translational wavefunctions ($N_x = N_y$)

| $N_y$ | $(\beta^y)^a$ | vibrational[b] overlap | translational overlap ($E_{sys}$ = 0.51 eV) |
|---|---|---|---|
| 10 | 18 | 0.85 | 0.93 |
| 12 | 19 | 0.82 | 0.84 |
| 14 | 10 to 18 | 0.94 to 0.97 | 1.00 |
| 20 | 30 to 36 | 0.90 to 0.91 | 0.96 |

[a]Average value or range of values which provided a normed final wavefunction.

[b]Overlap between the exact wavefunction and initial vibrational GWP expansion for the given value (or range of values) of $\beta^y$.

for $|\psi_{in}>$ were found. But for this lower range of $\beta^y$ values, the best solution to Eq. (47) yielded ~ 0.8 instead of unity. This lower range of $\beta^y$ failed to norm $|\psi_{out}>$ because there were not enough GWPs in both arrangement channels to adequately represent $|\psi_{out}>$. For $N_y$ = 14, upper and lower ranges of $\beta^y$ were also found. In this case, the lower range solution (corresponding to the values in Table II) for $|\psi_{out}>$ contained enough GWPs in each arrangement channel. $N_y$ = 14 also provided the best overall representation for $|\psi_{in}>$. The upper range solution (not shown) provided $\beta^y$ values that were too large and which resulted in the vibrational GWPs becoming too narrow to adequately represent $\phi_0(y)$. Similarly for the lower range solution to the $N_y$= 20 expansion (presented in Table II), the initial vibration GWPs were too narrow with $\beta^y$ = 30 to 36. Here we were packing too many GWPs onto a finite interval in the vibrational phase space. Therefore, the optimal GWP expansion of $N_y$ = 14 for this <u>specific</u> system was determined by the balance of two competing factors. In summary, too few GWPs yield a non-normalizable $|\psi_{out}>$, and too many GWPs yield an expansion for $\phi_0(y)$ which crowds the GWPs too closely in the vibrational phase space.

Using the $N_y$ = 14 GWP expansion, let us now compare the GWP reaction probabilities with the probabilities obtained from quantum ("exact") close-coupled calculations [22]. In Fig. 3, we present P(GWP,P) and the product channel reaction probability for the quantum treatment P(QM,P). $E_{sys}$ is restricted to the range between the classical reaction threshold and the onset of P(QCT,P) = 1. Also provided in Fig. 3 are the QCT results constructed from the 14 classical trajectories which serve as the GWP

Figure 3. Reaction probabilities for the $H + H_2$ collinear exchange reaction. The GWP results are derived from a $N_y = 14$ (vibrational) GWP basis. The absence of a point (+) at a given total system energy for the $N_x = 28$ (translational) GWP basis indicates that this probability is identical to the $N_x = 14$ result

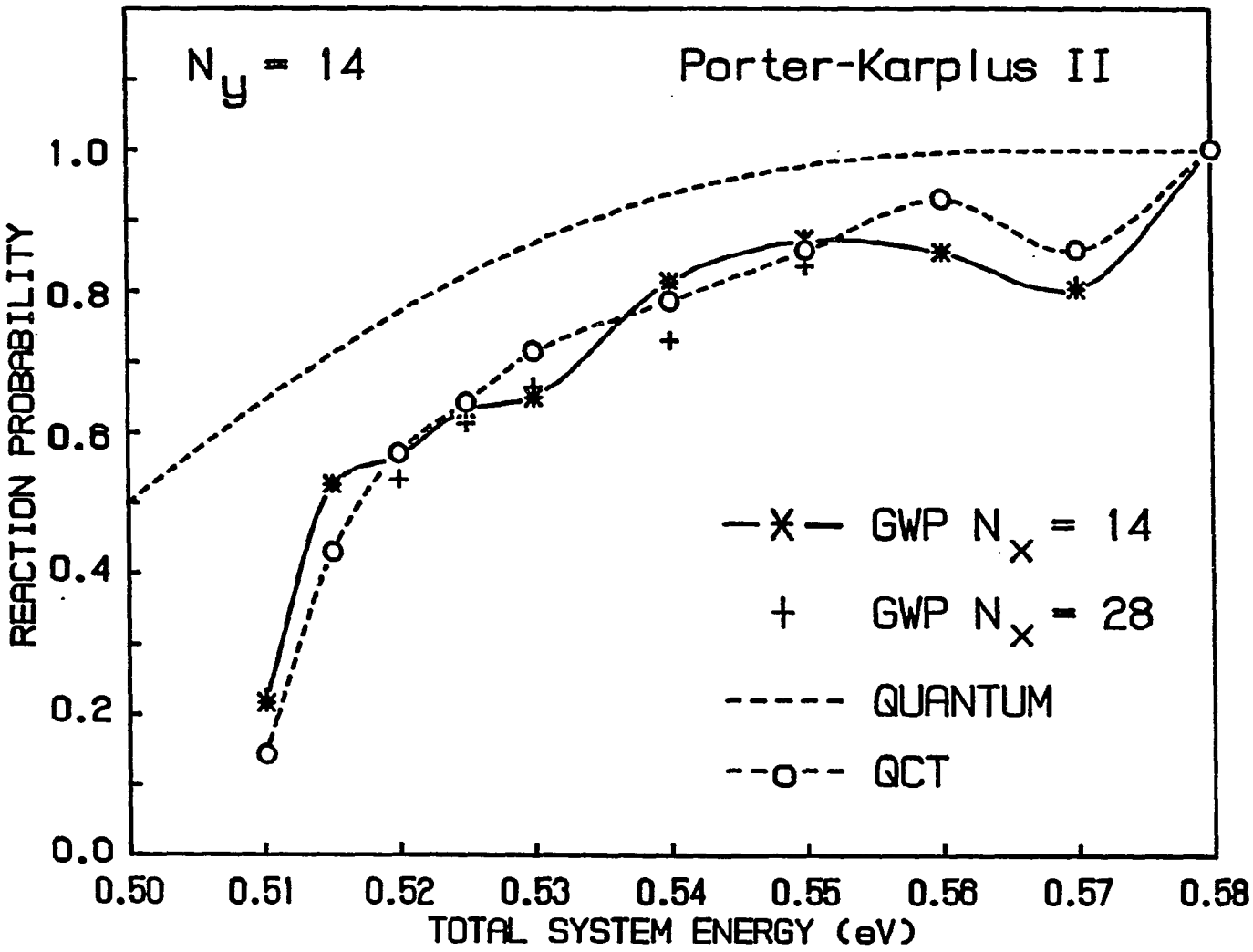
$N_y$ = 14
Porter-Karplus II
REACTION PROBABILITY
1.0
0.8
0.6
0.4
0.2
0.0
0.50
0.51
0.52
0.53
0.54
0.55
0.56
0.57
0.58
TOTAL SYSTEM ENERGY (eV)
GWP $N_x$ = 14
GWP $N_x$ = 28
QUANTUM
QCT

parameters. The QCT results are identical to the converged QCT curve [21] to within statistical uncertainty. Whereas our QCT reaction threshhold is achieved at $E_{sys}$ = 0.51 eV, the effective quantum reaction threshhold appears at ~ 0.41 eV due to quantum mechanical tunneling. At 0.50 eV, P(QM,P) = 0.5. The GWP results do not allow for tunneling because the center of each packet follows classical mechanics. But by examining the GWP points at 0.51 and 0.515 eV, the effects of constructive phase interference, (increased probability with respect to the QCT probability), is observed. As $E_{sys}$ increases, the GWP points oscillate about the QCT points where some of the GWP probabilities are actually less than QCT probabilities due to destructive interference effects in $|\psi_{out}>$. The uncertainty in P(QCT,P), due to the initial sampling of the total phase space, is the cause of the non-monotonic behavior of P(QCT,P) between 0.55 and 0.58 eV. Correlating P(GWP,P) with P(QCT,P) point by point over this $E_{sys}$ range, the value of P(GWP,P) is strongly influenced by the value of P(QCT,P) resulting in a non-monotonic function for P(GWP,P). The results for doubling the number of translational GWPs from 14 to 28 are also presented. Many of the $N_x$ = 28 probabilities are superimposed under the $N_x$= 14 points. From the general trend observed in Fig. 3, we can state that doubling the number of translational GWPs has little effect.

# CONCLUSIONS AND SUMMARY

We have presented a scheme to treat the atom-diatom collinear exchange reaction problem using the semiclassical propagation of Gaussian wavepackets. Two extensions to the present technology of Gaussian wavepackets dynamics were needed to adequately describe the scattering wavefunction which bifurcates into both the reactant's and product's channel. First, the interaction picture representation in each channel of the scattering wavefunction was explicitly evaluated by integrating the GWP equations of motion forwards in time using the full interaction Hamiltonian followed by a subsequent integration backwards in time using a channel Hamiltonian. Secondly, to provide more flexibility in the GWP basis, the initial translational wavefunction was linear least squares fit to a plane wave using GWPs, thus providing an expansion in both the translational and vibrational degree of freedom. The use of the interaction picture propagation of the scattering wavefunction expanded in both degrees of freedom provided a scheme which was independent of the choice of both the stopping time for the GWP equations of motion in the asymptotic region of the interaction potential and independent of the representation of the initial wavefunction. This approach was given the acronym IPGWD-M.

We applied the IPGWD-M procedure to the H-$H_2$ collinear exchange reaction using the Porter-Karplus II PES. Satisfactory results for the reaction probabilities, in comparison to the quantum results, were obtained for total system energies between the "practical" classical reaction threshold of 0.51 eV, and 0.58 eV.

The only previous treatment of the collinear exchange reaction using GWD was by Skodje [23] in which application of standard GWD to the F + $H_2$ system yielded a final scattering wavefunction which was not normed. The S matrix transition elements summed to less than 0.1. We believe the failure of this study, as well as the failure of our attempts to treat the H + $H_2$ system with standard GWD, was due mainly to two reasons. First, only a forward propagation in time was used thus creating an uncertainty in $|\psi_{out}>$. Second, and more importantly, the use of a single GWP representation for X(x) in a rearrangement type problem biased $|\psi_{out}>$ due to the non-invariance of the initial wavefunction coefficients with respect to a choice of $x_0$. The IPGWD-M procedure eliminates these two inaccuracies and provides a significant improvement in the application of the GWD formalism to the collinear reactive scattering problem.

A procedure similar in spirit to GWD was applied to the H + $H_2$ problem recently [24] using a method which semiclassically propagated the Wigner distribution function in phase space. This study focused on the tunneling region of the $E_{sys}$ scale. The shape of the product's channel reaction probability for the case in which they retained only the classical trajectories which conserve momentum upon interaction is very similar to the P(GWP,P) curve of Fig. 3. The quantum mechanical evaluation of the Wigner distribution function yielded increased tunneling which actually overestimated the exact quantum results. Another treatment similar to the GWD is the dynamical characteristic function (DCF) method [25]. This approach constructs a DCF by matching a trajectory governed by the full Hamiltonian with an outgoing trajectory governed by a channel Hamiltonian.

In this manner, the DCF method is similar to IPGWD. Numerical application of the DCF method to the reactive collinear exchange problem has not been reported.

## ACKNOWLEDGEMENT

This work was partially supported by NSF before October 1, 1986. It is a pleasure to acknowledge stimulating discussions with Professors E. Heller and D. Truhlar about various aspects of this work.

# APPENDIX

The transformation matrix parameters are defined in terms of the masses of the atoms, $m_A$, $m_B$, and $m_C$ and the total mass of the system $M = (m_A + m_B + m_C)$. They are

$$\gamma_{AB} = m_A / (m_A + m_B) \tag{A1}$$

$$\gamma_{BC} = m_C / (m_B + m_C) \tag{A2}$$

$$\gamma = m_B M / [(m_A + m_B)(m_B + m_C)] \quad . \tag{A3}$$

The reduced masses required in the Hamiltonians are also defined in terms of the atomic masses and the total system mass. They are

$$\mu_R = 1 \tag{A4}$$

$$\mu_P = m_C (m_A + m_B) / [m_A (m_B + m_C)] \tag{A5}$$

$$M_R = m_C (m_A + m_B)^2 / (M m_A m_B) \tag{A6}$$

$$M_P = (m_A + m_B)(m_B + m_C) / (m_B M) \quad . \tag{A7}$$

# REFERENCES


1. a) E. J. Heller, J. Chem. Phys. 62, 1544 (1975); b) R. D. Coalson and M. Karplus, Chem. Phys. Lett. 90, 301 (1982); c) R. T. Skodje and D. G. Truhlar, J. Chem. Phys. 80, 3123 (1984).
2. a) G. Drolshagen and E. J. Heller, J. Chem. Phys. 79, 2072 (1983); b) B. Jackson and H. Metiu, J. Chem. Phys. 82, 5707 (1985); c) B. Jackson and H. Metiu, J. Chem. Phys. 85, 4129 (1986); d) For a general review see R. B. Gerber, R. Kosloff and M. Berman, Comp. Phys. Reports 5, 61 (1986).
3. S.-Y. Lee and E. J. Heller, J. Chem. Phys. 76, 3035 (1982).
4. a) E. J. Heller, J. Chem. Phys. 64, 63 (1976); b) S. Mukamel, J. Phys. Chem. 88, 3185 (1984); J. Grad., Y.-J. Yan, A. Haque, and S. Mukamel, J. Chem. Phys. 86, 3441 (1987); c) S.-I. Sawada, R. Heather, B. Jackson and H. Metiu, J. Chem. Phys. 83, 3009 (1985); d) J. T. Muckerman, S. Kanfer, R. D. Gilbert, and G. D. Billing, Brookhaven National Laboratory, Brookhaven, New York, preprint.
5. A. D. McLachlan, Mol. Phys. 8, 39 (1964).
6. a) E. A. McCullough and R. E. Wyatt, J. Chem. Phys. 51, 1253 (1969), 54, 3578 (1971); b) A. Askar and A. S. Cakmak, J. Chem. Phys 68, 2794 (1978).
7. R. Kosloff and D. Kosloff, J. Chem. Phys. 79, 1823 (1983); D. Kosloff and R. Kosloff, J. Comput. Phys. 52, 35 (1983).
8. Z. H. Zhang and D. J. Kouri, Phys. Rev. A 34, 2687 (1986).
9. a) H. Tal-Ezer and R. Kosloff, J. Chem. Phys. 81, 3967 (1984); b) R. C. Mowrey and D. J. Kouri, J. Chem. Phys. 84, 6466 (1986).

10. A. P. Clark and A. S. Dickinson, Phys. B: Atom. Molec. Phys. 6, 164 (1973).

11. J. R. Taylor, "Scattering Theory: The Quantum Theory of Nonrelativistic Scattering", R. E. Krieger, Malabar, Florida, 1983, see Chapter 16.

12. R. D. Levine, "Quantum Mechanics of Molecular Rate Processes", Oxford, London, 1969, see Chapter 2.

13. M. J. Davis and E. J. Heller, J. Chem. Phys. 71, 3383 (1979).

14. A. Ralston, in "Mathematical Methods for Digital Computers", edited by A. Ralston and H. S. Wilf, Wiley, New York, 1960, pg. 100.

15. E. J. Heller, J. Chem. Phys. 75, 2923 (1981).

16. E. J. Heller, J. Chem. Phys. 65, 4979 (1976).

17. W. H. Miller, Adv. Chem. Phys. 25, 69 (1974).

18. W. C. DeMarcus, Am. J. Phys. 46, 733 (1978).

19. R. N. Porter and L. M. Raff, in "Dynamics of Molecular Collisions: Part B", edited by W. H. Miller, Plenum, New York, 1976.

20. R. N. Porter and M. Karplus, J. Chem. Phys. 40, 1105 (1964).

21. D. J. Diestler and M. Karplus, J. Chem. Phys. 55, 5832 (1971).

22. B. R. Johnson, Chem. Phys. Lett. 13, 172 (1972); D. K. Bondi, D. C. Clary, J. N. L. Connor, B. C. Garrett, and D. G. Truhlar, J. Chem. Phys. 76, 4986 (1982).

23. R. T. Skodje, thesis, "Topics in the Theory of Chemical Reactions", U. of Minnesota, Minneapolis, 1984, Chapter 7.

24. H.-W. Lee and T. F. George, J. Chem. Phys. 84, 6247 (1986).

25. K. Takasuka and H. Nakamura, J. Chem. Phys. 83, 3491 (1985).

# PAPER II.

## CORRECTED EFFECTIVE MEDIUM METHOD.
## I. ONE-BODY FORMULATION WITH APPLICATIONS TO
## ATOMIC CHEMISORPTION AND DIATOMIC MOLECULAR POTENTIALS

# CORRECTED EFFECTIVE MEDIUM METHOD. I. ONE-BODY FORMULATION WITH APPLICATIONS TO ATOMIC CHEMISORPTION AND DIATOMIC MOLECULAR POTENTIALS

Joel D. Kress and Andrew E. DePristo

Department of Chemistry
Iowa State University
Ames, IA 50011

# ABSTRACT

We have derived a corrected effective medium (CEM) theory which describes the binding between an atom and an inhomogeneous host. As in all EM theories, the zeroth order term of the interaction energy is provided by the embedding energy of the atom into a spin-unpolarized homogeneous electron gas, and is obtained from self-consistent calculations within the local density approximation. Higher order terms provide corrections of two sorts: 1) the Coulomb interaction is accounted for by an explicit evaluation of the electrostatic interaction between the atom charge density and the host charge density; and 2) the difference in kinetic, exchange and correlation energies between the atom/inhomogeneous system and the atom/homogeneous system is provided by a spin-polarized density functional evaluation. Both the Coulomb and difference energies are calculated non-self-consistently within the superposition of atomic densities approximation. A sampling procedure to obtain the homogeneous electron density from the inhomogeneous host density is derived by minimization of the contributions from the non-self-consistent difference term.

Applications of the CEM theory are made to three types of systems that reflect a measure of difference in the spin polarization and inhomogeneity of both the atom and host spin density. We first describe the interaction of an H atom embedded into a spin-polarized homogeneous electron gas. Next, we calculate the binding potentials for a set of diatomic hydrides. Finally, we predict the interaction potentials for the chemisorption of H atoms on three transition metal surfaces, Ni(100), Cu(100), and Fe(110).

# INTRODUCTION

The prediction of spectroscopic and dynamical properties of a many-body atomic system requires an accurate estimate of the adiabatic potential energy surface (PES) governing the interaction among the various bodies. When each atom contains many electrons and the system has low symmetry, such predictions are rather difficult since treatment of all the electrons in either the Hartree-Fock (HF) [1] or the Kohn-Sham local density (LD) [2] approaches becomes complicated in terms of computational requirements and convergence criteria. A promising alternative approach is embodied in an effective medium (EM) [3] or quasi-atom [4] scheme whereby the electronic interaction of an atom within the many-body system is modeled by that between the same atom and a homogeneous electron gas.

Based upon density functional theory [5], the EM theory to zeroth order replaces the (low symmetry) self-consistent solution of an atom interacting with a many-body electron density with the (high symmetry) self-consistent Kohn-Sham LD solution of an atom interacting with an extended system of constant electron density and constant positive background charge [6]. This zeroth order interaction is not adequate to describe accurately the interaction of an atom with an inhomogeneous system of electrons. Corrections have been developed by Norskov and Lang [3] by considering the first-order perturbation contribution with the ion cores of the inhomogeneous electronic system included as weak pseudopotentials. Computation of these corrections requires very little effort compared to a fully self-consistent solution.

The EM theory has been applied to chemisorption of H, O, and C on transition metal surfaces [7]. For H atom chemisorption accurate results were obtained but for O the results were at best qualitative. Recently [8], cohesive energies for free electron bulk metals, such as Al, have also been predicted with good accuracy. To our knowledge, no attempts at describing extremely inhomogeneous systems like diatomic and polyatomic molecules have been published.

In this article, we present the initial development of a corrected effective medium (CEM) theory to predict potentials for a diverse set of chemically interesting systems ranging in size from diatomic molecules to bulk metals, and including the interaction of a small system with a large system (e.g., atomic chemisorption on a metal surface). The corrections to the zeroth order term of the EM theory are provided by using a spin-polarized analog of the Gordon-Kim electron gas [9] approximation. Within the electron gas approximation, the energy of a system is evaluated using spin density functionals (local and non-local) where the spin density of the many-body, many-electron system is provided by a superposition of atomic spin densities.

A fundamental driving force behind the development of the CEM theory was the need to describe molecular chemisorption of diatomics and polyatomics on metal surfaces. To provide an adequate PES for such systems one must be able to describe each asymptote of each distinct chemical arrangement. For example, diatomic molecular dissociative chemisorption contains three arrangements of importance: 1) the isolated diatomic molecule; 2) the intermediate arrangement of the molecule interacting with

the metal surface; and 3) the atomic chemisorption of the two dissociated atoms. If we consider polyatomic molecular chemisorption, even more asymptotic fragments are possible and each fragment must be described accurately. Note also that the second type of arrangement is most difficult to calculate with present self-consistent methods and is also of critical importance in the dynamics of dissociative chemisorption.

In this paper we apply the CEM theory to two asymptotic arrangements of the diatomic molecular chemisorption potential, that of diatomic binding and atomic chemisorption. The molecular-surface interaction will be addressed in a future publication [10].

# THEORY

We seek the energy difference between an interacting N-body system and the infinitely separated N bodies. Let $\{i\}$, $i = 1, \ldots, N$ denote the set of N bodies where one of the bodies may be more complex than an atom (e.g., a homogeneous electron gas or a polyatomic molecule). Thus, this treatment is not limited to interacting atoms.

The interaction energy is defined as

$$\Delta E_N = E[\sum_i^N] - \sum_i^N E[i] , \tag{1}$$

where $E[\sum_i^N]$ is the total energy of all N interacting bodies and $E[i]$ is the total energy of the $i^{th}$ body when isolated from the other N-1 bodies. For the applications in this paper we will only consider two-body systems N = 2, with N > 3 body systems deferred to a future publication [11] (which is included as Paper III in this dissertation). The two-body interaction energy reduces to a form analogous to the binding energy expression of an AB diatomic molecule

$$\Delta E_{AB} = E[AB] - E[A] - E[B] \tag{2}$$

with the difference that A is restricted to be an atom while B can represent an atom, a cluster, an electron gas, etc.

The EM approach to chemical binding replaces the interaction between atom A and the body B by that of A embedded into a homogeneous electron gas with compensating positive background (i.e., jellium), and provides a prescription for choosing the electron density of the homogeneous electron gas from the inhomogeneous electron density of the host. Puska et al. [6] have calculated the embedding energies for most atoms through Cu as a function of the electron density of the homogeneous electron gas $n_H$ using the self-consistent Kohn-Sham [2] method with the local Gunnarsson-Lundqvist interpolation of the exchange-correlation energy [12]. These embedding energies $\Delta E_A(n_H)$ are plotted in Fig. 1 for the embedded atoms F, O, and H.

To derive the CEM interaction expression, we write the embedding energy in the form of Eq. (2),

$$\Delta E_A(n_H) = E[A + H] - E[A] - E[H] , \tag{3}$$

where H denotes the homogeneous electron gas of electron density $n_H$. The next step is to eliminate the atom energy between Eqs. (2) and (3) which yields

$$\Delta E_{AB} = \Delta E_A(n_H) + \{[E[AB] - E[B]) - (E[A + H] - E[H])\} . \tag{4}$$

The term in braces provides a correction to the effective medium contribution, thus the name corrected effective medium (CEM) theory. The extent of this term will become apparent when we discuss applications to

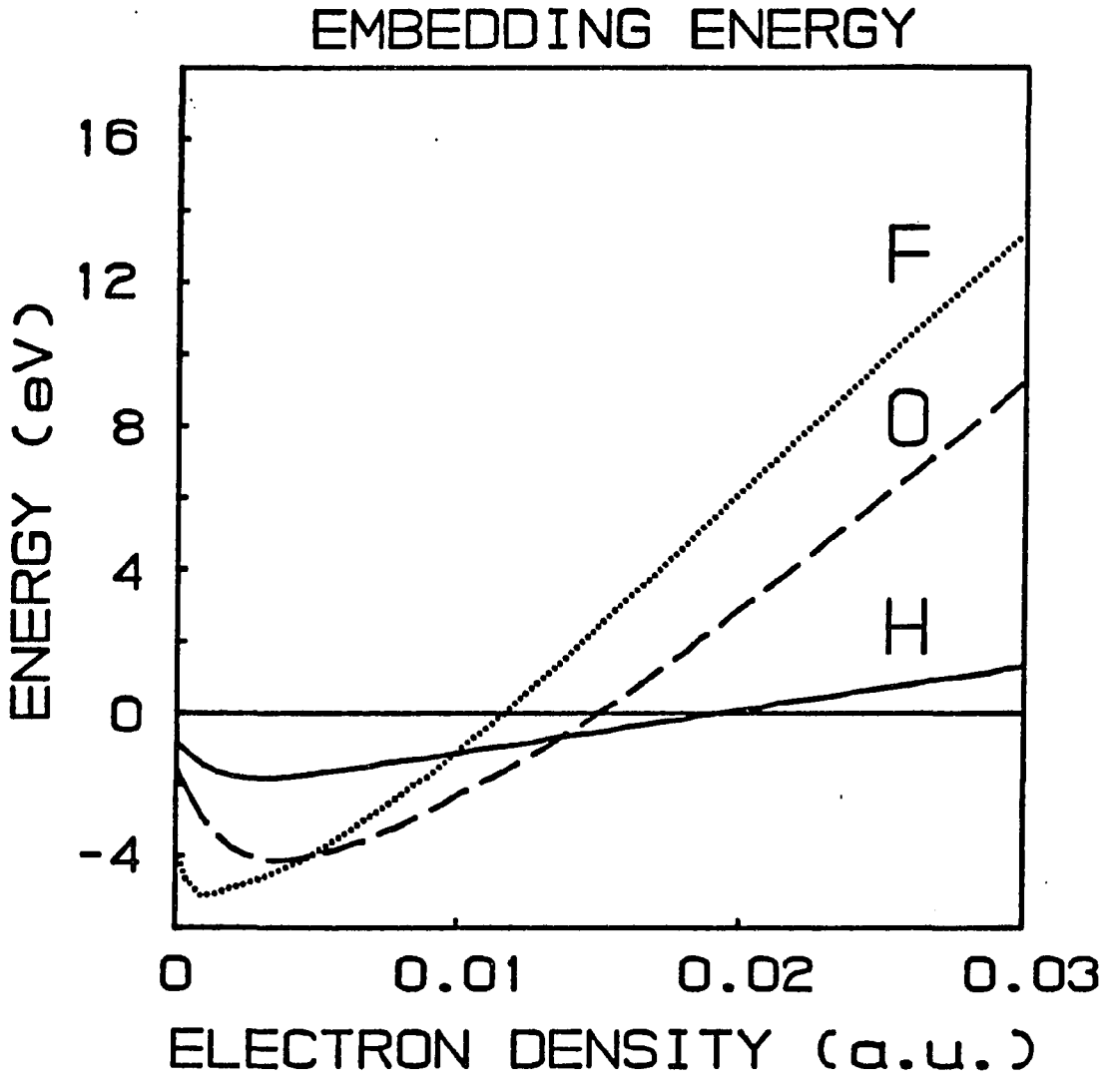


Figure 1. Embedding energies from SCF-LD calculations [6] for an atom in a homogeneous electron gas as a function of the electron density. Hydrogen, fluorine, and oxygen are shown

realistic systems (diatomic molecules and atomic chemisorption). We do note though by choosing only one atom, A, from the whole N-body system as our embedding atom we are using a one-body embedding scheme. Formally, the one-body embedding scheme means that only one $\Delta E_A(n_H)$ term appears in Eq. (4), and is referred to as CEM-1. We have derived the interaction expression analogous to Eq. (4) for a N-body embedding scheme and this is the topic of Paper III.

To implement Eq. (4), which is formally exact, we must evaluate the total energies (E[ ]). Hartree-Fock self-consistent field (SCF) methods, (with the various extensions of CI, MCSCF, perturbation theory) [13], and Kohn-Sham LD methods would not be of any utility here due to computational requirements. Instead, we employ the spin-polarized density functional formalism [14] in which the energy of a many-electron system is expressed as a functional of the one-electron spin density. For example, the total energy of the $i^{th}$ term in Eq. (1) is written as

$$E[i] = E[n\uparrow_i, n\downarrow_i] \ , \tag{5}$$

where $E[n\uparrow_i, n\downarrow_i]$ is a unique functional of the spin up and spin down electron density of the $i^{th}$ body. These are functions of position $\vec{r}$, $n\uparrow_i = n\uparrow_i(\vec{r})$ and $n\downarrow_i = n\downarrow_i(\vec{r})$. This unique (exact) functional has been proven to exist for ground states [14,15] but has not yet been found. However, various approximations to this exact functional exist with which to evaluate the total energy expressions required in the CEM theory. The details of these functionals are presented in the next section.

The practical utility of the CEM-1 theory for interacting many-body systems will depend upon the solution of three problems. First, the density functional must be specified to evaluate the total energies in the correction terms. Second, a procedure to determine the effective medium electron density must be defined. Third, the electron densities for both A and B must be provided. These densities are needed as input into the density functionals and effective medium sampling procedure.

## ASSUMPTIONS

In this section, we introduce the specific approximations used in application of the CEM-1 theory to a variety of "real systems". Atomic units are used unless otherwise specified.

### Density Functional

We write the density functional in the equivalent form $E[n,\phi]$, where the total electron density is

$$n = n\uparrow(\vec{r}) + n\downarrow(\vec{r}) \tag{6a}$$

and the spin polarization is

$$\phi = \frac{(n\uparrow(\vec{r}) - n\downarrow(\vec{r}))}{n} . \tag{6b}$$

The total density functional is broken up into two terms

$$E[n,\phi] = G[n,\phi] + V^{C}[n] , \tag{7}$$

where $V^{C}[n]$ is the Coulomb energy. The first term is composed of three parts

$$G[n,\phi] = T[n,\phi] + E_{x}[n,\phi] + E_{c}[n,\phi] , \tag{8}$$

where T, $E_X$ and $E_C$ are the kinetic, exchange and correlation energy functionals.

$T[n,\phi]$ is expanded in terms of the density gradient [16]

$$T[n,\phi] = T_0[n,\phi] + T_2[n,\phi] + \ldots \tag{9}$$

and truncated at second order in the present work. The zeroth order term is the Thomas-Fermi (LD) kinetic energy

$$T_0[n,\phi] = \frac{3}{10}(6\pi^2)^{2/3} \int d\vec{r}(n\uparrow^{5/3} + n\downarrow^{5/3}) \tag{10}$$

and is a functional of $n\uparrow$ and $n\downarrow$ only. The second order term is

$$T_2[n,\phi] = \frac{1}{72} \int d\vec{r} \left\{\frac{|\vec{\nabla}n\uparrow|^2}{n\uparrow} + \frac{|\vec{\nabla}n\downarrow|^2}{n\downarrow}\right\} \tag{11}$$

and is a functional of spin densities and gradients. Higher order terms to the series, $T_4$, $T_6$, etc., are known and methods to approximate the full series have been developed [17] using Padé approximants, but they are not utilized here.

For $E_X[n,\phi]$, we use the Dirac (LD) form [18],

$$E_X[n,\phi] = -\frac{3}{4}\left(\frac{6}{\pi}\right)^{1/3} \int d\vec{r}\ (n\uparrow^{4/3} + n\downarrow^{4/3}) \ . \tag{12}$$

Although a Padé approximant for $E_X$ exists [19], use of any <u>non-local</u> form

of $E_x$ would be inconsistent. It would not allow for the elimination of the energy of atom A between Eqs. (2) and (3) since the local Dirac form was used for the self-consistent solutions to Eq. (3) by Puska et al. Use of the non-local kinetic energy, $T_2$, in Eq. (4) is consistent since the kinetic energy contribution to the homogeneous embedding energies is provided exactly (thus non-locally) within the Kohn-Sham approach. For the correlation energy, we use the LD form

$$E_c[n,\phi] = \int d\vec{r}\; n\; \varepsilon_c(n,\phi)\;, \tag{13}$$

where $\varepsilon_c(n,\phi)$ is the local correlation energy density for a noninteracting electron gas. We use the Gunnarsson-Lundqvist [12] interpolation of $\varepsilon_c(n,\phi)$, in accord with the Puska et al. calculations, although other local [20a] and non-local [20b] forms exist.

The Coulomb energy is expressed as

$$V^C[n] = \frac{1}{2} \int\!\!\int' d\vec{r}_1\, d\vec{r}_2\, \frac{[n(\vec{r}_1) - \rho(\vec{r}_1)][n(\vec{r}_2) - \rho(\vec{r}_2)]}{|\vec{r}_1 - \vec{r}_2|}\;, \tag{14}$$

where $\rho(\vec{r})$ is the positive charge density distribution. For an atom with atomic number Z,

$$\rho(\vec{r}) = Z\, \delta(\vec{0})\;, \tag{15}$$

while for jellium, $\rho(\vec{r}) = n_H$. The prime on the integral denotes that the

nuclear-nuclear self-interactions are omitted.

## Effective Medium Embedding Schemes

Since applications of the CEM-1 theory in this paper are limited to two-body systems, we describe the embedding schemes in terms of the fictitious heteronuclear diatomic molecule AB. The schemes needed to describe the other two body systems considered in this paper, namely the atom/spin-polarized homogeneous gas and the atom/metal surface, are essentially the same. Applications of the CEM theory to 3-body systems (i.e., diatomic chemisorption) and the complications which arise when considering the embedding schemes and homogeneous electron gas density sampling procedures are covered in Paper III.

First, consider the case when neither A nor B are embedded into an effective medium, a zero-body embedding scheme. Eq. (4) becomes

$$\Delta E_{AB} = E[AB] - E[A] - E[B] \; . \tag{16}$$

The zero-body embedding scheme corresponds to a spin polarized variant of the Gordon-Kim [7] electron gas approximation if additive atomic electron densities are used to represent the AB molecular electron density. Gordon and coworkers have made numerous calculations [7,21] on many different systems using this model. We will not attempt to describe their findings here except to note that such a theory is not capable of describing covalent binding.

Another choice is to embed atom A into the host atom B. We call this scheme (A→B). The interaction energy becomes

$$\Delta E_{AB} = \Delta E_A(n_H) + (E[AB] - E[B]) - (E[A + H] - E[H]) \ . \qquad (17)$$

(Eq. (17) is identical to Eq. (4) and is provided for clarity.) The effective medium contribution is that of embedding atom A into the homogeneous electron gas H of electron density $n_H$. The correction terms provide the interaction energy difference between the AB diatomic molecule and the (A + H) "diatomic molecule" using the density functionals discussed in the last section. To determine the homogeneous electron gas density $n_H$ we sample the host total electron density $n_B(\vec{r})$ with an effective medium sampling functional $F(n_A(\vec{r}), \rho_A(\vec{r}))$. This yields

$$n_H = \int d\vec{r}\ F(n_A(\vec{r}), \rho_A(\vec{r}))\ n_B(\vec{r}) \ , \qquad (18)$$

where F is a normalized functional of the embedded atom density $n_A(\vec{r})$ and positive charge density $\rho_A(\vec{r})$. The specific form of the F functional is discussed in the next section. For now, F serves as a device to yield a constant (coordinate independent) effective medium electron density from the inhomogeneous electron density distribution of atom B.

By symmetry we can embed atom B into atom A, which is denoted (B → A). The interaction energy is determined by interchanging A and B in Eq. (17) to yield

$$\Delta E_{AB} = \Delta E_B(n_H) + (E[AB] - E[A]) - (E[B + H] - E[H]) \ . \qquad (19)$$

No confusion should arise in using H and $n_H$ to denote the homogeneous

electron gas system and density again.

The choice of whether to embed atom A into atom B (A → B) or atom B into atom A (B → A) for a given diatomic molecule AB is addressed when we consider the binding potentials of heteronuclear diatomic molecules later. Obviously, the two embedding schemes are identical for a homonuclear diatomic molecule since A = B.

## Effective Medium Sampling Procedures

The concept of the effective medium sampling functional was introduced in the last section. Here we discuss the specific sampling functionals that we and others have tried. For this discussion we embed atom A into the host atom B (A → B). The procedures are equally applicable to embedding atom B into atom A (B → A) by interchanging A and B in the resulting expressions.

In the original form of the quasiatom theory of Stott and Zaremba [4], the embedded atom was envisioned as an impurity in the host yielding the effective medium electron density as the value of the host electron density at the position of the impurity (embedded) atom. This is a <u>pointwise</u> sampling procedure since it results from the <u>pointwise</u> sampling functional

$$F = \delta(\vec{r} - \vec{r}_A) \ , \tag{20}$$

which in combination with Eq. (18) yields

$$n_H = n_B(\vec{r}_A) \ . \tag{21}$$

The pointwise effective medium electron density is the electron density of the host at the nucleus of the embedding atom $\vec{r}_A$.

In the EM theory of Norskov and Lang [3], corrections to the EM term were derived for atomic chemisorption based on a pseudopotential treatment of the metal atoms as a perturbation to the homogeneous electron gas. By averaging the host electron density over the electrostatic potential of the embedded atom a partial cancellation of the perturbation energy arising from the pseudopotential correction resulted. This is an electrostatic sampling procedure since it results from the electrostatic sampling functional

$$F = \chi_A(\vec{r}) / \int d\vec{r}\ \chi_A(\vec{r}) \ , \tag{22}$$

where

$$\chi_A(\vec{r}) = \int d\vec{r}' \ \frac{[n_A(\vec{r}') - \rho_A(\vec{r}')]}{|\vec{r} - \vec{r}'|} \ , \tag{23}$$

which in combination with Eq. (18) yields

$$n_H = \frac{\int d\vec{r}\ \chi_A(\vec{r})\ n_B(\vec{r})}{\int d\vec{r}\ \chi_A(\vec{r})} \ . \tag{24}$$

One disadvantage to this scheme is that the electrostatic potential does not always provide a positive definite sampling function. For

non-spherical $n_A(\vec{r})$, Eq. (24) can result in a negative value for $n_H$, which is not meaningful.

Since we do not base our CEM formalism on pseudopotentials and perturbation theory, there is no basis to use the electrostatic sampling procedure. The requirement of a positive definite sampling function provides further motivation for a new sampling procedure. Instead of averaging over the electrostatic potential of the embedded atom, we average the host electron density over the electron density of the embedded atom. Since the electron density is a positive definite function, the resulting sampled electron density will be positive. The <u>averaged</u> sampling functional is

$$F = n_A(\vec{r}) \; / \; \int d\vec{r} \; n_A(\vec{r}) \; , \tag{25}$$

which yields

$$n_H = \frac{1}{Z_A} \int d\vec{r} \; n_A(\vec{r}) \; n_B(\vec{r}) \; . \tag{26}$$

The physical basis for this <u>averaged</u> sampling is tied to the "size" of an atom. Since the "size" of atom A can be measured in terms of an average value of r over $n_A(\vec{r})$, the averaged sampling procedure averages the host electron density over the "size" of the embedded atom. In addition, it is interesting to note that the use of overlapping wavefunctions (or electron densities) between the two atoms is a natural measure of bonding in a

simplistic view. The readers wishing for a more rigorous derivation will find one based upon a minimization procedure in the next section.

## Electron Densities and Other Approximations

The last assumption involves the construction of the explicit spin densities which are needed as input into the density functionals and effective medium sampling procedures. Since the CEM-1 interaction expression is not solved self-consistently with respect to the spin densities, a good approximation is needed. We used the Hartree-Fock atomic spin densities [22] whenever atomic densities were required.

To construct many-body spin densities, we used a superposition of atomic spin densities [9]. For example, the spin up density for the AB diatomic is represented as

$$n_{AB\uparrow}(\vec{r}) = n_{A\uparrow}(\vec{r}) + n_{B\uparrow}(\vec{r}) \ , \tag{27}$$

where the atomic densities are centered about the position of the nuclei, $\vec{r}_A$ and $\vec{r}_B$, respectively. For the total electron density of the system consisting of an atom and a homogeneous electron gas, the superposition approximation yields

$$n(\vec{r}) = n_A(\vec{r}) + n_H \ . \tag{28}$$

The analogous result for the N-body system is

$$n(\vec{r}) = \sum_{i}^{N} n_i(\vec{r}) \ , \tag{29}$$

where $n_i(\vec{r})$ is the total electron density of the $i^{th}$ atom with nucleus located at $\vec{r}_i$.

The superposition approximation is zeroth order since it does not allow the electron densities of the AB system to redistribute as the bodies begin to interact. To improve on the superposition approximation the actual many-body electron densities from approximate MO calculations could be used. Alternatively, to allow redistribution for the spin density of the system, we might minimize the CEM-1 total interaction energy expression self-consistently with respect to a variation in the spin densities. If a solution of this accuracy is desired, then the direct minimization of the original energy expression [Eq. (2)] would be easier to implement. Two arguments can be made against such a procedure. First, such a first principles method is much more time consuming than the CEM-1 theory. Second, the CEM-1 theory does include electron redistribution in the AH system via the self-consistently determined embedding energy functions. Only the corrections are evaluated non-self-consistently.

The use of the superposition approximation simplifies the evaluation of the CEM-1 correction energies. With the help of Eq. (7) we obtain

$$\Delta E_{AB} = \Delta E_A^h + \Delta G_{AB} + \Delta V_{AB}^C \ , \tag{30}$$

where

$$\Delta V^{C}_{AB} = \iint d\vec{r}\, d\vec{r}' \, \frac{[n_A(\vec{r}) - \rho_A(\vec{r})][n_B(\vec{r}') - \rho_B(\vec{r}')]}{|\vec{r} - \vec{r}'|} \, . \tag{31}$$

The notation $\Delta E^{h}_{A}$ is used to represent $\Delta E_A(n_H)$. The Coulomb interaction between the total charge distributions on atom A and host B, $\Delta V^{C}_{AB}$, is <u>independent</u> of $n_H$ for two reasons: 1) the positive background and electron densities of the homogeneous gas are coincident; and 2) the intra-atomic coulomb energies are subtracted out. Thus, $\Delta V^{C}_{AB}$ is independent of embedding scheme.

Within the superposition approximation, a mathematical derivation of the averaged sampling procedure is obtained by considering the simplified $\Delta E_{AB}$. Since $\Delta E^{h}_{A}$ is the self-consistently determined homogeneous embedding energy function and $\Delta V^{C}_{AB}$ is independent of the homogeneous electron gas density, $\Delta G_{AB}$ provides the least accurate contribution to the total interaction $\Delta E_{AB}$ which depends upon $n_H$. To minimize this term we find the zero of $\Delta G_{AB}$ with respect to $n_H$, and use this value as our optimal effective medium electron density. Setting $\Delta G_{AB}$ equal to zero within the (A → B) embedding scheme yields

$$(G[A + H] - G[H]) = (G[AB] - G[B]) \, . \tag{32}$$

Note that this equation properly equates kinetic, exchange and correlation energies of both systems.

An analytic solution to Eq. (32) in terms of $n_H$ is not possible due to the non-linear behavior of the density functionals which make up G[n]. An approximate solution can be found by considering the dominant terms of the local kinetic and exchange energies, which are approximated very well by the quadratic density functional

$$G[n] = \int d\vec{r} \{C_2[n(\vec{r})]^2 + C_1[n(\vec{r})]\} , \qquad (33)$$

as shown in Fig. 2. The constants are $C_2 = 3.48864$ and $C_1 = -0.06080$ in atomic units. Inserting Eq. (33) into Eq. (32), performing some algebra, and solving for $n_H$ gives the <u>averaged</u> sampling procedure result for $n_H$. Note that this minimizes the approximate correction energy $\Delta G_{AB}$ in the same spirit that the electrostatic sampling procedure minimizes the pseudopotential contribution to the EM interaction expression [3]. When the full density functionals are used in Eq. (30), $\Delta G_{AB}$ is non-zero due to the correlation energy, non-local kinetic energy contribution, and the deviation of the local exchange-correlation energy from the approximate quadratic fit. As we show later in the paper, $\Delta G_{AB}$ is small compared to $\Delta \mathring{E}_A^h$ and $\Delta V_{AB}^C$ but still plays a crucial role in determining the position of the minimum in $\Delta E_{AB}$ for binding in diatomic molecules and atomic

Figure 2. The exact and quadratic fit to the sum of the local kinetic and exchange energy densities

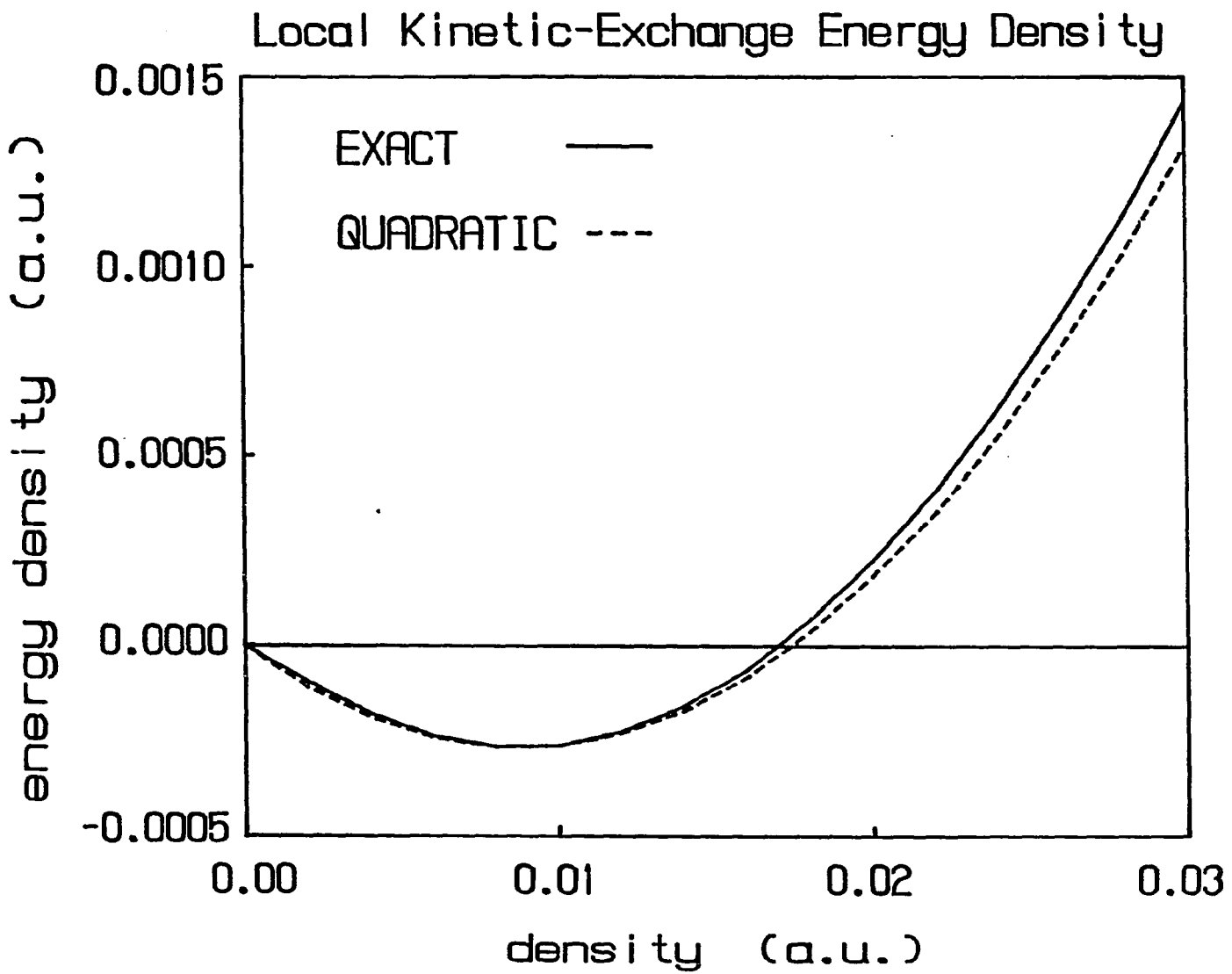
Local Kinetic-Exchange Energy Density
EXACT
QUADRATIC
0.0015
0.0010
0.0005
0.0000
-0.0005
energy density (a.u.)
0.00
0.01
0.02
0.03
density (a.u.)

chemisorption systems. It is clear that a correction to the homogeneous electron gas embedding energy is needed whether it be from pseudopotential perturbation theory or from spin density functional theory.

Even within the superposition approximation there is still some remaining flexibility in the specification of the Hartree-Fock atomic spin densities. Formally, the total electron density for a given atom is expressed as

$$n(\vec{r}) = \sum_{(n,\ell,m)} \sum_{m_s} N(n,\ell,m,m_s) \left| \psi_{n,\ell,m}(\vec{r}) \right|^2 , \qquad (34)$$

where $\psi_{n,\ell,m}(\vec{r})$ is the atomic basis orbital of quantum numbers n, $\ell$, and m and $m_s$. $N(n,\ell,m,m_s)$ is the occupation number of the $(n,\ell,m,m_s)$ spin orbital. The choice of the set of occupation numbers $\{N(n,\ell,m,m_s)\}$ for the occupied orbitals is somewhat arbitrary. The natural choice is the set corresponding to the ground state of the Hartree-Fock atom. For example, a Li atom would have an electronic configuration of $(1s^2,2s^1)$ corresponding to the choice of non-zero occupation numbers $\{N(100,1/2) = N(100,-1/2) = N(200,1/2) = 1\}$. Another possible representation of the total electron density is the set $\{N(100,1/2) = N(100,-1/2) = 1, N(200,1/2) = N(200,-1/2) = 1/2\}$. Here, there is a total of 3 electrons but now the electron density is spin-unpolarized. Yet another representation of the Li atom is $\{N(100,1/2) = N(100,-1/2) = N(210,1/2) = 1\}$. This corresponds to a unrelaxed 2p excited state of the Li atom. Although it is unlikely the excited state configuration would better model Li embedded in the homogeneous gas system or Li interacting with another atom, the excited

state configuration for transition metal atoms may play a more subtle role in binding. The point is that the electron density contribution from an atom participating in a bond in the CEM-1 theory may not necessarily be the Hartree-Fock ground state atomic spin electron density.

A minor approximation was made to alter the behavior of the homogeneous embedding energy functions at low electron density. Stott and Zaremba [4] showed that

$$\lim_{n_H \to 0} \Delta E_A (n_H) = -(E.A.)_A , \tag{35}$$

where $(E.A.)_A$ is the electron affinity of atom A. In this limit, the atom attracts electron density from the sparse homogeneous electron gas which is only weakly attracted to the sparse positive background. It is this attraction which results in the minima in the embedding energy curves for atoms not in group VIII. (c.f. Fig. 1.) Since the right hand side of Eq. (35) is not zero, the CEM-1 results will not dissociate correctly. To see this more clearly, let us look at the (A → B) embedding scheme for a diatomic molecule in the limit that the separation between the two atoms becomes infinite, $r_{AB} \to \infty$. All of the sampling procedures yield $n_H = 0$ since the two bodies are isolated. The interaction expression in Eq. (20) then yields

$$\lim_{r_{AB} \to \infty} \Delta E_{AB} = \lim_{n_H \to 0} \Delta E_A(n_H) . \tag{36}$$

Since infinite separation of the two bodies A and B is defined as the zero of energy, Eq. (36) should approach zero, which contradicts Eq. (35). A simple remedy for this discrepancy was to set $\Delta E_A(n_H = 0) = 0$ when generating the homogeneous embedding energy functions using a cubic spline interpolation from points determined from the original figures [6]. Obviously, this will alter the low electron density behavior of $\Delta E_A(n_H)$, but for the systems considered later changing the $n_H = 0$ cubic spline knot to $-(E.A.)_A$ in the embedding energy function has only minor significance in the important region of the potential minimum. We have noted this low density modification in order to allow duplication of our results.

The integrals required for the density functionals and sampling procedures are evaluated using a numerical quadrature scheme with a spherical coordinate system centered on the embedded atom for one center integrals and coordinate systems centered on pairs of atoms for the two center Coulomb integrals. The numerical quadrature schemes are summarized by three parameters (nlag, nleg, nphi). The radial integration is performed by a $nlag^{th}$ order Gauss-Laguerre quadrature, the polar angle integration by $nleg^{th}$ order Gauss-Legendre quadrature, and the azimuthal angle integration by a $nphi^{th}$ order Gauss-Chebychev quadrature on the half circle. To increase efficiency of the computer code, the radial dependence of the atomic electron densities and derivatives are fit to a large radial grid for each electronic shell and linearly interpolated. This yields negligible error when compared to calculations using the true electron densities.

# APPLICATIONS

In this section, we apply the CEM-1 theory to various two-body systems for which either experimental or first principles interaction energies are known. The goal is to delimit the range of validity for the CEM-1 method and not to illustrate its full power. We test the choice of embedding scheme, effective medium sampling procedure, and spin polarization and electronic configuration for the Hartree-Fock atomic electron densities. To see how such choices enter, consider the CEM-1 theory with regards to the relationship with the "zeroth" order term. The homogeneous embedding energy function describes an atom embedded into a spin-unpolarized homogeneous electron gas. The $\Delta V^C$ and $\Delta G$ terms correct for the embedding of an atom into a spin-polarized and locally varying electron density of an inhomogeneous electron gas. The two-body systems that we examine provide examples of these deviations from the zeroth order term in a systematic manner.

## Atom in a Spin-Polarized Homogeneous Electron Gas

The first case we examine provides a test of the treatment for the interaction of an atom with a spin-polarized system without complications due to the inhomogeneity of the host electron density. We identify body B as a spin polarized homogeneous electron gas H' of total electron density $n_{H'}$ and spin-polarization $\phi_{H'}$. Using the $(A \rightarrow B)$ embedding scheme the CEM-1 interaction energy expression becomes

$$\Delta E_{AH'} = \Delta E_A(n_H) + (G[A + H'] - G[H']) - (G[A + H] - G[H]) \ . \qquad (37)$$

The effective medium total density $n_H$ equals $n_{H'}$ independent of the choice of sampling function. However, the $\Delta G$ term of Eq. (37) does not vanish because $\phi_H = 0$ while $\phi_{H'} \neq 0$. Thus, the $\Delta G_{AH'}$ term provides a correction for the embedding energy of A in a polarized electron gas of density $n_{H'}$ which is due entirely to the dependence of the kinetic, exchange and correlation energy functionals on the spin polarization.

Using a Kohn-Sham self-consistent LD approach, Stott and Zaremba have calculated [4] the embedding energies for the H atom with $\phi_{H\ atom} = 1$ in two different spin-polarized homogeneous gases; $\phi_{H'} = 1$ and -1. These embedding energies are plotted in Fig. 3 as a function of $n_{H'}$. Also presented in Fig. 3 are the CEM-1 results using $\Delta E_{AH'}$ for three different polarizations of the host electron gas ($\phi_{H'} = -1, 0, 1$). The $\phi_{H'} = 0$ values correspond to the original embedding energy function of Puska et al. for the hydrogen atom which were also obtained by Stott and Zaremba. For $\phi_{H'} = 1$, the SCF-LD embedding energy curve is repulsive over the full range of $n_{H'}$ due to the large kinetic energy repulsion between the H atom and $n_{H'}$ which are both spin up. The CEM-1 curve for $\phi_{H'} = 1$ shows increased repulsion with respect to the curve for $\phi_{H'} = 0$, but becomes negative for low values of $n_{H'}$. The corrections cannot overcome the dominance of the zeroth order CEM-1 term as $n_{H'} \to 0$. By contrast, the CEM-1 curve is almost parallel to the SCF-LD result for large $n_{H'}$ at $\phi_{H'} = 1$. At the other extreme is the $\phi_{H'} = -1$ case. Here the spin of the H atom is antiparallel to the host electron gas, thus resulting in correlation energy spin attraction. The SCF-LD curve and the CEM-1 curve are in rather good agreement, although at large $n_{H'}$ the CEM-1 curve does not decrease as quickly as the SCF-LD $\phi_{H'} = -1$ curve.

Figure 3. Embedding energies of a spin up hydrogen atom into a spin-polarized homogeneous electron gas. Both the SCF-LD results [4] and the CEM-1 results are shown as a function of electron density for three different spin polarizations of the gas. $\phi = 1$ is spin up; $\phi = 0$ is unpolarized; $\phi = -1$ is spin down. (The $\phi = 0$ CEM-1 result is identical to the $\phi = 0$ SCF-LD result by definition.)

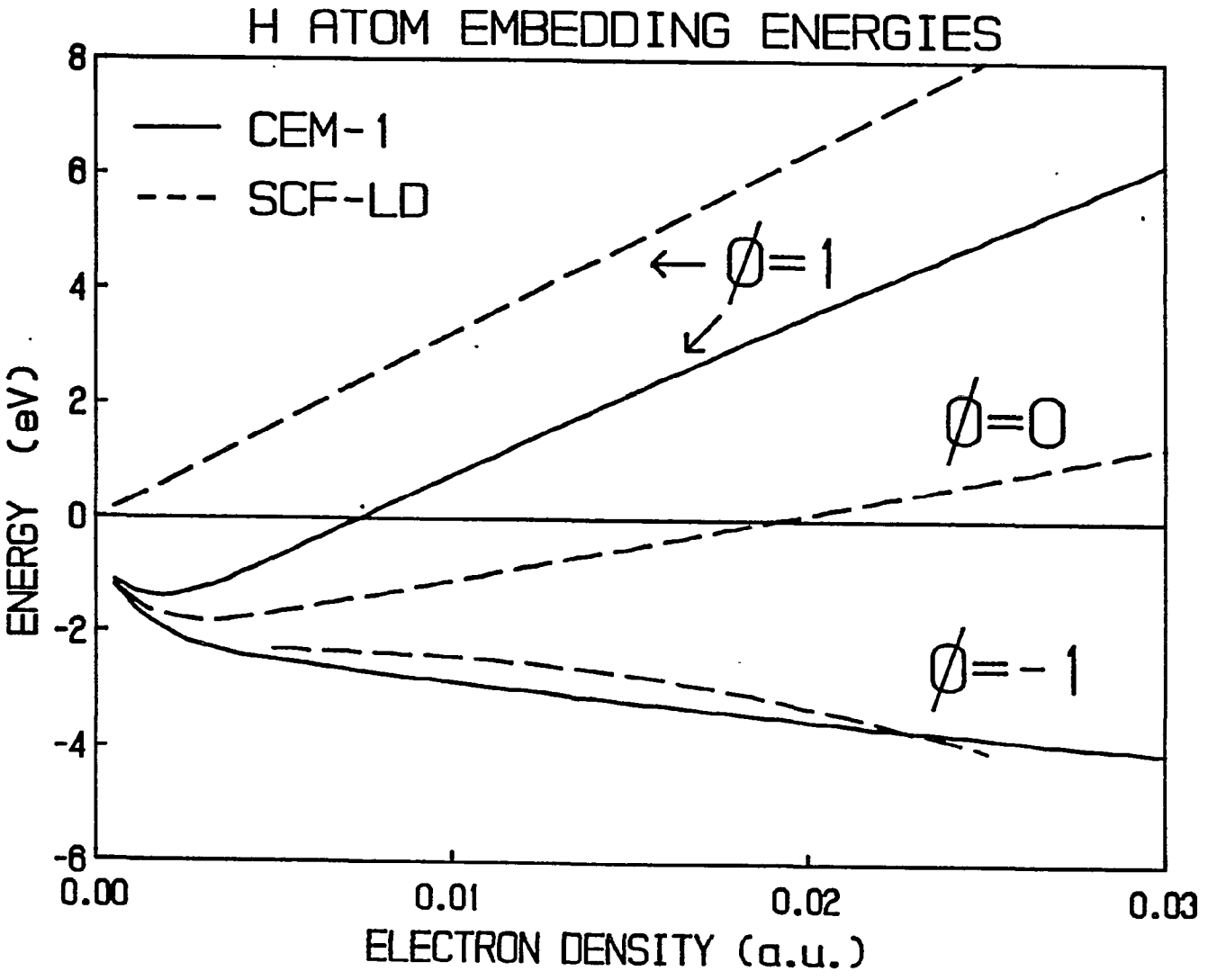
H ATOM EMBEDDING ENERGIES
CEM-1
SCF-LD
← ∅=1
∅=0
∅=-1
ENERGY (eV)
8
6
4
2
0
-2
-4
-6
0.00
0.01
0.02
0.03
ELECTRON DENSITY (a.u.)

## Diatomic Molecules

To calculate the interaction energy for a diatomic molecule using the CEM-1 theory, we embed one atom into the spin-polarized and inhomogeneous electron density of the other host atom. When compared to the electron gas, this type of host electron density is extremely inhomogeneous since it decays exponentially away from the nucleus. Since the CEM-1 theory is required to predict the interaction energy for a system far from the CEM-1 zeroth order term, we find that the binding energies and equilibrium bond lengths are sensitive to: 1) the embedding scheme; 2) the effective medium sampling procedure; 3) the degree of spin polarization of the Hartree-Fock atomic spin densities; and 4) the electronic configuration of the Hartree-Fock atomic spin densities. Each of these specific points is examined for diatomic molecules.

The $H_2$ molecule has been studied extensively since it is the simplest molecule which exhibits the basic characteristics present in two center bonds of many-electron systems: electron exchange and electron correlation between two bound spin-paired valence electrons. Since $H_2$ is homonuclear, the two embedding schemes (A → B) and (B → A) are identical. Because the averaged and electrostatic values of $n_H$ were in close agreement and the electrostatic sampling yielded negative $n_H$ for the OH system, we only present results for the pointwise and averaged sampling. The $H_2$ molecule provides a critical test of the choice of spin polarization for the atomic electron densities. Two different spin configurations were tried representing the two extremes of an unpolarized and a polarized bond. In the former, the occupation numbers for atom A and atom B were chosen as

A: N(100, +1/2) = 0.5, N(100, -1/2) = 0.5,

B: N(100, +1/2) = 0.5, N(100, -1/2) = 0.5

which corresponds to placing a spin-unpolarized 1s electron on each H atom. For the latter, the occupation numbers were chosen as

A: N(100, +1/2) = 1.0, N(100, -1/2) = 0.0,

B: N(100, +1/2) = 0.0, N(100, -1/2) = 1.0

which corresponds to a spin paired bond.

Table I contains the results of the CEM-1 theory for the $H_2$ molecule, along with the values from Hartree-Fock, LD, and experiment. The use of either sampling procedure (case 1 vs. case 2 and case 3 vs. case 4) yields the same binding energy and bond distance to within 5%. Large variations occur when the results for the two different spin polarization choices are compared within the same sampling procedure. The spin-polarized case provides a binding energy approximately 1 eV larger than that for the unpolarized bond and a bond distance approximately 0.8 bohr shorter. Both spin-polarized bond distances are within 15% of the experimental value. This is strong evidence that spin paired electron densities must be used to adequately describe a bond between two atoms within the CEM-1 theory. This result is not surprising since the spin-polarized density functional theory also improves the spin-unpolarized LD description of binding in solids and diatomic molecules when calculated self-consistently. The spin-polarized CEM-1 binding energy is not as accurate (-3.1 eV vs. exact -4.75 eV). These same features are seen in the Hartree-Fock potentials which provide good bond distances and too little binding energy, as evidenced in Table I for $H_2$.

Table I. $H_2$ molecule binding characteristics

| Case | H Atom Spin Polarization | Sampling Procedure | $r_e$(bohr) | $D_e$(eV) |
|---|---|---|---|---|
| 1 | unpolarized | averaged | 2.46 | 1.93 |
| 2 | unpolarized | pointwise | 2.46 | 1.82 |
| 3 | polarized | averaged | 1.62 | 3.09 |
| 4 | polarized | pointwise | 1.59 | 3.10 |
| LD[a] | | | 1.42 | 4.84 |
| Hartree-Fock[a] | | | 1.39 | 3.67 |
| experiment[b] | | | 1.41 | 4.74 |

[a]Self-consistent results of ref. [23].

[b]Ref. [24].

Although the pointwise and averaged sampling procedures yield virtually the same bond length and binding energy for the $H_2$ molecule, the homogeneous embedding energy and $\Delta G_{AB}$ contributions to the potential energy curve are distinctly different for the two procedures. In Figs. 4(a) and 4(b) we plot $\Delta E$, $\Delta E^h$, $\Delta V^C$and $\Delta G$ for the $H_2$ molecule corresponding to case 3 and 4, respectively, in Table I. (We drop the subscript AB for convenience.) The binding curves, $\Delta E$, are nearly identical over the bond length range of 1-3 bohr. $\Delta V^C$, is independent of the sampling procedure but the individual contributions of $\Delta E^h$ and $\Delta G$ are quite different. $\Delta G$(averaged) <u>increases</u> more slowly than $\Delta G$(pointwise) while $\Delta E^h$(averaged) <u>decreases</u> more slowly than $\Delta E^h$(pointwise) in the 1-2 bohr region. The faster variations in the pointwise sampling values nearly compensate for each other with the net result that $\Delta E$(pointwise) is similar to the $\Delta E$(averaged).

The $\Delta E^h$ and $\Delta G$ curves in Fig. 4(a) for the pointwise case diverge towards $\pm\infty$, respectively, much more quickly than do the averaged sampling curves as the bond length is compressed towards zero. Examining the behavior of $\Delta E^h$ first, note that within the range of 1-1.6 bohr, $n_H$(pointwise) > $n_H$(averaged). Either value of $n_H$ is large enough such that $\Delta E_A(n_H)$ (see Fig. 1, H atom) is on the repulsive wall where $\Delta E_A(n_H)$ is a monotonically increasing function of $n_H$. Thus, $n_H$(pointwise) yields a larger embedding energy than does $n_H$(averaged) over this range.

To understand why the $\Delta G$(pointwise) curve drops off faster than $\Delta G$(averaged) in Fig. 4(a), we must inspect the individual contributions to $\Delta G$, written as

Figure 4. CEM-1 energy components for $H_2$ molecule using both the averaged and pointwise sampling procedure. The curves are plotted as a function of bond length. (a) Embedding energy and correction energy. (b) Coulomb energy and binding potential

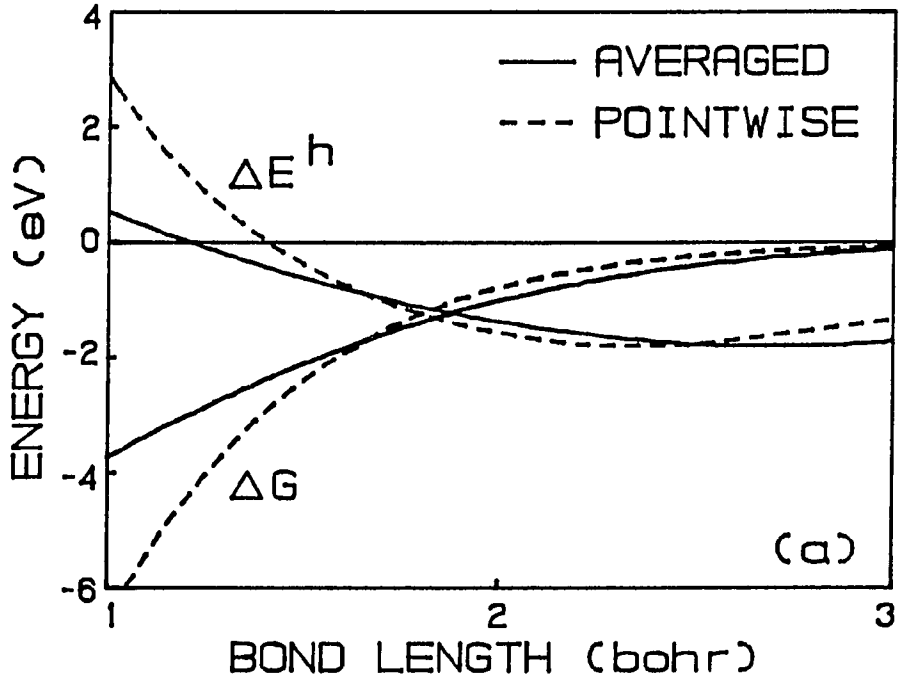
AVERAGED
POINTWISE
ΔE h
ΔG
(a)
ENERGY (eV)
BOND LENGTH (bohr)
4
2
0
-2
-4
-6
1
2
3

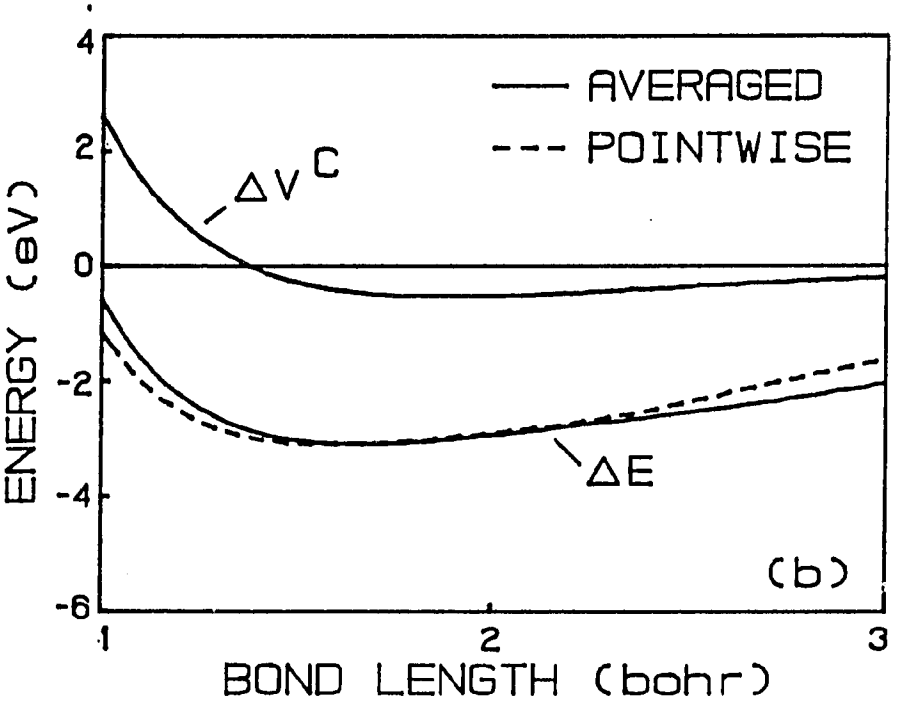
AVERAGED
POINTWISE
ΔV C
ΔE
(b)
ENERGY (eV)
BOND LENGTH (bohr)
4
2
0
-2
-4
-6
1
2
3

$$\Delta G = (G[AB] - G[A] - G[B]) - (G[A + H] - G[H] - G[A]) , \qquad (38)$$

where we have added and subtracted G[A] for illustrative purposes. The first term in parentheses is independent of $n_H$ and hence contributes equally to $\Delta G$ for any sampling procedure. This second term is the analog of a spin-polarized Gordon-Kim electron gas approximation to the embedding energy function

$$\Delta E_A^{GK}(n_H) = (G[A + H] - G[H] - G[A]) . \qquad (39)$$

We have verified numerically that $\Delta E_A^{GK}(n_H)$ behaves exactly as $\Delta E_A(n_H)$ in the large $n_H$ limit, increasing linearly with $n_H$. Since $n_H$(pointwise) is larger than $n_H$(averaged) in the range 1-1.6 bohr and since the second term in Eq. (38) is a subtraction of $\Delta E_A^{GK}(n_H)$, $\Delta G$(pointwise) decreases more quickly towards $-\infty$ than does $\Delta G$(averaged) as the bond distance is compressed towards zero.

The above discussion is extremely important since it indicates why slight variations in $n_H$ are compensated between $\Delta G$ and $\Delta E^h$ inside of the equilibrium bond length, (i.e., at large $n_H$). By contrast, out beyond 3 bohr where $n_H$ is small, $\Delta E^h$ dominates $\Delta E$ since $\Delta V^c$and $\Delta G$ both become negligible. $\Delta E^h$ remains significant because a vestige of the zero density value $\Delta E^h = -(E.A.)_A$ still occurs at these densities. This casts doubt on the accuracy of the binding curve in this region since the potential is governed completely by $\Delta E^h$.

Figs. 4(a) and 4(b) also provide information on the effect of $\Delta E^h$ on the equilibrium bond distance and well depth. Focus on the results of the average sampling procedure. If one models the binding of one H atom to another one by using only $\Delta E_A^h$, $\Delta E$ would correspond to $\Delta E^h$ in Fig. 4(a). Both the minimum energy of -1.81 eV and the bond distance of ~ 3 bohr are considerably worse than the corresponding values for $\Delta E$. Since the overlap of the two 1s H atom densities at this distance yields the value of $n_H$ corresponding to the minimum of $\Delta E_A(n_H)$, it is clear that the depth and position of the minimum of the $\Delta E^h$ curve does not determine the depth and the position of the minimum of the CEM-1 predicted $\Delta E$. For the latter, the depth is increased to -3.1 eV and the equilibrium bond distance is compressed to 1.6 bohr by the contribution from $\Delta G$, and by a smaller contribution from $\Delta V^C$.

As a test for heteronuclear diatomics we applied the CEM-1 theory to the first row monohydrides. Spin-polarized configurations were used for all open shell atoms, with the spin orbitals for the first row atoms filled according to Hund's rules using the Hartree-Fock ground state wavefunctions. The H atom was set oppositely spin-polarized with respect to the other atom resulting in a spin paired bond between the two atoms. Note that the atomic electron densities were not made spherically symmetric, a popular (but unjustified) approximation within electron gas theories [4,25]. Use of spherical electron densities changes the spatial shape of the atomic configurations which contain partially filled 2p orbitals. If we choose the z-axis to lie along the bond axis, electron density from the $2p_0$ contribution which lies along the bond axis is removed

and placed into the $2p_{\pm 1}$ densities which are perpendicular to the z-axis. This spatial change modifies the sampled homogeneous electron gas density and the Coulomb interaction yielding differences in the resulting potentials on the order of eV.

Application of the CEM-1 theory to heteronuclear diatomic molecules requires a decision as to whether the (A → B) or (B → A) embedding schemes should be used since these yield different binding energy curves. Choosing the OH molecule as an extreme example, we note that the embedding energy functions for the H and O atoms in Fig. 1 differ both with respect to the depth and location of the minimum. The effect of this difference in embedding functions is evident in the results presented in Table II for OH, and the other diatomics. (The averaged density sampling procedure was employed because the pointwise sampling procedure was found to be inadequate for describing these heteronuclear diatomic molecules.) It is apparent that the two sets of predicted binding potentials are very different except for the BH molecule. Better agreement with the experimental binding energies is found when the more electrognegative atom is embedded into the less electronegative one.

To explain this trend we consider choosing the host as the atom from the diatomic pair which most resembles, in terms of physical properties, a homogeneous electron gas. At low electron gas densities, the embedding energy approaches the -(E.A.) of the embedded atom. This implies that the host donates electron density to the embedded atom. Hence, when considering a pair of atoms forming a chemical bond, the atom with the smaller electronegativity value is chosen as the host since it will donate electrons to the atom with the larger value (i.e., the embedded atom).

Table II. CEM-1 diatomic hydride binding energies and bond lengths using averaged density sampling

| | E. N.[a] of A | Embedding Scheme | | | | | |
|---|---|---|---|---|---|---|---|
| | | (H → A)[b] | | (A → H)[c] | | expt.[d] | |
| | | $r_e$(bohr) | $D_e$(eV) | $r_e$(bohr) | $D_e$(eV) | $r_e$(bohr) | $D_e$(eV) |
| HH | 2.2 | | | 1.63 | 3.07 | 1.41 | 4.74 |
| LiH | 1.0 | 2.81 | 2.49 | 3.56 | 0.78 | 3.02 | 2.52 |
| BeH | 1.6 | 3.11 | 2.17 | 3.13 | 0.29 | 2.54 | 2.16 |
| BH | 2.0 | 2.21 | 3.91 | 2.11 | 4.40 | 2.33 | 3.57 |
| CH | 2.5 | 3.03 | 2.20 | 1.97 | 3.44 | 2.22 | 3.60 |
| OH | 3.4 | 2.16 | 2.58 | 1.75 | 7.95 | 1.83 | 4.62 |
| FH | 4.0 | 2.57 | 2.23 | 2.27 | 6.35 | 1.73 | 6.13 |

[a]Pauling Electronegativitiy

[b]H atom embedded into non-H atom.

[c]Non-H atom embedded into H atom.

[d]Experimental results of ref. [24].

CEM-1 binding energies predicted with the above embedding scheme, experimental binding energies, and Pauling electronegativities are provided in Table II. We note that the CEM-1 and experimental energies are in good agreement for LiH, BeH, BH, CH using the (H → A) embedding scheme and for CH and FH using the (A → H) scheme, thus supporting the embedding scheme choice based on the electronegativities of the atoms. OH and BH provide examples where the CEM-1 binding energy is greater than the experimental energy thus demonstrating that a minimum principle does not exist for the CEM-1 theory.

The worst case in Table II is the OH molecule for which the CEM-1 potential is over 3 eV deeper than the experimental one. Since oxygen is the more electronegative atom, $\Delta E_O(n_H)$ is used in the CEM-1 interaction. In comparison to the fluorine embedding energy function, the oxygen one obtains a minimum at a value of $n_H$ three times larger than the value for the fluorine, and more importantly the ratio $\Delta E_A(n_H = \text{minimum})/\Delta E_A(n_H = 0)$ is 4.1/1.5 for O and 5.1/3.5 for F. Both differences, we believe, are due to the fact that oxygen interacting with the homogeneous electron gas attempts to form a doubly charged anion, thus stabilizing the embedding energy relative to a singly charged anion. However, in the OH bond such an $O^{2-}$ species is an impossibility. This reflects the breakdown of the additive density approximation since the densities for the real and atom-homogeneous electron gas system are too different.

Finally, we note that the EM calculations [7] for H, C, and O atoms chemisorbed onto metal surfaces are in accord with our embedding scheme postulate. Their choice of the chemisorbed atom as the embedded atom and

the metal surface as the host body is consistent since a metal surface with a work function of only a few eV is electropositive when compared to the adsorbed atom.

## Atomic Chemisorption

In this section we consider the interaction of an atomic absorbate with a metal surface. We let the top layer of surface atoms define the z = 0 plane and specify the z-axis as perpendicular to the surface pointing out into vacuum. Although exhibiting nearly perfect homogeneity in the x and y directions, the electron density distribution provided by the conduction band electrons decays exponentially from the surface plane towards positive z. Thus the degree of inhomogeneity of the host density falls between that of the two previously considered systems. The homogeneous embedding energy provides a first approximation to the interaction energy with corrections due to the inhomogeneous nature of the surface furnished by the CEM-1 theory.

The form of the CEM-1 energy expression for an adatom A interacting with a metal surface B is analogous to the expression for the AB diatomic molecule upon replacement of atom B from the diatomic pair with the metal surface B throughout the interaction energy expression. Within the superposition approximation, we represent the metal surface by a finite cluster of metal atoms whose geometry is constructed to reproduce a specific face of a crystal with the experimental bulk lattice constant. Centered on each of these metal atoms in the lattice we place the Hartree-Fock atomic electron density. The electron density of the metal is

then used as input into the density functionals and homogeneous electron gas sampling procedures as specified by the choice of interaction expression.

The specific form for the interaction of adatom A with an N-member cluster of metal B atoms within the (A → B) embedding scheme is

$$\Delta E_{AB} = \Delta E_A\ (n_H) + \sum_i^N \Delta V_{Ai}^C + \Delta G_{AB}\ , \tag{40}$$

where the summation extends over the atoms in the metal cluster B. $\Delta G_{AB}$ is the correction energy given by Eq. (38). (We define the first term in parenthesis of Eq. (38) as the density functional interaction energy and denote it by $\Delta G[AB]$.) Due to the superposition of atomic densities, the Coulomb interactions and sampling procedures are pairwise additive.

Before discussing the results for atomic chemisorption, we compare the formal structure of the EM theory with that of the CEM theory. The EM interaction energy [7a] for an atom A embedded into an inhomogeneous host B is expressed as

$$\Delta E_{AB} = \Delta E_A(n_H) - \alpha_A\ n_H + \Delta E_A^{hyb}\ . \tag{41}$$

This equation only results upon use of the <u>electrostatic</u> sampling procedure and first-order perturbation theory using weak pseudopotentials for the ion cores of the host. The EM theory, as in the CEM-1 theory, utilizes a zeroth order approximation to the energy which is the embedding energy function. The second term of Eq. (41) accounts for the electrostatic

Coulomb interaction under the assumption that within a given finite radius about the A atom, the density of the host is nearly constant and void of the ionic core. Thus, the Coulomb interaction reduces to a product of a polarizability for atom A, $\alpha_A$, times $n_H$. The last term in Eq. (41) describes covalent binding effects (resonances) between the atomic states of A and any localized host electronic states (such as occupied d bands). This hybridization term also contains a small electrostatic contribution and a contribution from the hopping matrix elements between the atomic states and localized host states.

Comparing the CEM-1 and EM interaction expressions, we note that the Coulomb interaction is accounted for explicitly in the CEM-1 theory by using the actual host charge density within the superposition approximation to evaluate the Coulomb integrals. The term in the CEM-1 theory analogous to the $\Delta E_A^{hyb}$ term is the correction energy $\Delta G_{AB}$. Instead of considering the atom-host interaction in terms of a tight binding scheme, $\Delta G_{AB}$ provides a spin-polarized density functional evaluation of the difference in kinetic-exchange-correlation energy between the atom in the homogeneous electron gas and the atom in the inhomogeneous electronic distribution of the real host B.

Another theory similar in spirit to the EM and CEM theories is the embedded atom (EA) method [26] which incorporates a (semiempirical) embedding energy term for the host body, $\Delta E_B(n_H)$, as well as empirical repulsive two-body potentials. The former has the desirable property of simultaneously embedding atom A into the host and the host body B into atom A (using a pointwise sample of the host density), thus allowing the

embedding atom A to perturb the host. The inclusion of this backbinding of the host into the embedded atom is possible within the CEM theory by considering the simultaneous embedding scheme (A → B; B → A). A study incorporating this simultaneous embedding procedure as applied to diatomic molecules is considered in Paper III.

Returning to the CEM-1 treatment of atomic chemisorption, we next choose the atomic spin densities for the adatom and the atoms of the metal cluster. The latter offer considerable flexibility. For the first row transition metal elements considered here (Fe, Ni and Cu), the ground state Hartree-Fock spin electron configuration consists of a fully occupied 4s shell and a partially occupied 3d shell for the valence electrons ($3d^n, 4s^2$). The partial occupation of the 3d shell provides an electron density which is both spin-polarized and non-spherical. Constructing a metal cluster of spin-polarized atoms by a superposition of atomic densities results in a net spin moment. To eliminate this artifact of non-self-consistency, we treat the metal clusters as paramagnetic by populating equally the up and down spin density. To prepare this unpolarized density we alter the ground state Hartree-Fock spin density by changing the occupation numbers of any partially filled spatial orbital. For example, to unpolarize a singly filled 3d orbital density we change {N(320,+1/2) = 1, N(320,-1/2) = 0} to {N(320,+1/2) = 1/2, N(320,-1/2) = 1/2}. We also made the 3d shell spherical for these metal atoms, which alters the spatial dependence of the electron density slightly but allows a much more efficient numerical evaluation of the Coulomb integrals and density overlap integrals.

For clusters of Cu and Ni atoms we also considered the electron densities constructed from a Hartree-Fock excited state. In the bulk, Cu exists [27] with a full d-band and a partially filled s-band implying a valence electron occupation of $(4s^1, 3d^{10})$. In the gas phase [28], the $(4s^1, 3d^9)$ state of Ni is only 0.03 eV lower than the $(4s^2, 3d^8)$. When constructing the cluster electron density for transition metals from a superposition of atomic densities, it is unclear whether the Hartree-Fock ground state $(4s^2, 3d^n)$ or the state $(4s^1, 3d^{n+1})$ better represents the true surface electron density. Therefore, cluster electron densities were also constructed by removing a 4s electron and filling an additional 3d orbital still using the ground state Hartree-Fock basis (i.e., no atomic relaxation). This allows for a comparison of effects due to the spatial compactness of the atomic electron density since a 4s orbital is more diffuse than a 3d orbital.

One other approximation was used when constructing the metal atom electron densities. The inner core (1s, 2s, 2p) electrons are so tightly bound that they were assumed to shield an amount of positive nuclear charge equal to the number of electrons in these inner shells. Thus, the inner core density was not used. The Coulomb interactions are of sufficiently long range to validate the screening argument. However, the lack of inner shell electron density does have an effect on the sampled homogeneous electron gas densities. Without the inner shells the homogeneous electron density is smaller. The change in the contribution from the embedding energy function to the interaction energy is offset by an opposite and almost equal change from the correction energy. This approximation has

been tested for some of the H atom chemisorption potentials where the equilibrium values were found to be within 5% of the all-electron densities values.

The coordinates and geometrical arrangements of the adatom and metal cluster atoms are described here. The adatom is placed at a height z above the surface atom plane. We vary z and fix the x and y coordinates so that the adatom lies above a specific symmetry site on the surface. The size and composition of the metal cluster is determined by constructing a half sphere of radius $r_{cut}$, centered in the surface plane at the x,y coordinate of the specific symmetry site being investigated. The lattice atoms which reside within this half sphere are then retained.

For each symmetry site considered, the equilibrium binding heights and binding energies are presented in Tables III and IV for H atom chemisorption on Cu(100), Fe(110), and Ni(100). The H atom density was set as a fully spin-polarized ($\phi$ = 1), 1s electron except where specified otherwise. The results in Tables III and IV provide information on: 1) symmetry site differences on a given lattice face; 2) the influence of Hartree-Fock ground state ($4s^2$, $3d^n$) and promoted state ($4s^1$, $3d^{n+1}$) electronic configurations, and 3) the effect of the averaged versus pointwise homogeneous electron gas sampling. The numerical quadrature parameters used were (nlagu, nlege, nphi) = (160, 40, 20) which converged the binding energies to within 0.01 - 0.02 eV and converged the binding heights to within 0.1 bohr. The values for the binding heights and energies listed in Tables III and IV were determined by fitting a cubic polynomial to the potential points calculated every ~ 0.3 bohr in z around

Table III. CEM-1 H atom chemisorption potentials for selected symmetry sites on Ni(100)

| Sampling, Valence Shell Configuration | CENTER | | BRIDGE | | ATOP | |
|---|---|---|---|---|---|---|
| | $z_e$(bohr) | $D_e$(eV) | $z_e$(bohr) | $D_e$(eV) | $z_e$(bohr) | $D_e$(eV) |
| Averaged $(3d^8, 3s^2)$ | 1.8 | 2.57 | 2.8 | 2.42 | 3.6 | 2.30 |
| Averaged $(3d^9, 4s^1)$ | 2.0 | 2.40 | 2.9 | 2.28 | 3.7 | 2.17 |
| Pointwise $(3d^8, 4s^2)$ | 2.8 | 2.31 | 3.2 | 2.23 | 3.6 | 2.14 |
| Averaged $(3d^8, 4s^2)$, unpolarized H atom | 1.4 | 2.82 | | | | |
| EM[a] | 1.4 | 2.7 | | | | |
| LD[b] | 0.6 | 3.61 | 1.8 | 3.53 | 2.7 | 3.29 |
| GVB[c] | 0.57 | 3.04 | 1.9 | 2.73 | 2.8 | 1.56 |
| Experiment[d] | 0.97 | 2.74 | | | | |

[a]Effective medium results of ref. [7a].

[b]Local Density results of ref. [29].

[c]Generalized Valence Bond results of ref. [30].

[d]Experimental results of ref. [31a] for $z_e$ and ref. [31b] for $D_e$.

Table IV. CEM-1 H atom chemisorption potentials for the center site on Cu(100) and Fe(110) using the averaged sampling procedure

| Valence Shell Configuration | Cu(100) | | Fe(110) | |
|---|---|---|---|---|
| | $z_e$(bohr) | $D_e$(eV) | $z_e$(bohr) | $D_e$(eV) |
| $(3d^n, 4s^2)$ | 1.4 | 2.58 | 2.1 | 2.45 |
| $(3d^{n+1}, 4s^1)$ | 1.0 | 2.44 | | |
| $(3d^n, 4s^2)$, unpolarized H atom | 1.0 | 2.89 | 1.0 | 2.68 |
| EM[a] | | 2.4 | | 2.7 |
| SCF-CI[b] | 1.7 | 2.6 | | |
| Experiment[c] | | 2.6 | | 2.8 |

[a]Effective medium results of ref. [7a].

[b]Hartree-Fock-CI embedded cluster results of ref. [32].

[c]Experimental results of ref. [33] for Cu and ref. [34] for Fe.

the minimum. The minima are accurate to within 0.02 eV and 0.1 bohr, except over the center sites where the latter number is 0.2 bohr.

For the Ni clusters, we used the experimental fcc lattice constant of 6.65 bohr [35]. The positions of the three symmetry sites are illustrated in Fig. 5 for both the fcc(100) and bcc(110) lattices. Clusters much larger than the four atom unit cell were used in the CEM-1 calculations. For the fcc(100) calculations, we used a 26 atom cluster for the atop site which consisted of 9 surface atoms, 12 second layer atoms and 5 third layer atoms. This arrangement is denoted by (9, 12, 5). The bridge site cluster consisted of 26 atoms but in a (12, 8, 6) arrangement. The center site cluster consisted of 25 atoms in a (12, 9, 4) arrangement. We found that, within the CEM-1 theory, these clusters provided well converged results. In fact, a smaller cluster could be used in the atop and bridge site case, (9, 4, 1) and (8, 6, 2), respectively, without changing the shape of the potentials around the minimum. The CEM-1 theory is much less sensitive to the metal cluster size, than is Hartree-Fock theory, since self-consistent molecular wavefunctions delocalized over the whole cluster are <u>not</u> needed.

To explain the trends in symmetry site dependence of the interaction potentials, consider the values for the $(3d^8, 4s^2)$ configurations with averaged density sampling. The binding height decreases and the binding energy increases in the order of: atop site, bridge site, center site. The individual energy contributions to the interaction energy are plotted in Figs. 6(a), 6(b), 6(c) and 7(a), 7(b), 7(c). The repulsive portion of the embedding energy $\Delta E^h$ gives a qualitative measure of the amount of metal cluster electron density sampled by the H atom since the H atom embedding

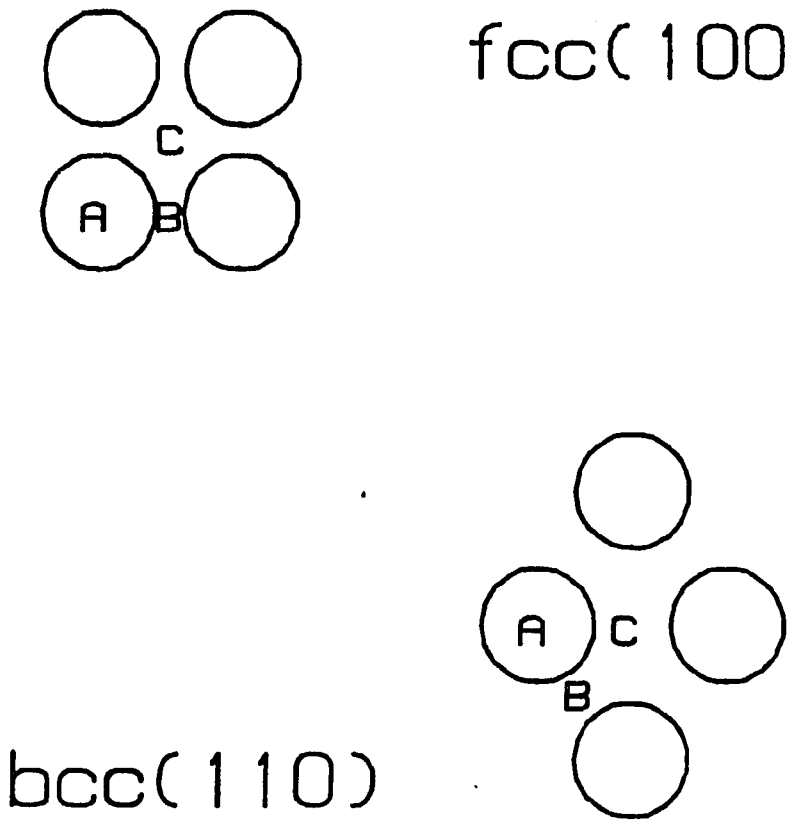


Figure 5. Definition of the atomic chemisorption sites within the fcc(100) and bcc(110) surface unit cells. A = Atop. B = Bridge. C = Center

Figure 6. CEM-1 embedding and correction energies for H atom chemisorption on Ni(100) using the averaged sampling procedure and the Ni ground state Hartree-Fock electronic configuration. The curves are plotted as a function of the height of the atom above the surface plane for the symmetry sites. (a) Atop. (b) Bridge. and (c) Center

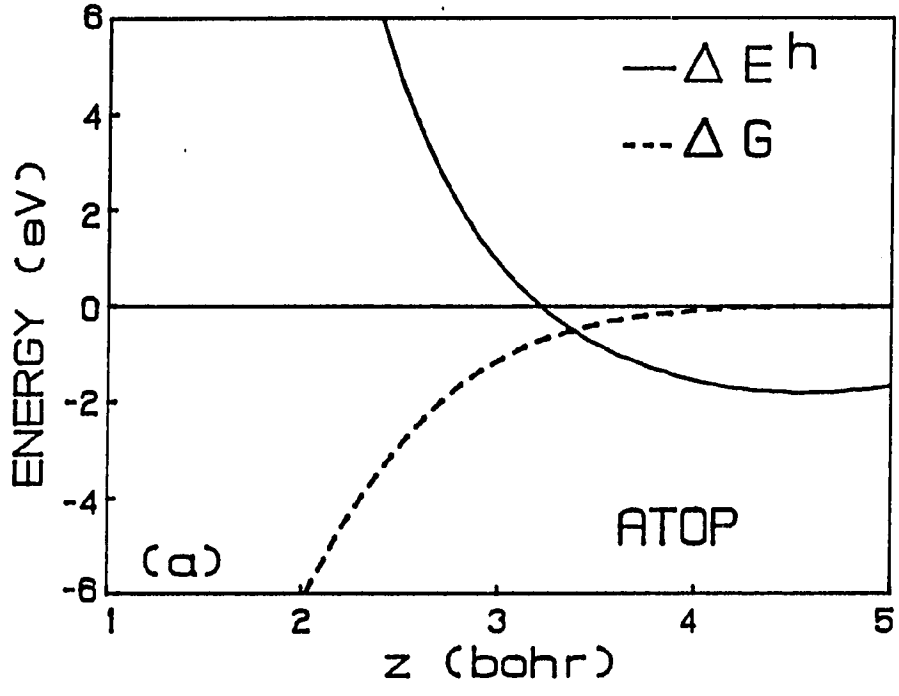
6
4
2
0
-2
-4
-6
ENERGY (eV)
—Δ E h
---Δ G
ATOP
(a)
1
2
3
4
5
z (bohr)

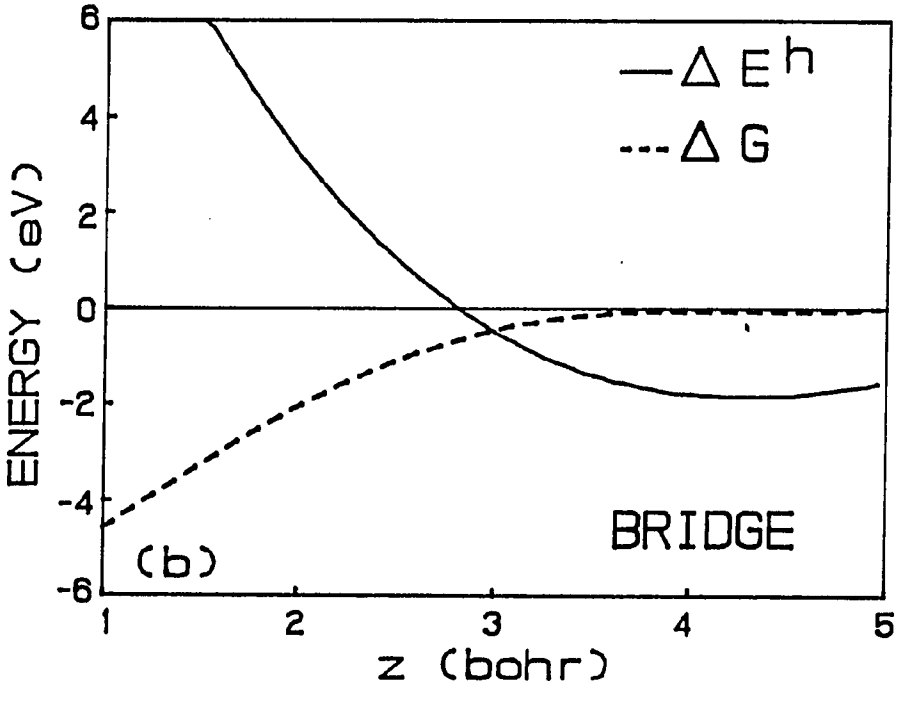
6
4
2
0
-2
-4
-6
ENERGY (eV)
—Δ E h
---Δ G
BRIDGE
(b)
1
2
3
4
5
z (bohr)

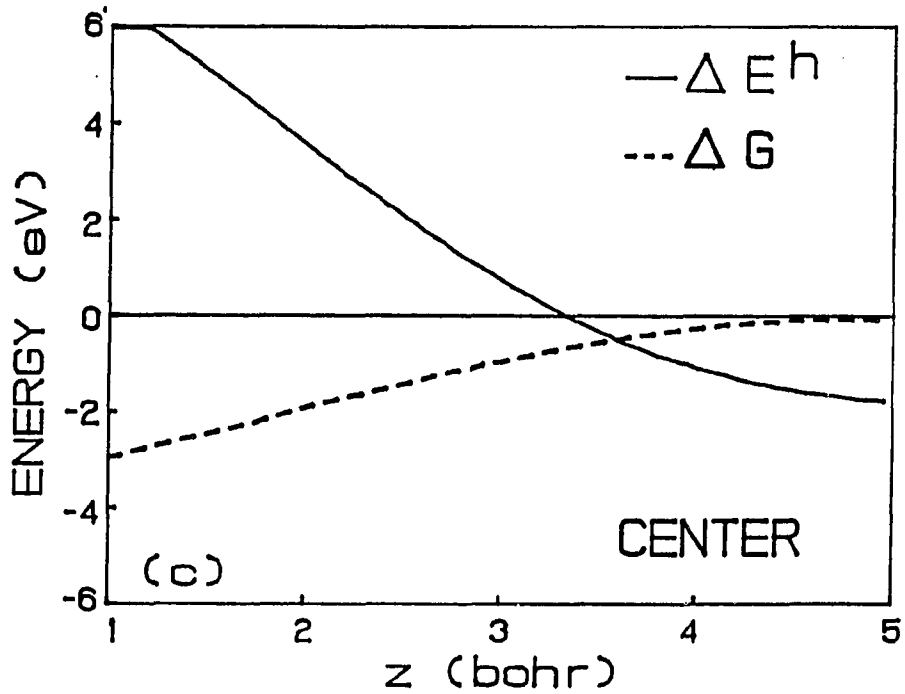


Figure 6 (Continued)

Figure 7. CEM-1 binding potential and Coulomb energy for H atom chemisorption on Ni(100) using the averaged sampling procedure and the Ni ground state Hartree-Fock electronic configuration. The curves are plotted as a function of the height of the atom above the surface plane for the symmetry sites. (a) Atop. (b) Bridge. and (c) Center

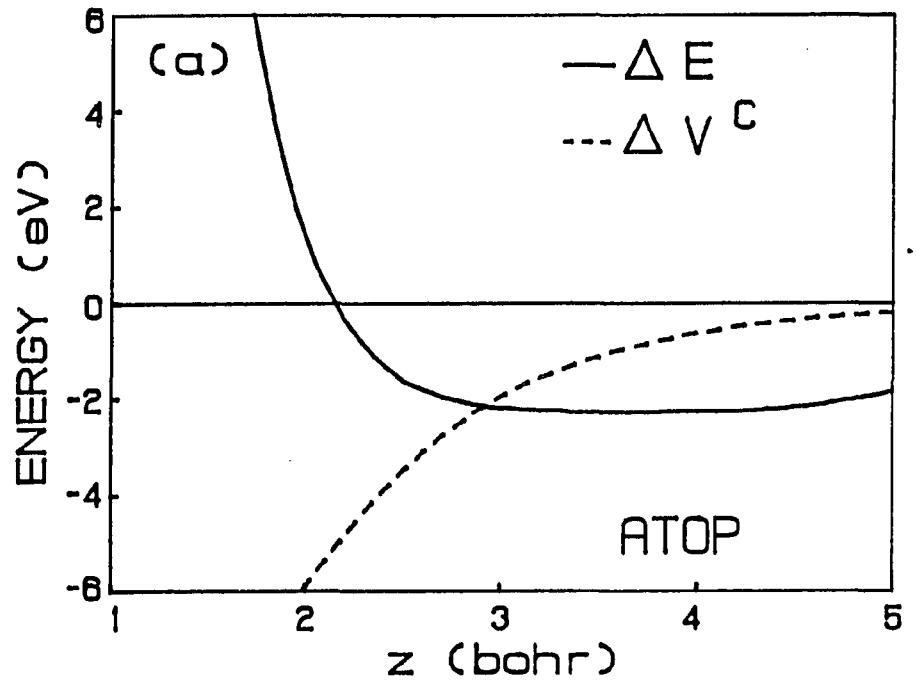
(a)
—Δ E
---Δ V C
ATOP
ENERGY (eV)
z (bohr)
6
4
2
0
-2
-4
-6
1
2
3
4
5

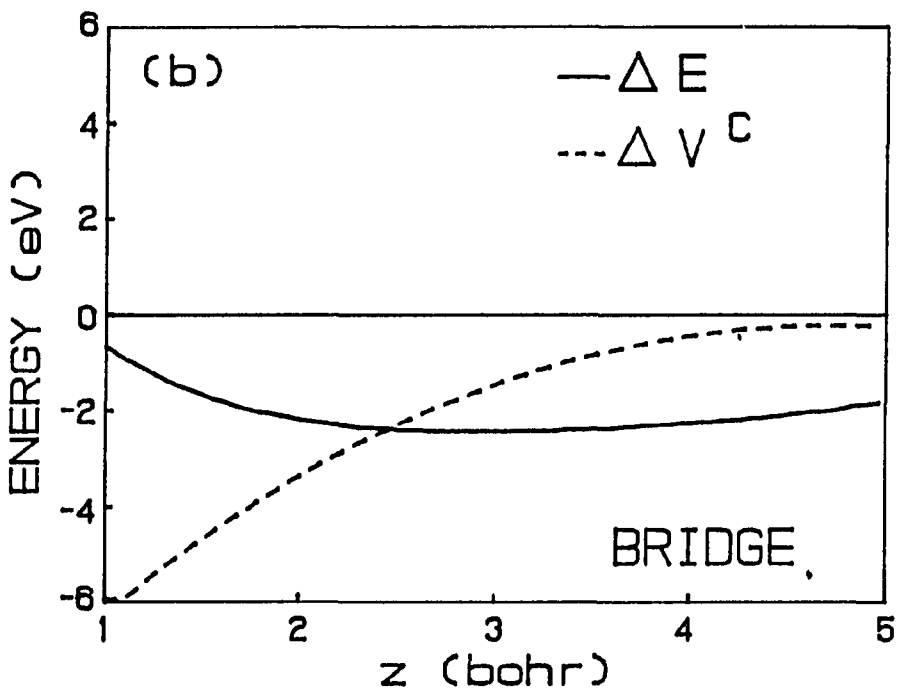
(b)
—Δ E
---Δ V C
BRIDGE
ENERGY (eV)
z (bohr)
6
4
2
0
-2
-4
-6
1
2
3
4
5

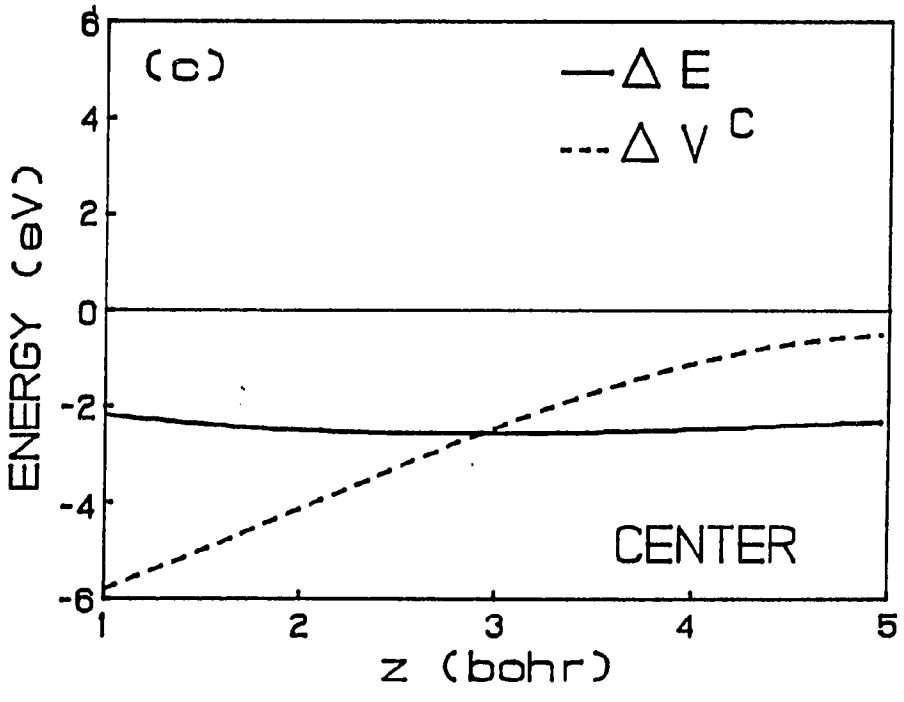


Figure 7 (Continued)

energy function $\Delta E_A(n_H)$ is nearly linear with respect to $n_H$ for $n_H > 0.005$ a.u. (see Fig. 1). Comparing $\Delta E^h$(atop), $\Delta E^h$(bridge) and $\Delta E^h$(center) indicates that the homogeneous electron density increases most quickly for the atop site as z is decreased. For the atop site the H atom samples the electron density of the Ni atom directly beneath it, whereas the bridge and sites lack a surface Ni atom directly below the H atom. This strong repulsion for $\Delta E^h$(atop) at larger z pushes the binding height out to 3.6 bohr. The difference in binding heights between the bridge and center sites is due to a combination of effects. The H atom does not have a Ni atom directly below on either site, but the bridge site provides 2 nearest Ni neighbors and the center site provides 4 nearest Ni neighbors to the H adatom. Comparing $\Delta E^h$(bridge) with $\Delta E^h$(center) indicates that the bridge site provides less sampled Ni electron density than the center site for $2 \leq z \leq 4.5$ bohr. If the binding was determined solely by $\Delta E^h$, the bridge site binding height would be less than the center site binding height. The correction energies are nearly identical for the two sites. But, $\Delta V^c$(center) drops off more quickly than $\Delta V^c$(bridge); thus $\Delta E$(center) minimizes at a smaller value of z than $\Delta E$(bridge). It is interesting to note the very shallow interaction potentials for the chemisorption onto the more open symmetry sites. As z decreases, $\Delta E^h$ approaches a large positive value and $\Delta V^c$ approaches a large negative value, with the sum of the two terms nearly canceling. This balance between $\Delta E^h$ and $\Delta V^c$ is similar to the balance between kinetic and potential energy provided by the virial theorem for diatomic molecules [36].

The variation in the binding energy with respect to symmetry site is

less pronounced and thus more difficult to understand. It is due to the same cancellation between $\Delta E^h$ and $\Delta V^c$ with $\Delta G$ remaining nearly constant between sites. In detail, we note that as the H atom approaches the surface, $\Delta E^h$ rises, $\Delta V^c$ decreases and $\Delta G$ decreases. Very subtle changes in the rate of increase and decrease in these three terms as we go from the atop site to the center site provide for an increase in binding energy of only 0.27 eV as shown in Table III.

Now we examine the sampling procedures for H atom chemisorption on the center site of Ni(100) using the $(3d^8, 4s^2)$ electron configuration. Potential energy curves and the components are shown in Figs. 8(a) and 8(b), for both the averaged and pointwise sampling procedures. Since $\Delta V^c$ is independent of the homogeneous electron gas density, any difference in the potentials due to the sampling procedure results from $\Delta E^h$ and $\Delta G$. $\Delta E^h$(averaged) rises much more steeply than $\Delta E^h$(pointwise) since the average sampling of the H atom electron density overlapping with the Ni cluster electron density provides a larger value of $n_H$ than the pointwise averaging procedure, at a given point z above the Ni surface (see Fig. 1, H atom). For a fixed position above the surface, $\Delta G$ becomes large and negative for large $n_H$ and $n_H$(averaged) is sufficiently large to be in this regime. However, $\Delta G$(averaged) does not become negative as quickly as $\Delta E^h$(averaged) becomes positive. By contrast, $n_H$(pointwise) is so much smaller that $\Delta G$(pointwise) increases as $\Delta E^h$(pointwise) increases. The net effect is that $\Delta E$(averaged) minimizes at a slightly larger binding energy and at a significantly smaller distance from the Ni surface than does $\Delta E$(pointwise). In fact, the nearly 1 bohr difference in binding height is the major

Figure 8. CEM-1 energy components for H atom chemisorption on the center site of Ni(100). Comparison of the averaged (AV) and pointwise (PW) sampling procedures using the Ni ground state Hartree-Fock electronic configuration. (a) Embedding energy and correction energy. (b) Binding potential and Coulomb energy

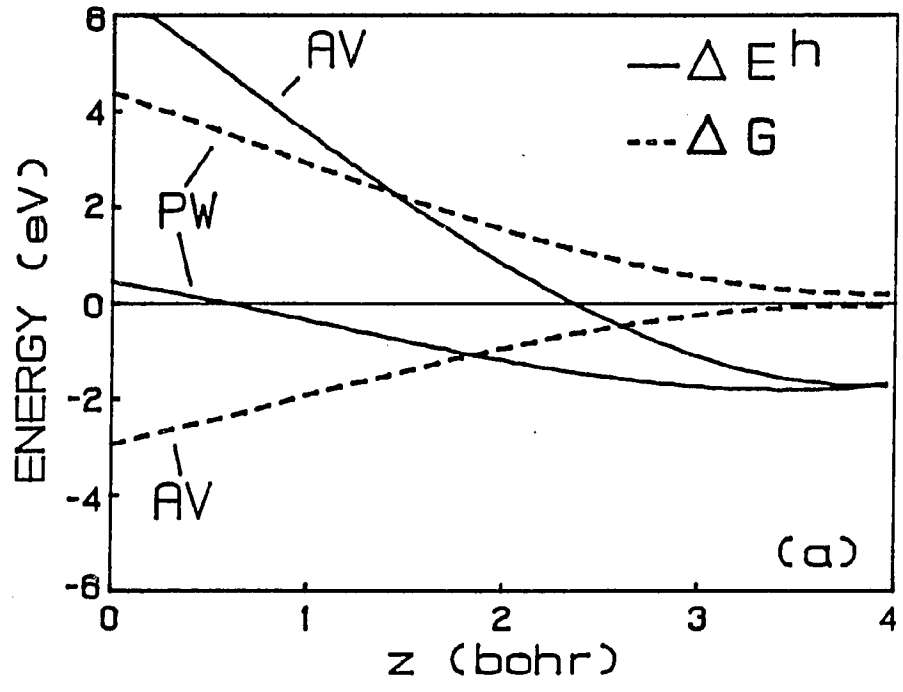
AV
—Δ Eh
---Δ G
PW
AV
(a)
ENERGY (eV)
z (bohr)
6
4
2
0
-2
-4
-6
0
1
2
3
4

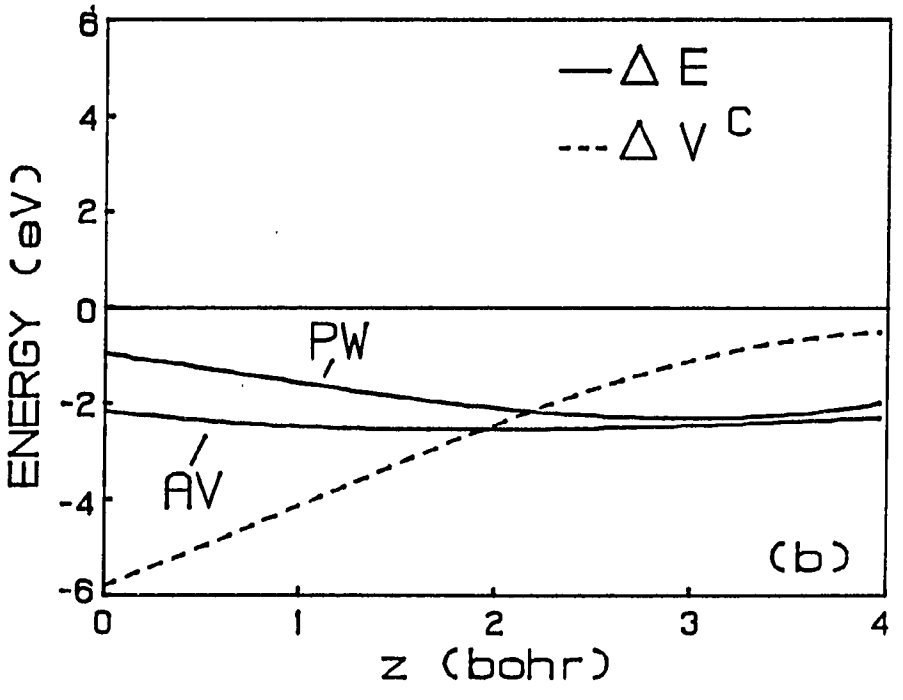
—Δ E
---Δ V C
PW
AV
(b)
ENERGY (eV)
z (bohr)
6
4
2
0
-2
-4
-6
0
1
2
3
4

practical reason for preferring the averaged sampling procedure over the pointwise sampling procedure. Of course, the averaged sampling procedure has the additional theoretical support of minimizing the correction energy and describing the binding through the use of overlapping electron densities between atomic centers.

Next we consider the effect of the valence electron configuration of the transition metal on the interaction potentials. This was investigated using the test case of H atom chemisorption on the center site of the Ni(100) surface. The Hartree-Fock (valence) ground state for Ni in this basis is $(3d^8, 4s^2)$. We compared energy curves using this Ni electron density with those calculated using the s → d promoted but unrelaxed configuration of $(3d^9, 4s^1)$ as presented in Fig. 9(a) and 9(b). The averaged sampling procedure was employed for both configurations. The main difference between the chemisorption potentials at the minimum, $z \sim 2.0$ bohr, is due to the contributions from $\Delta E^h$ and $\Delta V^c$. Again, the $\Delta E^h$ curves result from the repulsive part of $\Delta E_A(n_H)$. The overlap of the H atom electron density with the doubly occupied 4s orbitals of the $(3d^8, 4s^2)$ configuration is larger than the overlap with the singly occupied 4s orbital of the $(3d^9, 4s^1)$ configuration. This provides a larger value of $n_H$, yielding $\Delta E^h(3d^8) > \Delta E^h(3d^9)$. Removal of a 4s electron also affects the Coulomb interaction through a change in the shielding of the nuclear charge of the Ni which yields $\Delta V^c(3d^8) < \Delta V^c(3d^9)$. The decreased Coulombic energy barely beats the increase in the embedding and correction energies, thereby yielding a larger binding energy for the $(3d^8, 4s^2)$ configuration by $\sim 0.15$ eV.

Figure 9. CEM-1 energy components for H atom chemisorption over the center site on Ni(100). Comparison of the Ni ($3d^8$, $4s^2$) ground state and the ($3d^9$, $4s^1$) promoted state electronic configurations (denoted by 3d8 and 3d9 respectively), using the averaged sampling procedure. (a) Embedding energy and correction energy. (b) Binding potential and Coulomb energy

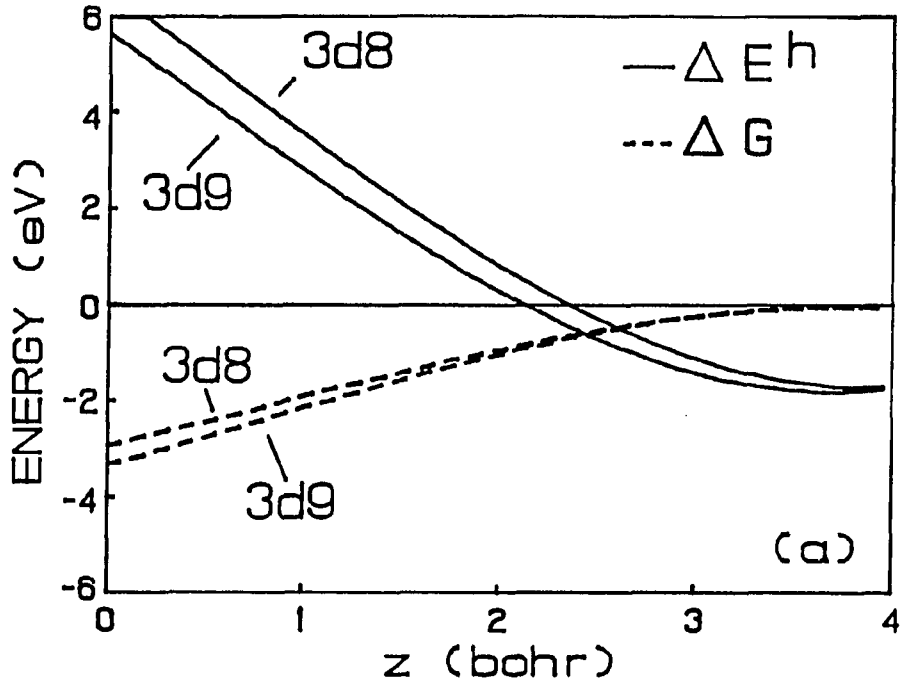
6
4
2
0
-2
-4
-6
ENERGY (eV)
3d8
3d9
—Δ E h
---Δ G
3d8
3d9
(a)
0
1
2
3
4
z (bohr)

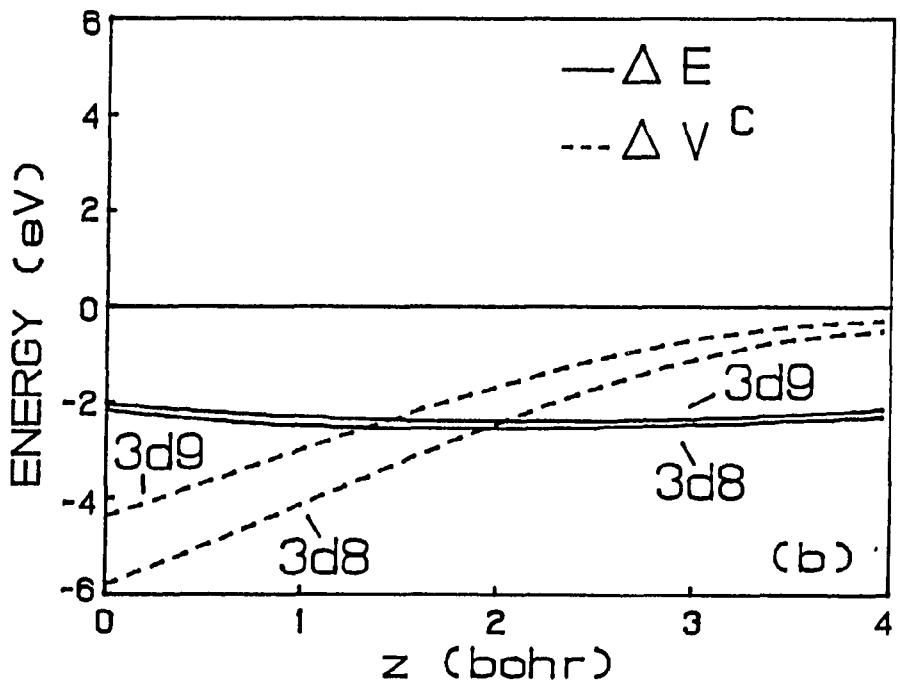
6
4
2
0
-2
-4
-6
ENERGY (eV)
—Δ E
---Δ V C
3d9
3d9
3d8
3d8
(b)
0
1
2
3
4
z (bohr)

We might emphasize that the valence electron configuration yields a small difference for the interaction potential of an H atom with clusters of metal atoms. A much larger effect would be expected if one calculated Ni-Ni interactions in bulk Ni metal or clusters of Ni atoms. The only role of the Ni cluster in CEM-1 theory is to provide a source of electron density for the H-Ni interaction.

Finally we address the question as to whether spin-polarized or spin-unpolarized electron densities should be used. For all our previous discussion on H atom chemisorption, we used a spin-polarized, $\phi = 1$, 1s electron density for the H atom. Consider the interaction of a spin-unpolarized ($\phi = 0$), 1s electron of an H atom with the unpolarized Ni cluster of $(3d^8, 4s^2)$ configuration. We will refer to the polarized H atom case as POL and the unpolarized H atom case as UNPOL.

Since the sampling procedures, embedding energy functions, and Coulomb interactions are independent of spin density, the only difference between the POL and UNPOL potentials is the contribution from the correction term. As shown in Table III, the UNPOL binding energy is ~ 0.25 eV larger than the POL binding energy. Upon examination of the contributions to the correction energy, we found that the many-body energy $\Delta G[AB]$ is nearly the same (to within 0.06 eV) for $\Delta E$(POL) and $\Delta E$(UNPOL) around the minima. The 0.3 eV difference is due solely to $-\Delta E_A^{GK}(n_H)$. The effect of the latter can be determined by noting that the kinetic energy of interaction for a spin-unpolarized atom A in jellium is greater than for a spin-polarized atom in jellium for the same value of $n_H$. (Here, interaction energy $\equiv \{E[A + H] - E[A] - E[H]\}$ with $E[\ ]$ evaluated with the appropriate functionals.) The

exchange and correlation energies act in exactly the opposite manner, but at high $n_H$ the kinetic energy dominates. Near $z_e$, the values of $n_H$ are in this high $n_H$ limit. Thus, $\Delta E_A^{GK}(n_H)(UNPOL) > \Delta E_A^{GK}(n_H)(POL)$, and the binding energy of the UNPOL system is greater by 0.25 eV than the binding energy of the POL system. As confirmation of this argument, we used the pointwise sampling procedure in the above analysis which leads to a decrease of $n_H$ by an order of magnitude. This decrease in $n_H$ changes the relative sizes of $\Delta E_A^{GK}(n_H)(UNPOL)$ and $\Delta E_A^{GK}(n_H)(POL)$ so that the kinetic energy effect discussed above vanishes, and thus $\Delta E(POL) \approx \Delta E(UNPOL)$ at the minimum of the two curves.

It is interesting to note that the EM results in Table III are in excellent agreement with the CEM-1 values using the unpolarized H atom. This indicates that the CEM-1 theory yields results equivalent to the EM theory upon use of unpolarized densities. It also provides a quantitative estimate of the accuracy of the approximations in the EM theory.

We believe that the description of the H atom on the metal cluster surface using the spin-polarized atom is appropriate for the following reason. When employing the CEM-1 theory we do <u>not</u> adjust the spin density of an interacting system as a function of internuclear separations within that system. We must use a reasonable "guess" for the spin density which will approximate the self-consistently determined density in all situations. As we saw earlier in the paper, the description of the $H_2$ molecule with the CEM-1 theory using spin-unpolarized densities was considerably worse than using spin-polarized densities. There the spin played a more important role in forming a spin paired bond, which lowered

the interaction potential considerably. In addition, for the treatment of $H_2$ dissociative chemisorption onto metal surfaces, H atom chemisorption is an asymptote of the reaction coordinate for molecular dissociation. Consistency in the CEM theory requires that we use spin-polarized densities for the $H_2$ molecule and for the H atom chemisorption.

Finally, we compare the CEM-1 potentials to those derived using other methods and to the experimentally determined bonding characteristics as presented in Table III. For the CEM-1 results, we use the potential derived from the averaged density sampling, a spin-polarized H atom, and the Hartree-Fock ground state configuration ($3d^8$, $4s^2$). This potential predicts a binding energy of only 0.17 eV less than the experimental value, while the predicted binding height is almost twice as large as the experimental number. The apparent lack of agreement for the binding height is due to the fact that the CEM-1 potential curve is very flat in the region around the minimum for the center site on Ni(100). This flatness provides an uncertainty of $\sim 0.2$ bohr in $z_e$ simply due to the finite number of points calculated on the curve. In addition, the precision of the CEM-1 calculations may also yield uncertainties in this value.

Other calculations of these potentials are based upon self-consistent solutions of the Kohn-Sham LD problem for a monolayer of H atoms on a slab of Ni atoms corresponding to the LD values [29] in Table III. As is the case for the application of LD calculations applied to many different types of interacting systems, the predicted equilibrium geometries agrees fairly well with experiment, but the binding energies are overestimated by a large percentage.

The most rigorous calculations of absorbate-metal surface interactions involve self-consistent ab initio molecular orbital (MO) or Generalized Valence Bond (GVB) methods (including CI). A cluster of metal atoms is constructed and the total energy is minimized for the absorbate bound to this cluster. The binding energy converges slowly with respect to metal cluster size since the methods do not describe the delocalized behavior of the conduction band electrons on the metal surface very well. Upton and Goddard [30] used the GVB method (with an effective core potential for Ni) to predict H atom chemisorption potentials using a 20 atom Ni cluster. Their binding height compares favorably to the experimental value but the binding energy is too large with respect to the experimental number. Note that Upton and Goddard pointed out that even for a 28 atom Ni cluster the GVB orbital structure near the Fermi level of the cluster fails to mimic the bulk band structure.

The CEM-1 chemisorption binding energies and binding heights for H atom on two other transition metal surfaces, Fe(110) and Cu(100), are provided in Table IV. Only the center site potentials are presented using the averaged density sampling procedure. The metal cluster electron densities were constructed as for Ni and the H atom was assigned a spin-polarized 1s electron. The experimental lattice constants (Cu = 6.82 bohr, Fe = 5.42 bohr) were used to fix the geometries of the respective clusters. The Cu(100) surface contained the same 25 atom arrangement as Ni(100) for the center site, whereas for the Fe(110) center site we used a 22 atom cluster consisting of the arrangement (10, 10, 2). The position of the center site within the surface unit cell is illustrated in Fig. 5.

Also presented in Table IV are the experimental, EM, and Hartree-Fock (available for Cu only) binding energies, along with the CEM-1 potentials calculated with an unpolarized H atom and with the promoted ($s \rightarrow d$) configured electron density. The use of an unpolarized H atom increases the binding energy by 0.2-0.3 eV with respect to the polarized H atom potential, just as for the Ni(100) surface. The ($3d^{10}$, $4s^{1}$) configured Cu cluster more closely mimics the true bulk Cu band structure by filling the d-band and partially occupying the s-band. But, like on the Ni(100) surface, the binding energy is decreased by 0.14 eV. The H atom prefers the additional diffuse electron density provided by the two 4s electrons in the ($3d^{9}$, $4s^{2}$) configuration. Comparing the three CEM-1 potentials for Ni, Cu and Fe determined using the ($3d^{n}$, $4s^{2}$) configuration, we find that the binding energies are equal to within 0.2 eV. The CEM-1 binding heights show a larger variation which reflects the packing of the various surface atoms on each of the metal surfaces.

The binding height and energy from the Hartree-Fock SCF-CI calculation of Madhaven and Whitten [32] for the chemisorption on Cu(100) is in excellent agreement with the CEM-1 calculated value and both values are in good agreement with the experimental binding energy. Although, the binding energies predicted by the CEM-1 theory are comparable in accuracy to the EM values, the CEM-1 calculations do not correctly predict the trend of increased binding energy for the Fe(110) surface versus the Cu(100) surface while the EM calculations do predict this trend correctly. Perhaps the additive density approximation is less adequate for Fe versus Cu and this affects the CEM-1 values more than the EM values.

# SUMMARY AND CONCLUSIONS

We have derived an effective medium theory, CEM-1, which describes the binding between an atom and an inhomogeneous host. The zeroth order term of the CEM-1 interaction is represented by the embedding energy of the atom into a spin-unpolarized homogeneous electron gas. The Coulomb interactions between the atom and the host are accounted for by an explicit evaluation of the electrostatic interactions between the atom charge density and the host charge density. The difference in kinetic, exchange and correlation energies (the correction energy term) between the homogeneous electron gas and the inhomogeneous host is provided by using a spin-polarized density functional evaluation. Both the Coulomb and correction energy terms are calculated using a superposition of atomic densities approximation. The contribution from the correction energy can be minimized by constructing the appropriate homogeneous electron gas density using the averaged sampling procedure. This minimization ensures that the non-self-consistent terms which depend upon the homogeneous electron gas density are as small as possible. The embedding energy provides the many-electron energy, which is difficult to calculate self-consistently for a real inhomogeneous host, via a self-consistent treatment of the atom embedded in an homogeneous electron gas. It is worthwhile to note that the CEM formalism can be interpreted as a spin-polarized generalization of the Gordon-Kim electron gas model where a self-consistent reference system, the atom in jellium, is used instead of the original reference system, vacuum.

We applied the CEM-1 theory to the description of an H atom embedded into a spin-polarized homogeneous electron gas and obtained good results in comparison to SCF-LD values. This application provided a test of the ability of the correction energy term to predict the effects of a spin-polarized perturbation to the zeroth order CEM-1 system.

We also used the CEM-1 theory to calculate the binding potentials for a set of hydrogen containing diatomic molecules. In general, we found that the use of spin-polarized atomic densities and an averaged homogeneous density sample provided the best CEM-1 potentials both in terms of binding energy and equilibrium bond length. Also, the CEM-1 potentials were better when we embedded the more electronegative atom into the more electropositive one. This trend was explained in terms of the ability of the host atom to mimic the homogeneous electron gas with respect to donation of electrons to the embedded atom.

The most detailed application involved chemisorption of H atoms on three different transition metal surfaces, Ni(100), Cu(100) and Fe(110). Representing the metal surface by a finite cluster of spin-unpolarized metal atoms, we examined the chemisorption binding potentials as a function of: 1) the symmetry site within the surface unit cell, 2) the homogeneous electron density sampling procedure, 3) the spin polarization of the H atom, and 4) the occupation of the valence 4s electron density of the metal. The H atom preferred the symmetry site which provided the most metal atom nearest neighbors because the electrostatic attraction slightly exceeds the kinetic-exchange-correlation energy repulsion between the H atom electron density and the metal atom electron densities. For example,

the center site on Ni(100) is more stable than the bridge and atop sites by ~ 0.1 and ~ 0.2 eV. The options implemented within the CEM-1 theory which generated potentials most consistent with experiment were the use of the averaged sampling procedure and spin-polarized H atom spin density. Within the superposition approximation of atomic Hartree-Fock spin densities, we compared the CEM-1 potentials generated with both the ground state valence configuration ($3d^n$, $4s^2$) and the promoted but unrelaxed configuration ($3d^{n+1}$, $4s^1$) for both Cu and Ni. The resulting CEM-1 potentials predicted that the H atom bond with the ground state cluster is stronger than the bond with the promoted cluster by 0.14 eV for Cu and 0.17 eV for Ni over the stable center site.

Although the CEM-1 theory provided an adequate description of chemical binding, we can envision a couple of extensions to the theory. Future atomic chemisorption investigations could include experimentation with the metal cluster spin density by spin pairing the surface cluster atoms nearest to the absorbate with the spin density of the absorbate, thus forming a multicenter spin paired bond. This spin pairing could be determined via a limited self-consistent CEM-1 calculation by allowing only these spin densities in question to vary. Another desirable feature, which is neglected in the CEM-1 theory, is the description of the host back-bonding with the embedded atom. In terms of the (A → B) embedding scheme, both the perturbation of the embedding atom A on the energy of the B cluster of atoms, as well as the binding between the atoms in B, is not included. In short, CEM-1 is a one-(active)-body theory. Backbinding can be included by deriving a N (active)-body theory (the subject of Paper III)

where each body within the set of N-bodies is embedded into each other. Using this formalism, a consistent treatment of molecular chemisorption is then possible. Consider the 3-(active)-body system of an $A_2$ molecule chemisorbing onto a B surface. Here we would embed each A atom into both the surface B and the other A atom as well as embed the surface B into both A atoms, thus allowing for backbinding. Molecular chemisorption is the subject of a forthcoming paper [10].

## ACKNOWLEDGEMENTS

We thank Professor J. K. Norskov for a preprint of ref. [8] and Dr. M. J. Puska for the communication of unpublished results. Support of this work by NSF grant CHE-8403820 is gratefully acknowledged.

# REFERENCES


1. "Modern Theoretical Chemistry", edited by H. F. Schaefer, III, Plenum, New York, 1977, Vols. 3 and 4.
2. W. Kohn and L. J. Sham, Phys. Rev. A 140, 1133 (1965).
3. J. K. Norskov and N. D. Lang, Phys. Rev. B 21, 2131 (1980); J. K. Norskov, Phys. Rev. B 26, 2875 (1982).
4. M. Stott and E. Zaremba, Phys. Rev. B 22, 1564 (1980).
5. a) "Many-Body Phenomena at Surfaces", edited by D. Langreth and H. Suhl, Academic, New York, 1984, Chapters 1, 2, and 3; b) W. Kohn, in "Theory of the Inhomogeneous Electron Gas", edited by S. Lundqvist and N. H. March, Plenum, New York, 1983.
6. a) M. J. Puska, R. M. Nieminen and M. Manninen, Phys. Rev. B 24, 3037 (1981); b) supplemented by M. J. Puska, Helsinki University of Technology, Helsinki, Finland, private communication.
7. a) P. Nordlander, S. Holloway, and J. K. Norskov, Surf. Sci. 136, 59 (1984); b) B. Chakraborty, S. Holloway, and J. K. Norskov, Surf. Sci. 152/153, 660 (1985); c) K. W. Jacobsen and J. K. Norskov, Surf. Sci. 166, 539 (1986).
8. a) K. W. Jacobsen, J. K. Norskov and M. J. Puska, Phys. Rev. B 35, 7423 (1987); b) M. Manninen, Phys. Rev. B 34, 8486 (1986).
9. R. G. Gordon and Y. S. Kim, J. Chem. Phys. 56, 3122 (1972).
10. J. D. Kress and A. E. DePristo, "Corrected Effective Medium Method. IV. Applications to hydrogen molecular chemisorption potentials", in preparation.

11. J. D. Kress and A. E. DePristo, "Corrected Effective Medium Method. II: N-body formulation", J. Chem. Phys., submitted.

12. O. Gunnarsson and B. I. Lundqvist, Phys. Rev. B 13, 4274 (1976).

13. P. Carsky and M. Urban, "Ab Initio Calculations", Springer, Berlin, 1980.

14. U. von Barth and L. Hedin, J. Phys. C 5, 1629 (1972); G. L. Oliver and J. P. Perdew, Phys. Rev. A 20, 397 (1979).

15. P. Hohenberg and W. Kohn, Phys. Rev. 136, B864 (1964).

16. C. H. Hodges, Can. J. Phys. 51, 1428 (1973).

17. A. E. DePristo and J. D. Kress, Phys. Rev. A 35, 438 (1987).

18. P. A. M. Dirac, Proc. Cambridge Philos. Soc. 26, 376 (1930).

19. A. E. DePristo and J. D. Kress, J. Chem. Phys. 86, 1425 (1987).

20. a) S. H. Vosko, L. Wilk, and M. Nusair, Can. J. Phys. 58, 1200 (1980); b) J. P. Perdew. Phys. Rev. B 33, 8822 (1986).

21. M. Waldman and R. G. Gordon, J. Chem. Phys. 71, 1325 (1979); M. J. Clugston and R. G. Gordon, J. Chem. Phys. 66, 244 (1977).

22. P. S. Bagus, T. L. Gilbert and C. J. Roothaan, J. Chem. Phys. 56, 5195 (1972); NAPS Document No. 01767 from ASIS National Auxillary Publication Service, c/o CCM Information Corp., 866 Third Ave. New York, NY 10022.

23. G. Kemister and S. Nordholm, J. Chem. Phys. 83, 5163 (1985).

24. K. P. Huber and G. Herzberg, "Molecular Spectra and Molecular Structure. IV. Constants of Diatomic Molecules", Van Nostrand and Reinhold, New York, 1979.

25. M. L. Plummer and M. J. Stott, J. Phys. C 18, 4143 (1985).

26. M. S. Daw and M. I. Baskes, Phys. Rev. B 29, 6443 (1984); S. M. Foiles, M. I. Baskes, and M. S. Daw, Phys. Rev. B 33, 7983 (1986).

27. F. J. Arlinghaus, J. G. Gay, and J. R. Smith, in "Theory of Chemisorption", edited by J. R. Smith, Springer, Berlin, 1980 and references therein.

28. M. D. Morse, Chem. Rev. 86, 1049 (1986).

29. C. Umrigar and J. W. Wilkins, Phys. Rev. Lett. 54, 1547 (1985).

30. T. H. Upton and W. A. Goddard III, Phys. Rev. Lett. 42, 472 (1979).

31. a) I. Stansgaard and F. Jacobsen, Phys. Rev. Lett. 54, 711 (1985); b) S. Anderson, Chem. Phys. Lett. 55, 185 (1978).

32. P. Madhavan and J. L. Whitten, J. Chem. Phys. 77, 2673 (1982).

33. a) G. D. Kubiak, G. O. Sitz, and R. N. Zare, J. Chem. Phys. 83, 2538 (1985); b) A. R. Gregory, A. Gelb, and R. Silbey, Surf. Sci. 74, 497 (1978) as deduced from J. Pritchard and F. C. Tompkins, Trans. Faraday Soc. 56, 500 (1977) for Cu thin films.

34. F. Bozso, G. Ertl, and M. Weiss, J. Catalysis 50, 519 (1977).

35. C. Kittel, "Introduction to Solid State Physics", Wiley, New York, 1971.

36. I. N. Levine, "Quantum Chemistry", 2nd ed., Allyn and Bacon, Boston, 1974.

# PAPER III.

## CORRECTED EFFECTIVE MEDIUM METHOD.

## II. N-BODY FORMULATION

# CORRECTED EFFECTIVE MEDIUM METHOD.

# II. N-BODY FORMULATION

Joel D. Kress and Andrew E. DePristo

Department of Chemistry
Iowa State University
Ames, Iowa 50011

## ABSTRACT

A general corrected effective medium (CEM) theory is presented which yields the interaction energy of an N atom system, in contrast to the previous version of the CEM theory which provides the energy of one atom interacting with the other (N-1) atoms acting as a host. The CEM method presented herein treats all N atoms on an equal basis without identifying all but one as a host, and is referred to by the acronym CEM-N. The basis for this theory involves expressing the interaction energy for the real system in terms of the sum of the interaction energies for each atom embedded into a homogeneous electron gas with compensating positive background (i.e., the effective medium is jellium). Minimization of the difference in kinetic-exchange-correlation energy between the real and effective system, evaluated using density functionals, yields the prescription for choice of the electron densities of each jellium system. The full interaction energy then consists of three terms: the embedding energy, Coulombic energy, and kinetic-exchange-correlation difference energy. Applications and tests for a variety of homonuclear diatomic molecules are presented. These results illustrate the need for a new set of "covalent" embedding energies, which are constructed semi-empirically in the present article.

# INTRODUCTION

The calculation of interaction energies in systems of more than a few many-electron atoms is a formidable problem. Conventional methods of *ab initio* quantum chemistry, including extensive configuration interaction, provide the most accurate methodology for such calculations in principle, but are limited in practice to the smallest clusters by the sheer number of electrons in many-particle systems [1]. For larger systems, one is restricted to the use of rather small basis sets and either SCF or very limited CI calculations [2-5]. Density functional methods in the Kohn-Sham local density formalism (i.e., SCF-LD) address the difficulties involved with the incorporation of electron correlation but still suffer from basis set limitations [6-10]. In addition, the exchange-correlation energy functional of the electron density, $E_{xc}(n)$, is not represented to chemical accuracy for systems of atoms within this local density approximation [11-13]. This problem may be alleviated by the recent development [11-13] of accurate non-local $E_{xc}(n)$, but such a conclusion must await further numerical testing.

In a recent article [14], we presented an approach to the calculation of the interaction energy for an atom A interacting with a cluster of other atoms, B. Following the brilliant effective medium idea due to Norskov and coworkers [15-17] and Stott and Zaremba [18], we replaced the original A-B system, which has low spatial symmetry, by the atom embedded in a spin-unpolarized jellium system, which has a high spatial symmetry. The atom in jellium, A-J, is defined as the effective system where the jellium

is the effective medium. The A-J system is nearly ideal for the SCF-LD approach, and the results of self-consistent calculations for most atoms through Zn at a variety of densities of the electron gas are known [19]. Since the real system differs from the A-J one due to inhomogeneities and spin polarization of the electron density and due to the point charge of the nuclei, we determined non-self-consistent corrections between the two systems. These involved both Coulombic and kinetic-exchange-correlation energies. The latter were calculated using spin-polarized density functionals for the kinetic [20,21], local exchange and local correlation [22] energy. These corrections were minimized by proper identification of the homogeneous electron gas density corresponding to the real system. This theory is referred to as the corrected effective medium method for a one atom embedding scheme, or CEM-1 for short.

There are two major difficulties with the CEM-1 theory. Both stem from the fact that a single atom is identified as the active body with the remainder of the system identified as the host. The first problem involves the lack of symmetry which restricts the results of the CEM-1 method to the interaction energy of one atom with a host. For an N-body system, this asymmetry can be partially removed by sequentially identifying each atom as the active body and the remaining (N-1) atoms as the host, and repeating the calculations N times. Explicitly, one embeds atom 1 into 2 + 3 + ... + N; then, atom 2 into 1 + 3 + 4 + ... + N; etc.; up to atom N into 1 + 2 + ... + (N-1). However, this approach yields the interaction energies of N individual atoms in an (N-1) atom cluster, not the energy difference between the N atom cluster and the N isolated atoms. Furthermore, these N

individual interaction energies cannot provide a unique cluster stabilization energy. This lack of uniqueness occurs even in a more sophisticated sequential embedding scheme: atom 1 embedded into 2 + 3 + ... + N; atom 2 embedded into 3 + 4 + ... + N; etc.; up to atom (N-1) embedded into N. The second problem is more subtle. The division into an active atom and a host assumes that the active atom has a negligible influence on the bonding in the host system. Such an approximation will be adequate for weak chemical bonding but will become increasingly poor as the atom-host interaction becomes as strong as the interaction among the host atoms.

In this paper, we develop the theory for a completely symmetric treatment of all atoms in the system, referred to as CEM-N. As an added benefit, this formalism is sufficiently general to allow the derivation of any CEM theory with a reduced number of active atoms, M, chosen from the set of N atoms. Two different analytic formulae are derived for the determination of the proper jellium density for use in this CEM-N theory. A discussion of the factors leading to differences in binding between the real and homogeneous systems is presented, and new semi-empirical universal embedding functionals are determined. Applications are restricted to homonuclear diatomic molecules up to $F_2$ in order to illustrate the salient features of the CEM-N theory in the simplest bonding cases. These are also the most difficult cases for the CEM-N theory to treat since they are most unlike the bonding in extended near-homogeneous systems. In the Appendix, a point of considerable practical importance, namely the accurate numerical calculation of three-dimensional multicenter integrals, is addressed.

# THEORY

## N-body Corrected Effective Medium Formalism (CEM-N)

Consider an N-body system consisting of atoms $\{A_i, i=1,\ldots,N\}$, where the $A_i$ can be either the same or different types of atoms. We wish to determine the energy difference between the interacting and non-interacting system of atoms, denoted by

$$\Delta E(\{A_i\}) = E(\sum A_i) - \sum E(A_i) \ . \qquad (1)$$

The basic idea of the CEM approach is to evaluate this energy difference by using the energy of the atoms embedded into jellium [19], i.e., a homogeneous electron gas with compensating positive background. The motivation for this approach is clear when the number of atoms becomes large, with each one interacting with the 'nearly-uniform' electron density due to all of the others. However, it is not apparent that such an approach is useful in treating much smaller and/or much more inhomogeneous systems. Since many phenomena which are chemically interesting involve the interaction of a small molecule with a large cluster, (e.g., dissociation of a diatomic molecule on a metal surface), it is necessary to develop a formalism which can treat both small inhomogeneous systems and large nearly-uniform systems with comparable accuracy.

The mathematical implementation of the CEM idea involves rewriting the energy difference in Eq. (1) in terms of the embedding energy for atom $A_i$ in jellium of density $n_i$, defined by

$$\Delta E_J(A_i;n_i) = E_J(A_i;n_i) - E_J(n_i) - E(A_i) \ . \qquad (2)$$

Here, $E_J(n_i)$ and $E_J(A_i;n_i)$ are the energies of the jellium and jellium plus atom $A_i$ system, respectively. The atom energy $E(A_i)$ common to Eqs. (1) and (2) can be used to combine the two equations. This leads to the first fundamental relationship of the CEM-N theory:

$$\Delta E(\{A_i\}) = \sum \Delta E_J(A_i;n_i) + E(\sum A_i) - \sum [E_J(A_i;n_i) - E_J(n_i)] \ . \qquad (3)$$

In this equation, the first term on the right hand side is the sum of the embedding energies for each atom in jellium of some (as yet unspecified) density $n_i$. These energies can be evaluated from the self-consistent local density calculations of Puska et al. [19] or from other semi-empirical methods as discussed later in this section. We emphasize three points concerning these embedding energies: 1) they already contain self-consistent solutions and/or experimental information; 2) they are readily available; 3) for each atom, they are universal <u>functions</u> of only the jellium density. The form of the remaining three terms in Eq. (3) and the choice of the densities $n_i$ are addressed next.

The energy is composed of Coulombic, kinetic, exchange and correlation parts. We denote this separation by

$$E(\{A_i\}) = V_C(\{A_i\}) + G(\{A_i\}) \ , \qquad (4)$$

where $V_C$ is the Coulombic energy and G is the sum of the kinetic and exchange-correlation energies, T and $E_{XC}$ respectively. Substitution of

Eq. (4) into Eq. (3) yields the second fundamental relationship of CEM-N theory

$$\Delta E(\{A_i\}) = \sum \Delta E_J(A_i;n_i) + \Delta V_C + \Delta G(\{A_i\}) \ , \tag{5a}$$

where

$$\Delta G(\{A_i\}) = G(\sum A_i) - \sum [G_J(A_i;n_i) - G_J(n_i)] \ . \tag{5b}$$

Eq. (5a) expresses the stabilization energy of the N-body cluster as a total of three terms:

1. the sum of the embedding energies for the atoms in jellium;
2. the difference in the Coulombic energy between the real system and all the atoms in jellium; and
3. the difference in the sum of the kinetic, exchange, and correlation energies between the real system and all the atoms in jellium.

This decomposition is useful since the physical factors contributing to $\Delta V_C$ and $\Delta G$ can be identified. (This should be contrasted with purely empirical treatments such as the embedded atom method [23] which would replace the last two terms in Eq. (5a) by an empirical summed two-body potential, and would not use the same procedure to determine the $n_i$.)

For $\Delta V_C$, there are two physical effects. The first is the difference in homogeneity between the electron density distributions in the real and atom-jellium systems. The second is the difference between the uniform positive background in the jellium and the point nuclear charges in the

real system. For $\Delta G$, there are also two effects. The first, and most important, is again the difference in uniformity of the electron density distributions. The second is the difference in spin polarization between the real system and the unpolarized jellium. This spin difference was central to the description of spin pairing in chemical bonding for CEM-1 and will also be tested for CEM-N.

Since evaluation of Eq. (5a) from first principles would be as difficult as evaluation of the original Eq. (1), progress requires an approximate evaluation of Eq. (5a) based upon some ansatz about the relationships between the electron density of the N-atom system and that of the N individual atoms. (The same ansatz must be applied to the A-J system versus the A and J separately.) In this regard, we note that the effects described in the previous two paragraphs do not vanish even within the approximation of superposition of electron densities for each system. In addition, since a difference between the energetics in the real vs. jellium systems is calculated, we expect that this difference will be less sensitive to the use of accurate electron densities than the direct calculation of energetics in either system by itself, assuming of course that the proper density in the jellium is used. In other words, a self-consistent calculation is always being employed via the $\Delta E_J(A_i;n_i)$ and only the corrections due to inhomogeneity and spin polarization of the electron and positive charge distribution are being calculated non-self-consistently.

Accurate implementation of the CEM-N theory depends upon solution of three problems. First, a proper choice of the jellium density must be

determined. Second, accurate spin density functionals must be utilized for the kinetic, exchange and correlation energies. Third, the calculation of the multicenter three-dimensional integration over the functionals of the electron density must be performed precisely and efficiently. These are addressed after discussing the treatment of $\Delta V_c$.

We assume that the electron density at any point in space, $\underline{r}$, is the sum of the spin densities from each atom:

$$n+(\underline{r}) = \sum n+(\underline{r};A_i) \tag{6a}$$

$$n-(\underline{r}) = \sum n-(\underline{r};A_i) \ , \tag{6b}$$

where n+ and n- refer to spin-up and spin-down electrons, respectively. This superposition of atomic densities is the major approximation in implementation of the theory. But without this assumption or some analogous simplification, application of the CEM-N formalism would be just as complicated in principle as a self-consistent solution of the original N-body cluster problem, (using spin density functional theory within a density formulation and not within the Kohn-Sham [24] wavefunction approach). Since the additive density approximation is assumed to hold for each atom in the jellium also, the electrostatic interaction in the jellium system vanishes. The difference in Coulombic energies is then given by that of the real system only:

$$\Delta V_c = \sum_{i<j} \sum \int [n(A_i)-Z_i \delta(\underline{r}_1-\underline{R}_i)][n(A_j)-Z_j \delta(r_2-R_j)] \ r_{12}^{-1} \ d\underline{r}_1 \ d\underline{r}_2 \ , \tag{7}$$

where $n(A_i)$ is the total electron density of atom $A_i$ with nuclear charge $Z_i$ located at $\underline{R}_i$. This summation of standard electron-electron, electron-nuclear, and nuclear-nuclear integrals can be evaluated either by analytical methods [25], or by direct numerical quadrature provided either $n(A_i)$ or $n(A_j)$ is spherically symmetric.

The determination of the jellium electron density is considered next. Since the non-self-consistent part of the CEM-N formalism is not expected to be as accurate as the self-consistent part, we propose to minimize the former just as in CEM-1 [14]. For the same reasons detailed in the CEM-1 development, this requires minimization of $\Delta G$ with respect to the $\{n_i\}$. Now,

$$G(n) = T(n) + E_X(n) + E_C(n) \ , \tag{8}$$

where the right hand terms are the kinetic, exchange and correlation energy functionals of the electron density, expressed as integrals of the general form,

$$F(n) = \int \{f[n+(\underline{r}), \nabla n+(\underline{r})] + f[n-(\underline{r}), \nabla n-(\underline{r})]\} \, d\underline{r} \ . \tag{9}$$

Since the integrands are complicated functions of both the spin densities and their gradients, an analytic minimization of $\Delta G$ is not possible, and a numerical minimization would not provide insight into the proper choice of the jellium densities. However, we can make progress by using the following argument just as in CEM-1 [14].

Let f=t, $\varepsilon_x$, and $\varepsilon_c$ denote the integrands of the functionals T, $E_x$ and $E_c$, respectively. We focus on the spin-up density n+ for concreteness; the analogous argument holds for the spin-down density n-. It is true that $t > 0$ and $\varepsilon_x < 0$ for all densities and gradients, and that for large densities and/or gradients $t > \varepsilon_x$. Since the leading term in t is $C_k n+^{5/3}$ and that in $\varepsilon_x$ is $C_x n+^{4/3}$, (where $C_k = (3/10)(6\pi^2)^{2/3}$ and $C_x = -(3/2)(3/4\pi)^{1/3}$ are constants [11,12,20,21,26]), we examine the variation of the sum of these leading terms with n+. This is shown in Fig. 1 for the density range that is important in chemical bonding. The function can be approximated quite closely by a quadratic in n+, as is also shown in Fig. 1. Since $|\varepsilon_c| << t$ and $\varepsilon_c << |\varepsilon_x|$, we can use the quadratic form for G(n) in order to provide an analytic solution of the minimization. However, we emphasize that the full functional will be used in numerical calculations of ΔG and that the approximation is only necessary to find an analytic choice for the density $n_i$. The CEM-N energies are not invariant to arbitrary changes in $n_i$ because the ΔG terms are not calculated self-consistently, and thus an optimal choice of $n_i$ is important. However, small variations of $n_i$ do not alter the CEM-N energies because of a cancellation between the embedding energies and ΔG. Within the above quadratic approximation for both n+ and n-, we have

$$G(n) \approx C \int \{n+(\underline{r})^2 + n-(\underline{r})^2\}\, d\underline{r} + D \int \{n+(\underline{r}) + n-(\underline{r})\}\, d\underline{r} , \qquad (10)$$

where C and D are proportionality constants provided in Fig. 1. Using Eq. (10), the result for ΔG can be written as

Figure 1. Local kinetic-exchange spin-up energy density, $C_k(n+)^{5/3} + C_x(n+)^{4/3}$, where $C_k = (3/10)(6\pi^2)^{2/3}$ and $C_x = -(3/2)(3/4\pi)^{1/3}$, as a function of spin-up density $n^+$. Exactly the same function holds for $n^-$. A quadratic fit based upon duplication of the exact position and depth of the minimum is also shown

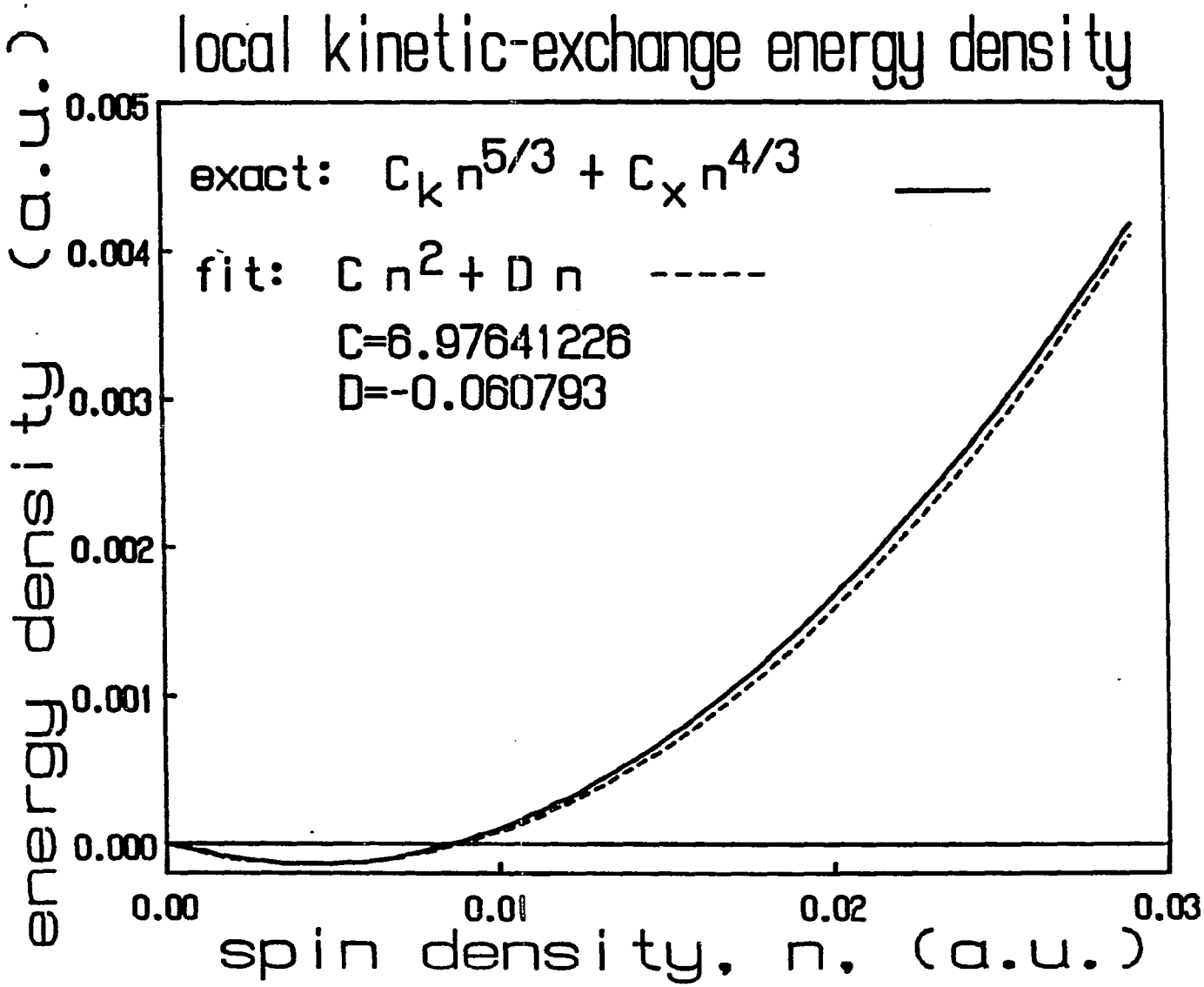
local kinetic-exchange energy density
exact: $C_k n^{5/3} + C_x n^{4/3}$
fit: $C n^2 + D n$
C=6.97641226
D=-0.060793
energy density (a.u.)
0.005
0.004
0.003
0.002
0.001
0.000
0.00
0.01
0.02
0.03
spin density, n, (a.u.)

$$\Delta G \sim 1/2\ C \sum_{i \neq j} \sum_{j} \int \{n+(A_i)\ n+(A_j) + n-(A_i)\ n-(A_j)\}\ d\underline{r}$$

$$- C \sum_{i} \int \{n+(A_i)\ n+_i + n-(A_i)\ n-_i\}\ d\underline{r}\ . \qquad (11)$$

Since the self-consistent jellium results utilize an unpolarized electron gas [19], we let $n+_i = n-_i = n_i/2$ in Eq. (11) and obtain the final equation which must be minimized:

$$\Delta G \sim 1/2\ C \sum_{i \neq j} \sum_{j} \int \{n+(A_i)\ n+(A_j) + n-(A_i)\ n-(A_j)\})\ d\underline{r}$$

$$- 1/2\ C \sum_{i} \int n(A_i)\ n_i\ d\underline{r}\ . \qquad (12)$$

One possible solution to the minimization of Eq. (12), i.e. $\Delta G=0$, is immediately apparent:

$$n_i = \sum_{j} (1-\delta_{ij}) \int \{n+(A_i)\ n+(A_j) + n-(A_i)\ n-(A_j)\}\ d\underline{r}\ /Z_i\ . \qquad (13)$$

This is clearly the most symmetrical solution, and also possesses a number of reasonable physical properties. First, the jellium density on atom $A_i$ due to atom $A_j$ is proportional to the electron spin density of $A_j$ averaged over atom $A_i$ with the weight function equal to the (normalized) spin density of $A_i$. Since the "size" of atom $A_i$ can be characterized by the atomic spin density, such an average makes good physical sense. Second, for the case of <u>spin-unpolarized</u> atoms, $n_i$ is 1/2 of the total

density average because of a division of electron density between the two atoms. This eliminates overcounting of embedding energies. (Note that for a given pair of atoms, i and j, the density overlap contribution is equal on each atom but the density contribution is not because of the inverse weighting by the atomic number.) Third, the integral in Eq. (13) is positive for all densities, a property which is not shared by other more complicated functionals of $n(A_i)$ and $n(A_j)$ such as the electrostatic weighting due to Stott and Zaremba [18] and Lang and Norskov cited in [15-17].

It is important to realize that Eq. (13) is not the most general solution of Eq. (12). If we define

$$n_i = \sum_j (1-\delta_{ij})\ \alpha(i,j) \int \{n+(A_i)n+(A_j) + n-(A_i)n-(A_j)\}\ d\underline{r}\ /Z_i, \qquad (14a)$$

then $\Delta G=0$ for all pairs of numbers $\alpha(i,j)$ satisfying

$$\alpha(i,j) + \alpha(j,i) = 2 \qquad i,j=1,\ldots,N \text{ for } j\neq i\ . \qquad (14b)$$

The solution in Eq. (13) corresponds to the special case of $\alpha(i,j) = 1$ for all i and j. In general, Eq. (14) must be supplemented by other information which relates pairs of $\alpha(i,j)$. Based upon the physical rational that the $\alpha(i,j)$ values effectively partition electron density between atoms $A_i$ and $A_j$, it is reasonable to utilize the ratios of the electron affinities, $EA(A_i)$. This yields

$$\alpha(i,j)/\alpha(j,i) = EA(A_i)/EA(A_j)\ . \qquad (15)$$

Note also that the $EA(A_i)$ is the negative of the zero density limit of the embedding energy [18]. The $n_i$ determined via Eqs. (14b) and (15) are denoted by $n_i(EA)$. Similarly, those determined by the equal partitioning in Eq. (13) are denoted $n_i(0.5)$.

The two solutions differ in their partitioning of the electron density between the two atoms. The $n_i(0.5)$ provide an equal sharing subject to the differences in the $Z_i$. By contrast, the $n_i(EA)$ provide a larger share of electron density to the atom with the larger electron affinity. However, for the case of identical atoms both solutions yield $\alpha(i,j) = 1$, as expected on physical grounds. Applications in this paper will be limited to homonuclear systems for which both solutions are the same. Examples of the use of each type of partitioning will be provided in future work.

The implementation of the CEM-N theory can now be accomplished once the functionals for the kinetic, exchange and correlation energy are specified. In our previous work [14], we used

$$T(n) = \int [t_0(n+) + t_0(n-) + t_2(n+) + t_2(n-)]\, d\underline{r} \tag{16a}$$

$$= T_0(n) + T_2(n) \tag{16b}$$

$$E_X(n) = \int [\varepsilon_{X0}(n+) + \varepsilon_{X0}(n-)]\, d\underline{r} \tag{17a}$$

$$= E_{X0}(n) \tag{17b}$$

$$E_C(n) = \text{Gunnarrson-Lundqvist form} . \tag{18}$$

These are referred to as second order gradient kinetic, local exchange and GL correlation [22] energy functionals, respectively. Since that work, we have developed a much more accurate kinetic energy functional [26] in which the integrand in Eq. (17a) is replaced by a Pade' approximation in $|\text{grad}(n)|/n^{4/3}$ which has the effect of approximately summing the full series in the gradients of the electron density. This is denoted by

$$T(n) = \int [t_p(n+) + t_p(n-)]\, d\underline{r} \tag{19a}$$

$$= T_p(n) \tag{19b}$$

and is used throughout the present work since it provides an accurate representation of the exact Kohn-Sham (wavefunction based) kinetic energy used in the self-consistent calculations [19]. Although we have also developed a much more accurate exchange energy functional [12a] via a Pade' approximation, we have continued to use the local exchange functional in Eq. (17) because the self-consistent solutions [19] of $\Delta E_J(A_i;n_i)$ utilized this functional. In particular, use of a non-local exchange functional in Eq. (1) would not allow for the elimination of the energy of atom $A_i$ between Eqs. (1) and (2) since $E_{X0}(n)$ was used for the solutions in Eq. (2). An identical argument forces continued use of the Gunnarrson-Lundqvist correlation energy [22] even though a more accurate non-local form has been presented by Perdew [13].

A numerical problem which must be addressed in the implementation of the CEM-N theory is the efficient numerical calculation of the three-

dimensional multicenter integrals over the kinetic, exchange, and correlation energy functionals. The solution which we have developed is presented in the Appendix.

Before considering the embedding energy functions in detail, it is worthwhile to indicate some of the flexibility within the present formalism. Consider the case where the first M atoms of the system of N atoms are active and the remaining (N-M) atoms are grouped together to form the host. The present derivation would be modified by eliminating only the atom energies $E(A_i)$ for i=1,...,M between Eqs. (1) and (2). The reader can easily verify that the end result of such a modification is equivalent to the following choice of all the $\alpha(i,j)$:

$$\alpha(i,j) + \alpha(j,i) = 2 \qquad i,j=1,\ldots,M \quad j\neq i \tag{20a}$$

$$\alpha(i,j) = 2 \qquad i=1,\ldots,M \quad j=M+1,\ldots,N \tag{20b}$$

$$\alpha(i,j) = 0 \qquad i=M+1,\ldots,N \quad j=1,\ldots,N\ . \tag{20c}$$

This allows for the M active bodies to interact with each other exactly as in a full M-body theory, while including the effect of the host by simply providing the <u>full</u> host electron density average to the effective medium of each active atom. The host is uninfluenced by the M active atoms since Eq. (20c) yields $n_i = 0$ for i=M+1,...,N. Clearly, CEM-1 corresponds to M=1. One situation where this generalization may be useful is when the embedding energy functions for some atoms are not known.

## Embedding Energy Functions

The most direct choice of the embedding energies $\Delta E_J(A;n)$ is simply that of the self-consistent solution of the local density equations for atom A in jellium of density n. These have been calculated for a number of atoms by Puska et al. [19] and such a choice will be referred to with the subscript P in place of the J to indicate the particular type of solution, $\Delta E_p(A;n)$.

The $\Delta E_p(A;n)$ function for an atom with positive electron affinity has the characteristic shape shown in Fig. 2 for B and F. The intercept at zero density is the negative of the electron affinity of atom A. The small decrease of $\Delta E_p(A;n)$ with increasing n at low n is due to reorganization of the originally uniform electron density in jellium around the atom. The large increase in energy at high n is due to the kinetic energy repulsion between the electrons of the atom and those of the jellium.

The troublesome behavior when using $\Delta E_p(A;n)$ to model the interactions in systems composed of atoms is the intercept at -EA. This feature is a direct result of the vanishing of the work function for jellium in the zero density limit. For real non-interacting systems, the electron density n will vanish via Eqs. (13) or (14a) and an artificial interaction energy will be introduced by the intercept at -EA. This cannot simply be subtracted out since the extent of any electron transfer at higher density will not be the same as at n = 0.

A more rigorous way of describing the difference between jellium and real systems is in terms of the work functions or ionization potentials. Consider a diatomic molecule AB for example. At a large separation r, the

Figure 2. SCF-LD embedding energies for B and F into jellium as a function of the jellium electron density [19, 20]

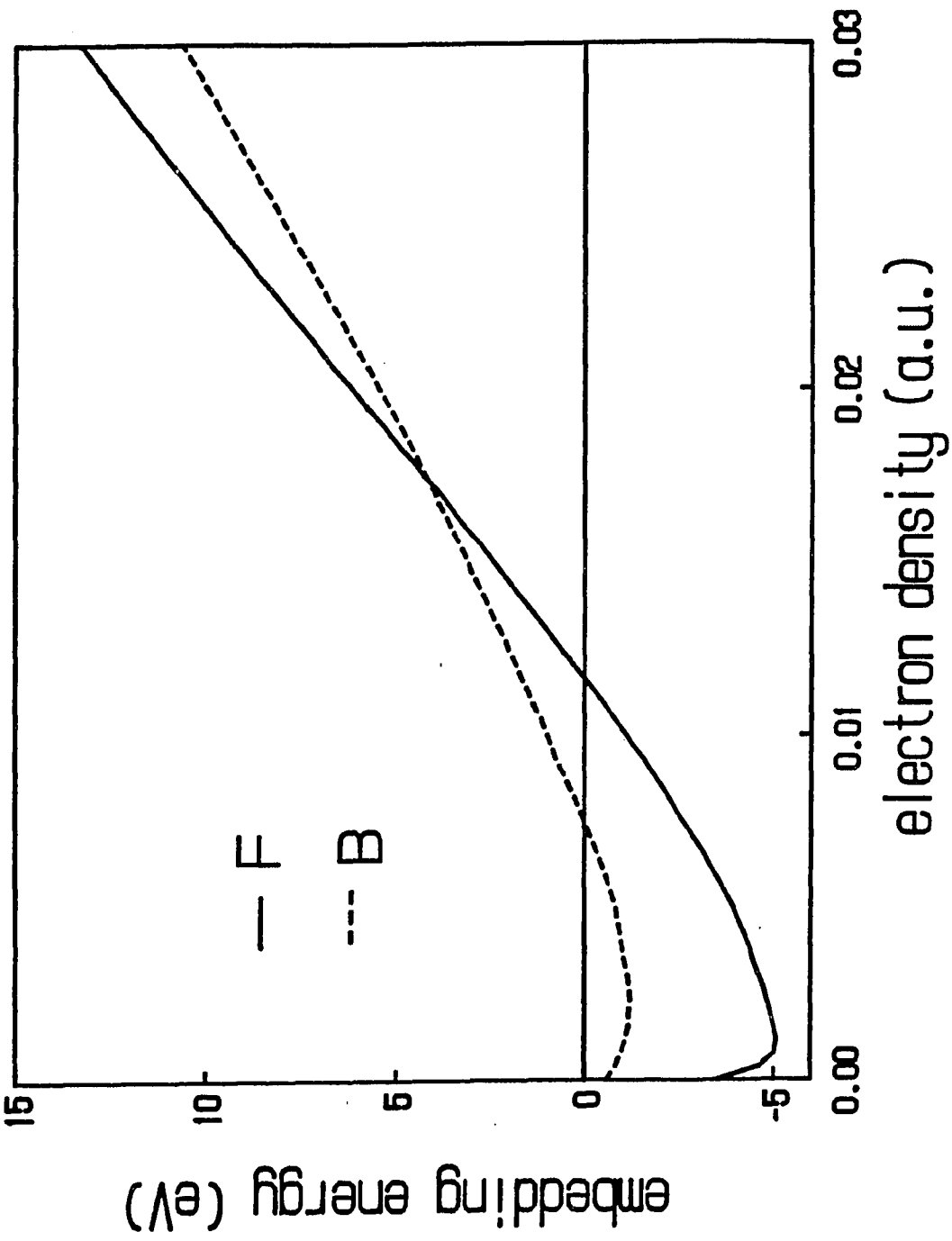
embedding energy (eV)
15
10
5
0
-5
0.00
0.01
0.02
0.03
electron density (a.u.)
F
B

energy required to transfer an electron from B to A is (to a good approximation)

$$\delta E(A,B) = IP(B) - EA(A) - 1/r \ , \tag{21}$$

in obvious notation. These components can be interpreted in the following manner: 1) IP(B) is the energy required to remove an electron from the highest occupied atomic orbital (HOAO) of the host which is located at -IP(B); 2) EA(A) is the energy gained by filling the lowest unoccupied AO (LUAO) of the embedded atom which is located at -EA(A); 3) -1/r is the reorganization energy gained in the interaction between the two atoms. Eq. (21) is only correct at large r since at small r, the last term would eventually become positive due to both electrostatic and kinetic energy overlap repulsions.

For atom A in jellium, the exact embedding energy can be written in an analogous form to Eq. (21):

$$\delta E(A,J) = WF(n) - EA(A) + \delta E_r(A;n) \ , \tag{22}$$

where WF(n) is the work function of the jellium and $\delta E_r(n)$ is the reorganization energy. (Note that $\delta E(A,J)$ and $\Delta E_J(A;n)$ are the same quantity with the former symbol being used here to indicate the analogy to $\delta E(A,B)$.) Also, WF(n) is the negative of the chemical potential of the jellium and is calculated from the local kinetic-exchange-correlation potential [19]. To see the differences between Eqs. (21) and (22), we inspect the terms in Eq. (22) more closely. The work function depends only

upon the jellium electron density and is shown in Fig. 3. The reorganization energy depends upon each individual atom, and can be calculated by setting $\Delta E(A,J)$ equal to $\Delta E_p(A;n)$. The result for F is typical and is also shown in Fig. 3. The reorganization energy behaves in an analogous manner to -1/r: both decrease from zero in the limit of non-interaction, $r \to \infty$ or $n \to 0$. In this limit both are simply an extra electrostatic reorganization. At large density $\delta E_r(A;n)$ becomes quite positive due to kinetic energy and electrostatic repulsion exactly as the modified -1/r term would behave in the real system. Thus the main distinction between the jellium and real systems is the difference between the donation of an electron from the Fermi level at -WF(n) in the former case and the donation of an electron from the HOAO at -IP(B) in the latter case.

The above discussion would indicate how to modify the embedding energy, at least for a diatomic system treated within CEM-N, if the bonding was due to a long-range electron transfer mechanism. However, the real situation is more complicated because the reorganization energy will depend upon the energy levels of the jellium (e.g., via the kinetic energy repulsion). In other words, the bonding is described as a mixture of covalent and ionic configurations. Under these circumstances, it is not clear how to modify $\Delta E_J(A;n)$ without further calculations on the atom embedded into jellium system. For example, a self-consistent calculation of $\Delta E_J(A;n)$ which allows for a variation in the Fermi level in the jellium could model the donation from the HOAO in the real system. This would allow more variation in the atom-jellium system by making the embedding energy a function of the Fermi level of the homogeneous gas. This in turn

Figure 3. Decomposition of the F atom embedding energy according to Eq. (22) of the text. The EA(F) would appear as a horizontal line at 3.52 eV.

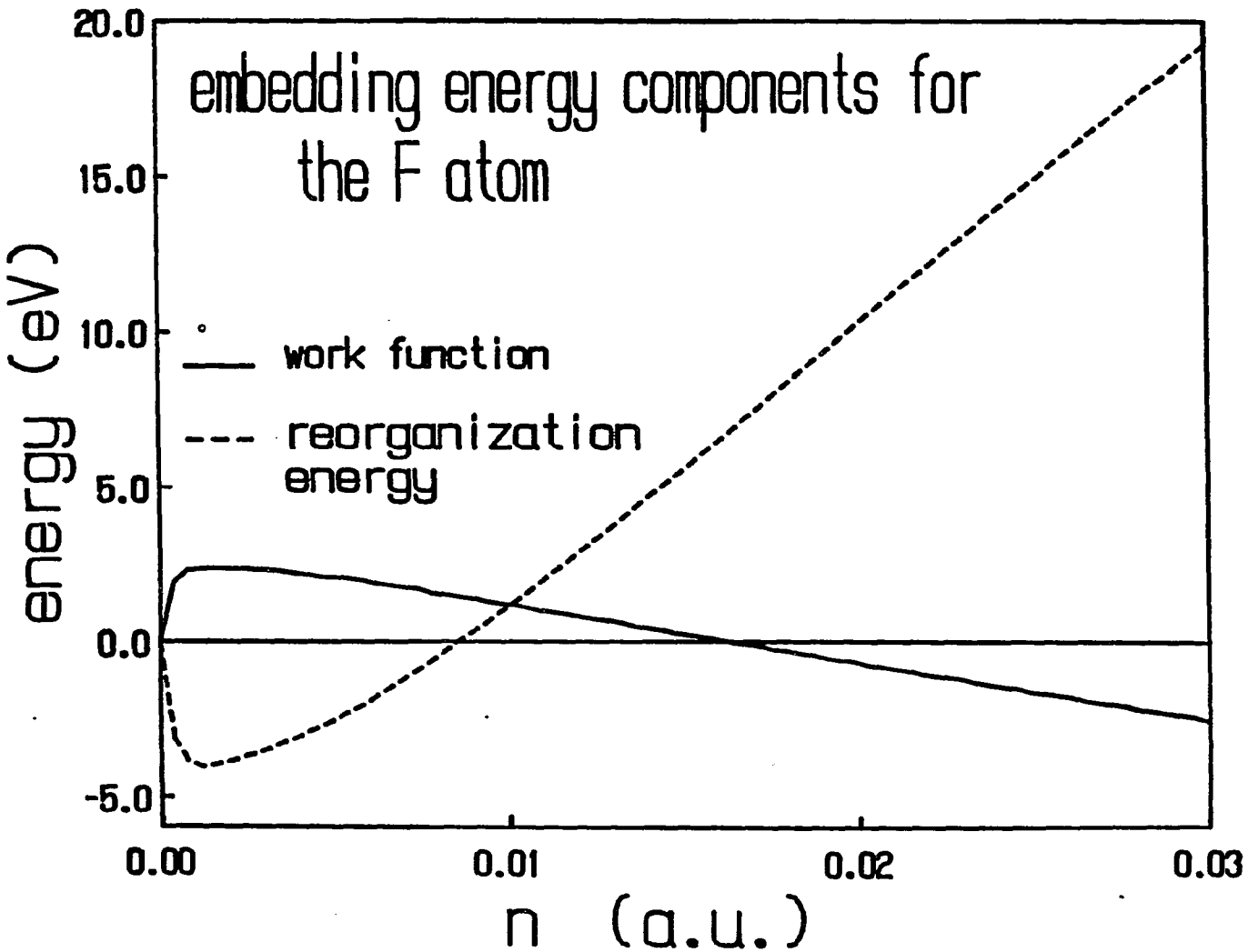
embedding energy components for
the F atom
work function
reorganization
energy
energy (eV)
20.0
15.0
10.0
5.0
0.0
-5.0
0.00
0.01
0.02
0.03
n (a.u.)

would yield a more complicated universal function, $\Delta E_J(A;n,E_f)$, with <u>two</u> parameters for each atom A. The Puska et al. [19] results are for the special case $E_f = -WF(n)$ while we would need results for $E_f = -IP(B)$.

Because of the above mentioned problems, a semi-empirical method has been devised to construct the $\Delta E_J(A;n,E_f)$ curves for the special case of a homonuclear diatomic molecule, i.e., $E_f = -IP(A)$. In this case, the choice of the n is unambiguous (EA ≡ 0.5 solution) and thus the only variation of the energy in the CEM-N theory can be due to variation of the embedding energy. Denoting this energy by $\Delta E_C(A;n)$, we then have from Eq. (5a)

$$\Delta E(A_2) = 2\Delta E_C(A;n) + \Delta V_C + \Delta G(A_2) \ . \tag{23}$$

The values for $\Delta E_C(A_2)$ can be found from this equation given the experimentally determined binding curve for $A_2$. These should mimic a covalent bonding situation. By contrast, the original $\Delta E_p(A;n)$ will describe an ionic bonding situation better for atoms with significant electron affinities. We shall present illustrations of each function in this article, and future work will be pointed towards delimiting the range and accuracy of these embedding functions. We should emphasize that these covalent embedding functions are <u>universal</u>, as long as $E_f = -IP(A)$, and thus they have intrinsic utility in the prediction of the properties of homogeneous many-atom clusters. Examples of such applications will be presented in future publications. We also leave for future research the solution of the rather difficult problem of how to use the two universal functions for $E_f = -IP(A)$ and $E_f = -WF(n)$ to predict the function for the general case $E_f = -IP(B)$ with $IP(B) \neq IP(A) \neq WF(n)$.

# APPLICATIONS AND DISCUSSION

This section is divided into a number of parts. The first contains a test of two choices for the determination of the jellium density. The latter sections contain applications to the homonuclear diatomic molecules, $H_2$, $Li_2$, $B_2$, $C_2$, $N_2$, $O_2$ and $F_2$. In one set of calculations, the spin configurations were set to be unpolarized, and the spatial configurations of the atoms in these molecules were assumed to be spherical, reflecting the symmetry property of atoms in free space. These are shown in Table I. This mimics the spin-spatial pairing in chemical bonding using molecular orbitals (in the language of quantum chemistry). In another set of calculations, the spin and spatial configurations of the atoms in these molecules were chosen as in Table II. These configurations mimic the spin-spatial pairing in chemical bonding using valence atomic orbitals (in the language of quantum chemistry). The atomic densities were generated from the Hartree-Fock results [27]. The diatomic potentials used to test the CEM-N theory were approximated by Morse potentials with the parameters shown in Table III as determined from experimental data [28]. In the CEM-N calculations enough quadrature points were included to converge the results to about .05 eV, which is sufficient for the following analyses.

## Determination of the Jellium Density

Flexibility within the CEM-N theory, due to the choice of the jellium density, was investigated. The particular choice in Eq. (13) arises from minimization of the difference in the sum of the local kinetic and exchange energies between the real and atom-jellium systems. Since the accurate

Table I. Spin-unpolarized and spherically symmetric[a] configurations of the first row homonuclear diatomic molecules

+ (-) up (down) spin

| atom#1 (atom#2) | 1s | 2s | $2p_0$ and $2p_{\pm 1}$ |
|---|---|---|---|
| H | +1/2,-1/2 | | |
| (H) | +1/2,-1/2 | | |
| Li | +1,-1 | +1/2,-1/2 | |
| (Li) | +1,-1 | +1/2,-1/2 | |
| B | +1,-1 | +1,-1 | +1/6, -1/6 |
| (B) | +1,-1 | +1,-1 | +1/6, -1/6 |
| C | +1,-1 | +1,-1 | +1/3, -1/3 |
| (C) | +1,-1 | +1,-1 | +1/3, -1/3 |
| N | +1,-1 | +1,-1 | +1/2, -1/2 |
| (N) | +1,-1 | +1,-1 | +1/2, -1/2 |
| O | +1,-1 | +1,-1 | +2/3, -2/3 |
| (O) | +1,-1 | +1,-1 | +2/3, -2/3 |
| F | +1,-1 | +1,-1 | +5/6, -5/6 |
| (F) | +1,-1 | +1,-1 | +5/6, -5/6 |

[a]The symmetry of the density about each atom.

Table II. Spin-polarized and non-spherically symmetric[a] configurations of the first row homonuclear diatomic molecules

+ (-) one up (one down) spin

| atom#1 (atom#2) | 1s | 2s | $2p_0$ | $2p_{\pm 1}$ | |
|---|---|---|---|---|---|
| H | + | | | | |
| (H) | | | | | |
| Li | +,- | + | | | |
| (Li) | +,- | - | | | |
| B | +,- | +,- | + | | |
| (B) | +,- | +,- | | | |
| C | +,- | +,- | + | + | |
| (C) | +,- | +,- | - | - | |
| N | +,- | +,- | + | + | + |
| (N) | +,- | +,- | - | - | - |
| O | +,- | +,- | + | + | +,- |
| (O) | +,- | +,- | - | - | -,+ |
| F | +,- | +,- | + | +,- | +,- |
| (F) | +,- | +,- | - | -,+ | -,+ |

[a]The symmetry of the density about each atom.

Table III. Morse parameters for selected homonuclear diatomic molecules[a]

| molecule | $D_e$ (eV) | $\alpha_e$ (bohr$^{-1}$) | $r_e$ (bohr) |
|---|---|---|---|
| $H_2$ | 4.7446 | 1.030 | 1.4100 |
| $Li_2$ | 1.07 | 0.4570 | 5.051 |
| $B_2$ | 3.085 | 1.0075 | 3.005 |
| $G_2$ | 6.32 | 1.2960 | 2.350 |
| $N_2$ | 9.906 | 1.4226 | 2.074 |
| $O_2$ | 5.214 | 1.4041 | 2.282 |
| $F_2$ | 1.66 | 1.5737 | 2.668 |

[a]The parameters were determined from the frequency, bond length and well depth provided in ref. [28].

energy functional includes the local correlation energy and utilizes the Pade' kinetic energy functional which depends upon the gradient of the density, it is important to determine the applicability of the density choice to minimization of Eq. (5b) using the accurate functional. We have done this by computing $\Delta G(A_2)$ for a variety of homonuclear diatomic molecules as a function of bond length for two different selections of the jellium density. For these calculations, the spin-spatial configurations in Table I were utilized.

Although an infinite number of possible choices of $n_i$ are possible, the one we have considered is simply twice the value in Eq. (13). This has one salutary effect: if the total density due to the 'host' atoms is uniform, then $n_i$ can be identified as this physical density.

Tests for all the diatomics mentioned in the preface were carried out for these two choices and it was found that the choice in Eq. (13) led to the smallest value of the correction in the region of the minimum in the molecular binding curve. Illustrations are shown in Figs. 4(a) and (b) for the $Li_2$ and $N_2$ molecules using the polarized configurations in Table II. The experimental equilibrium bond length is indicated by the arrow. Around the minimum of the molecular binding curves, the choice in Eq. (13) always leads to a smaller magnitude of the correction than that from using twice the value in Eq. (13). This is especially apparent in Fig. 4(b) for $N_2$. Thus the use of the choice that gives the physical density can be ruled out. Note that $\Delta G$ becomes large and negative at very short distances. This occurs where the densities become considerably larger than the values over which the quadratic fit in Fig. 1 is accurate and where the gradients

Figure 4. The kinetic-exchange-correlation correction energy is shown for two different definitions of the electron density average as a function of bond length. See the text for a full description of each choice. The experimental equilibrium bond length is denoted by a vertical arrow

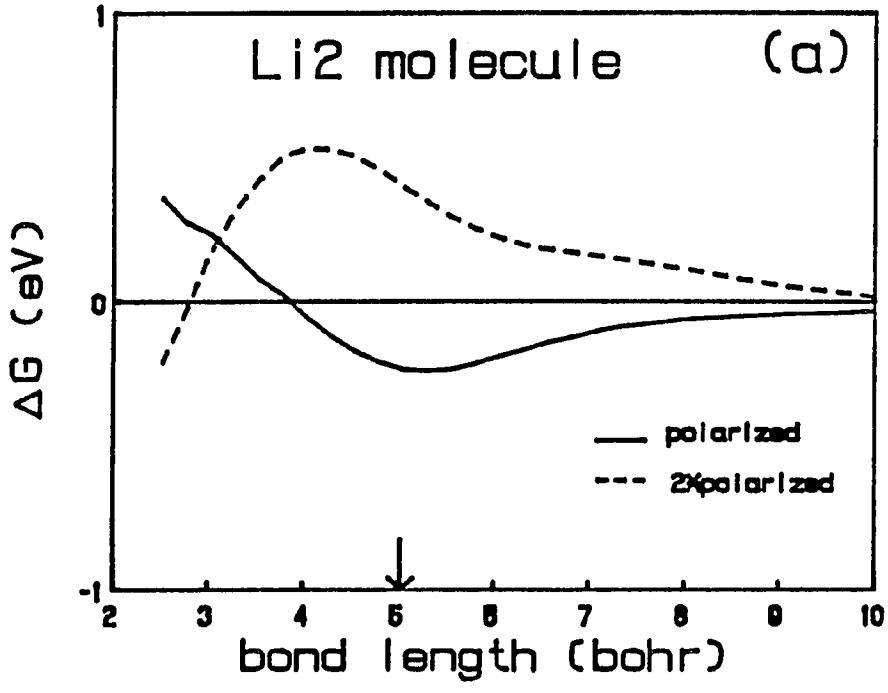
Li2 molecule
(a)
ΔG (eV)
1
0
-1
2
3
4
5
6
7
8
9
10
bond length (bohr)
polarized
2Xpolarized

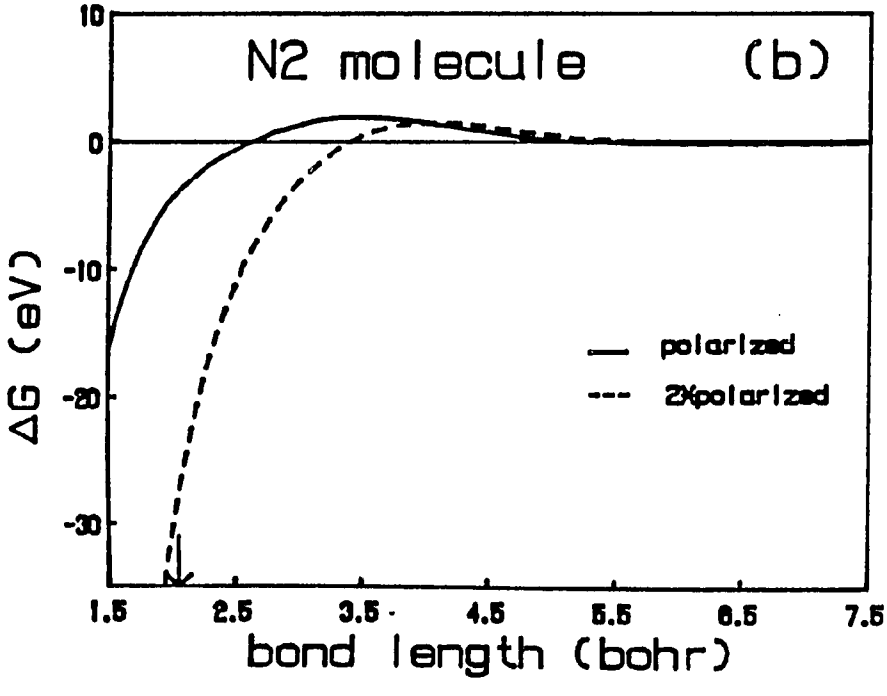
N2 molecule
(b)
ΔG (eV)
10
0
-10
-20
-30
1.5
2.5
3.5
4.5
5.5
6.5
7.5
bond length (bohr)
polarized
2Xpolarized

of the density make a large contribution to the kinetic energy functional. Although an iteration scheme could be used to determine the density which minimizes $\Delta G$ using the accurate functionals, we will show later that this region is dominated by the repulsion due to $\Delta E_J$ and thus the particular value of $\Delta G$ will be unimportant. In addition, the changes in $\Delta G$ and $\Delta E_J$ with respect to a change in the jellium density compensate for each other in this repulsive region, and thus the binding potential is less sensitive there.

## $H_2$ Molecule

The experimental equilibrium well depth and bond length are 4.75 eV and 1.4 bohr, respectively [28]. In the first calculation, we modeled the electron density of the $H_2$ molecule with two spherical, unpolarized H atoms (i.e., the configuration in Table I). The CEM-N and Morse diatomic potentials are shown in Fig. 5(a) along with the components of the CEM-N energy: $2\Delta E_p(H;n)$, $\Delta V_c$, and $\Delta G(H_2)$. The predicted potential minimizes at 2.0 bohr with a value of -3.45 eV. Note that $2\Delta E_p(H;n)$, which is -3.6 eV at a bond length of ~2.2 bohr and increases at shorter distances, is the dominant contribution. $\Delta V_c$ shifts the bond length slightly inward while $\Delta G(H_2)$ is nearly constant and decreases the binding energy. In addition, a short range repulsion occurs due to the rapid increase in $\Delta V_c$ and the slower increase in $2\Delta E_p(H;n)$. These features are rather particular to $H_2$. Note also that the CEM-N potential is quite smooth, even though the three components sometimes vary rapidly in different directions. Such smoothness is not guaranteed since a virial theorem does not hold. When contrasted with the results of SCF calculations [29,30], 3.63 eV and 1.38 bohr, the

Figure 5. $H_2$ molecule

(a) The diatomic Morse potential (solid line), the predicted potential using CEM-N with the Puska et al. [19] embedding function (dotted line), and the three components of the latter: homogeneous embedding energy (short dashed line), Coulombic energy (long-short dashed line), kinetic-exchange-correlation difference energy (long dashed line). All are given as a function of bond length. The H atoms are unpolarized.

(b) The semi-empirical covalent (unpolarized) and SCF-LD Puska et al. [19] embedding functions as a function of electron density. The density corresponding to the distance at which the Morse potential equals zero is denoted by the vertical down-arrow. The density corresponding to the equilibrium distance of the $H_2$ molecule is indicated by the up-arrow

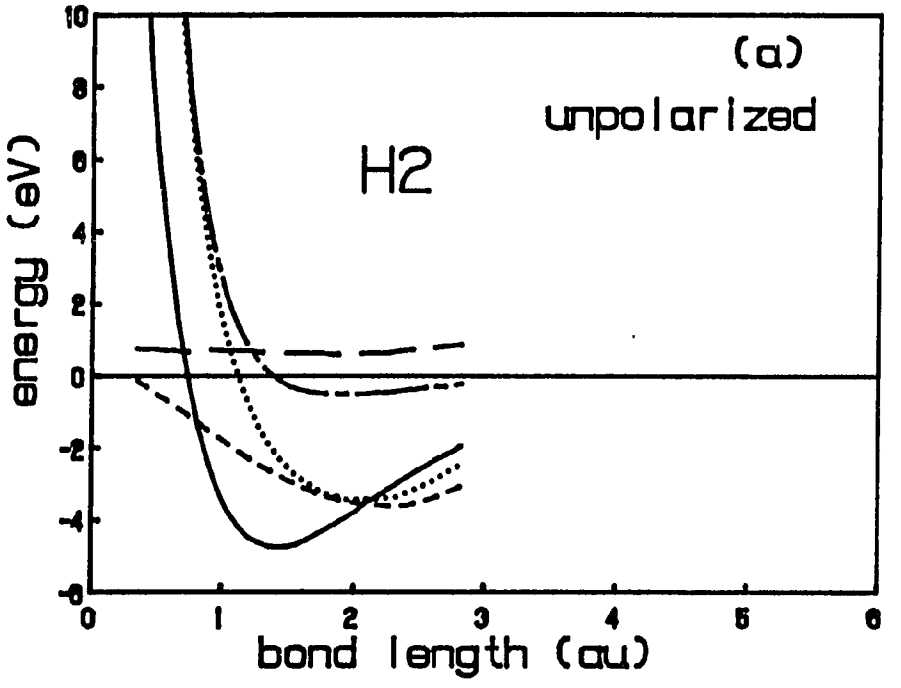


H atom embedding functions

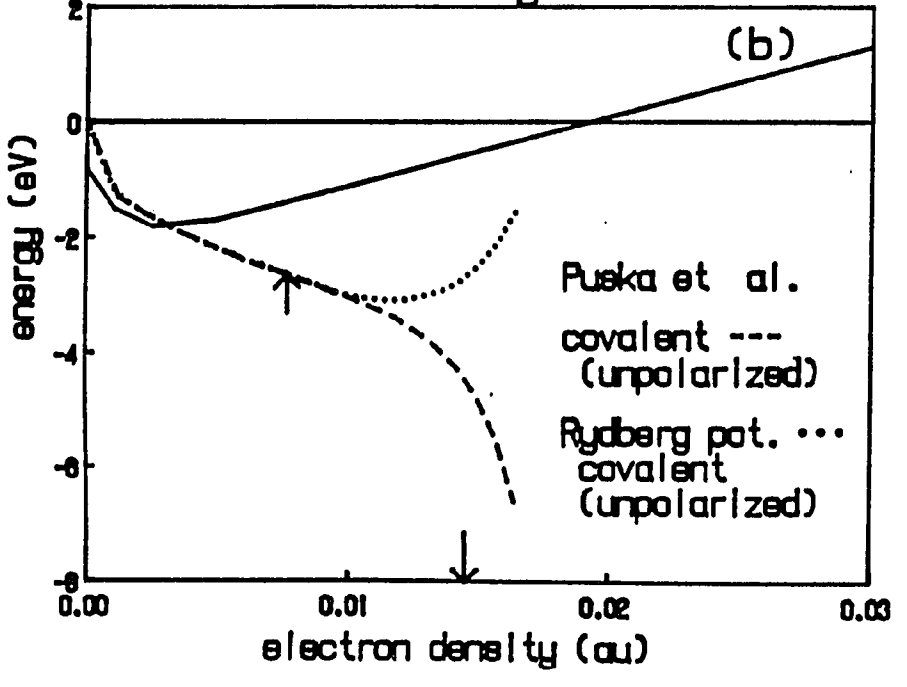

CEM-N values are adequate.

In the next calculation, we modeled the electron density of the $H_2$ molecule as in Table II. Since Eq. (13) utilizes the product of like spin densities, the jellium density is $n_j = 0$ for all nuclear separations. The CEM-N theory then yields a molecular well of 2.65 eV at a bond length of 1.75 bohr. When we used an unpolarized density average and retained spin polarization in the $\Delta G$ term, the molecular well deepens to 5.1 eV at a bond length of 1.6 bohr. While this is a significant improvement, it is not a satisfactory solution because of the inconsistency between the correction term and the density averaging procedure, which was derived by minimizing the correction term.

In Fig. 5(b), we show a comparison of the covalent (unpolarized) embedding function determined via Eq. (23) and the Puska et al. function. The up-arrow indicates the density corresponding to the experimental minimum of the $H_2$ binding potential; it is also the inflection point of $\Delta E_C$. The down arrow indicates the density corresponding to $\Delta E(H_2) = 0$. The covalent and Puska et al. functions are in disagreement, with the former displaying a completely different shape. This is not a major concern since the inflection point of $\Delta E_C$ occurs at the up-arrow, which also happens to occur at the minimum of the $H_2$ binding potential. On the repulsive wall of this potential, the Morse form used in Eq. (23) is too small which leads to an underestimate of the covalent function. Replacement of the Morse potential by the very accurate extended Rydberg form [31] yields the Rydberg covalent function also shown in Fig. 5(b). Note that this modified covalent function vanishes at $n = 0$, and thus eliminates the zero density electron transfer in $\Delta E_p$, a problem discussed

earlier.

## $Li_2$ Molecule and Embedding Functions

The experimental equilibrium well depth and bond length are 1.07 eV and 5.05 bohr, respectively [28]. In the first calculation, we modeled the electron density of the $Li_2$ molecule with two spherical, unpolarized Li atoms (i.e., the configuration in Table I). The CEM-N and Morse diatomic potentials are shown in Fig. 6(a) along with the components of the CEM-N energy: $2\Delta E_p(Li;n)$, $\Delta V_c$, and $\Delta G(Li_2)$. The predicted potential minimizes at ~5.0 bohr with a value of -1.0 eV. However, this is a metastable equilibrium because $2\Delta E_p(Li;n)$, and thus $\Delta E(Li_2)$, decreases to -1.2 eV as the equilibrium bond length increases to infinity. When contrasted with the well depth of 0.16 eV from SCF calculations [29], the CEM-N value is quite good. Note that $\Delta E_p$ does not have a minimum, but that $\Delta V_c$ and $\Delta G(Li_2)$ determine the location of this metastable equilibrium. The short range repulsion for $r < 4$ bohr is due to the rapid increase in all three components of the CEM-N energy; this is a feature which we have found only for the alkali metal diatomics. As for $H_2$, the CEM-N potential is quite smooth, even though the three components sometimes vary rapidly in different directions.

In the next calculation, we modeled the electron density of the $Li_2$ molecule as spin-polarized with the configuration in Table II. The CEM-N and Morse diatomic potentials are shown in Fig. 6(b) along with the components of the CEM-N energy. The predicted potential minimizes at slightly too short of a bond length, 4.8 bohr, with much too large of a

Figure 6. $Li_2$ molecule

The diatomic Morse potential (solid line), the predicted potential using CEM-N with the Puska et al. [19] embedding function (dotted line), and the three components of the latter: homogeneous embedding energy (short dashed line), Coulombic energy (long-short dashed line). (a) Spin-unpolarized Li atoms. (b) Spin-polarized Li atoms. All are given as a function of bond length.

Also, the semi-empirical covalent and SCF-LD Puska et al. [19] embedding functions as a function of electron density. (c) Spin-unpolarized Li atoms. (d) Spin-polarized Li atoms. The density corresponding to the distance at which the Morse potential equals zero is denoted by the vertical down-arrow. The density corresponding to the equilibrium distance of the $Li_2$ molecule is indicated by the up-arrow

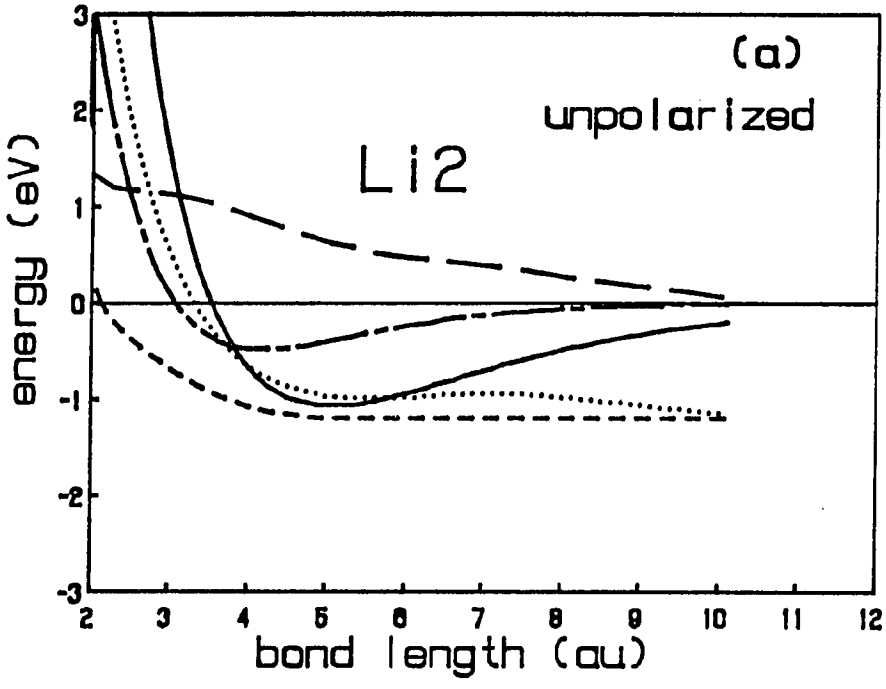
(a)
unpolarized
Li2
energy (eV)
bond length (au)
3
2
1
0
-1
-2
-3
2
3
4
5
6
7
8
9
10
11
12

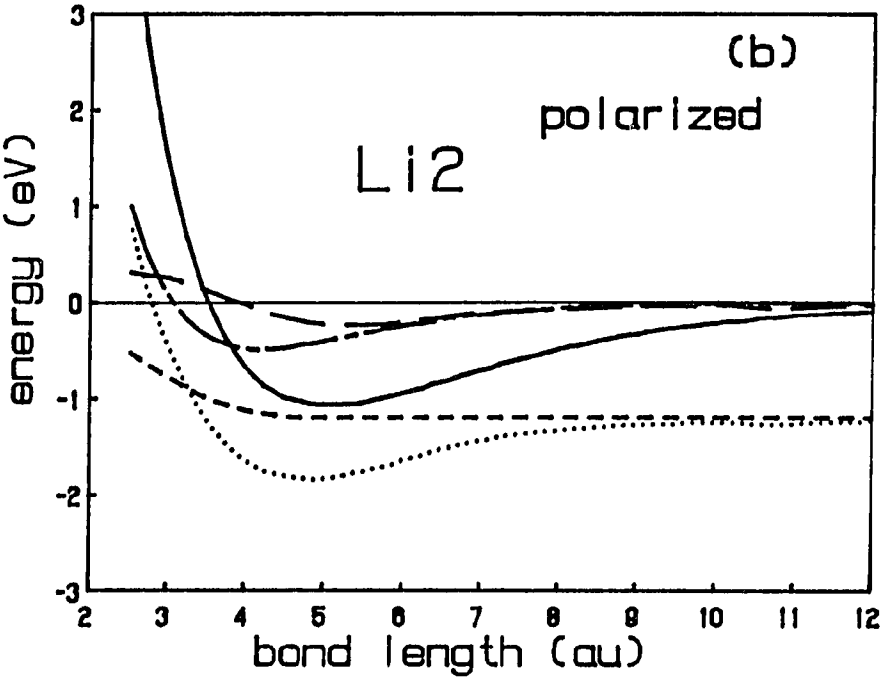
(b)
polarized
Li2
energy (eV)
bond length (au)
3
2
1
0
-1
-2
-3
2
3
4
5
6
7
8
9
10
11
12

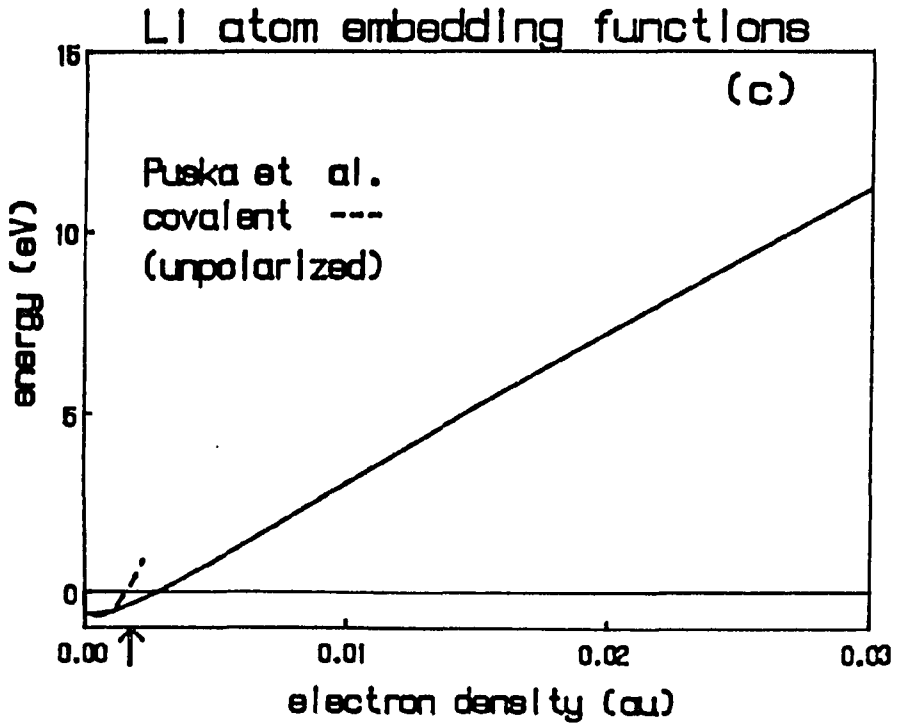


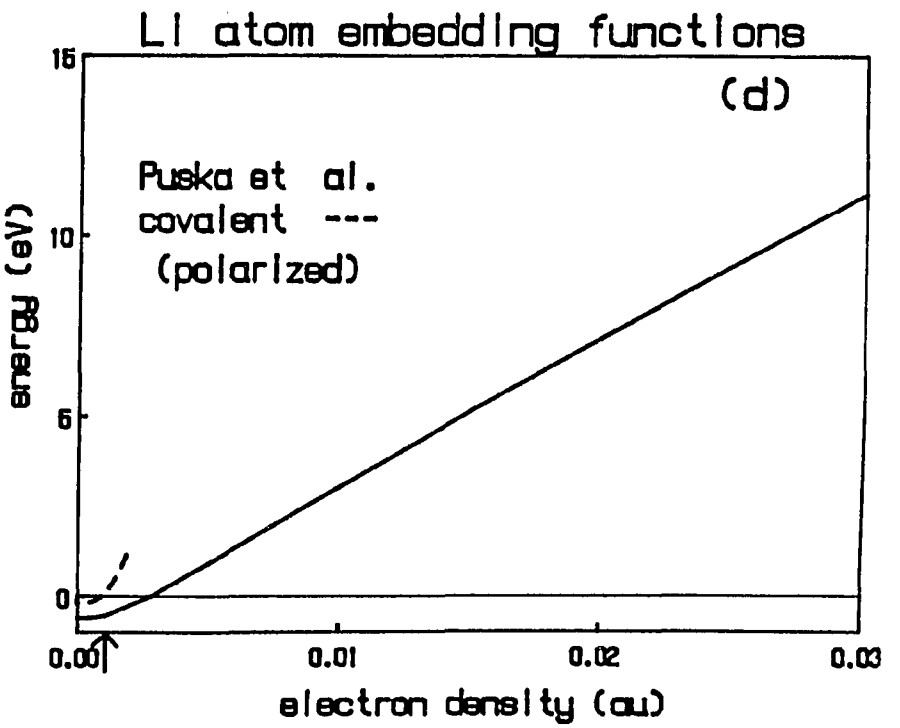


Figure 6 (Continued)

well, 1.84 eV. These are considerably worse than the results shown in Fig. 6(a), and indicate that it is better to model the molecular density as unpolarized within CEM-N.

In Fig. 6(c), we show a comparison of the covalent (unpolarized) embedding function determined via Eq. (23) and the Puska et al. function. The up-arrow indicates the density corresponding to $\Delta E(Li_2) = 0$. The covalent and Puska et al. functions are in disagreement as to the rate of increase with density on the repulsive portion of the curve, but are in remarkably good agreement with regards to the position and depth of the minimum. The former feature is quite similar to that found for the Ryberg covalent $H_2$ embedding function. It is difficult to see on Fig. 6(c) but the covalent function vanishes at n = 0 while the Puska et al. function equals -0.6 eV. The vanishing of the former eliminates the metastable behavior of the $Li_2$ binding potential in Fig. 6(a) by eliminating the zero density electron transfer associated with $\Delta E_p$, a problem discussed in detail earlier.

For completeness, we show the covalent (polarized) embedding function in Fig. 6(d). It is in substantially worse agreement with $\Delta E_p$ than was the covalent (unpolarized) function in Fig. 6(c).

### $B_2$ Molecule and Embedding Functions

The experimental equilibrium well depth and bond length are 3.09 eV and 3.01 bohr, respectively [28]. In the first calculation, we modeled the electron density of the $B_2$ molecule with two spherical, unpolarized B atoms (i.e., the configuration in Table I). The CEM-N and Morse diatomic potentials are shown in Fig. 7(a) along with the components of the CEM-N

Figure 7. $B_2$ molecule

The diatomic Morse potential (solid line), the predicted potential using CEM-N with the Puska et al. [19] embedding function (dotted line), and the three components of the latter: homogeneous embedding energy (short dashed line), Coulombic energy (long-short dashed line), kinetic-exchange-correlation difference energy (long dashed line). (a) Spin-unpolarized and spherical B atoms. (b) Spin-polarized and non-spherical B atoms. All are given as a function of bond length.

Also, the semi-empirical covalent and SCF-LD Puska et al. [19] embedding functions as a function of electron density. (c) Spin-unpolarized and spherical B atoms. (d) Spin-polarized and non-spherical B atoms. The density corresponding to the distance at which the Morse potential equals zero is denoted by the vertical down-arrow. The density corresponding to the equilibrium distance of the $B_2$ molecule is indicated by the up-arrow

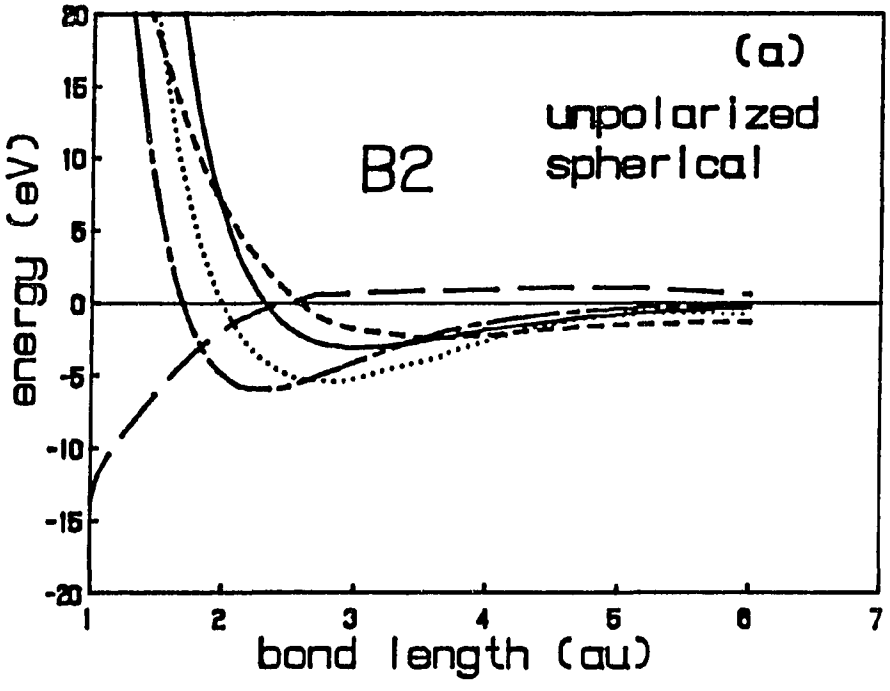
(a)
unpolarized
spherical
B2
energy (eV)
bond length (au)
20
15
10
5
0
-5
-10
-15
-20
1
2
3
4
5
6
7

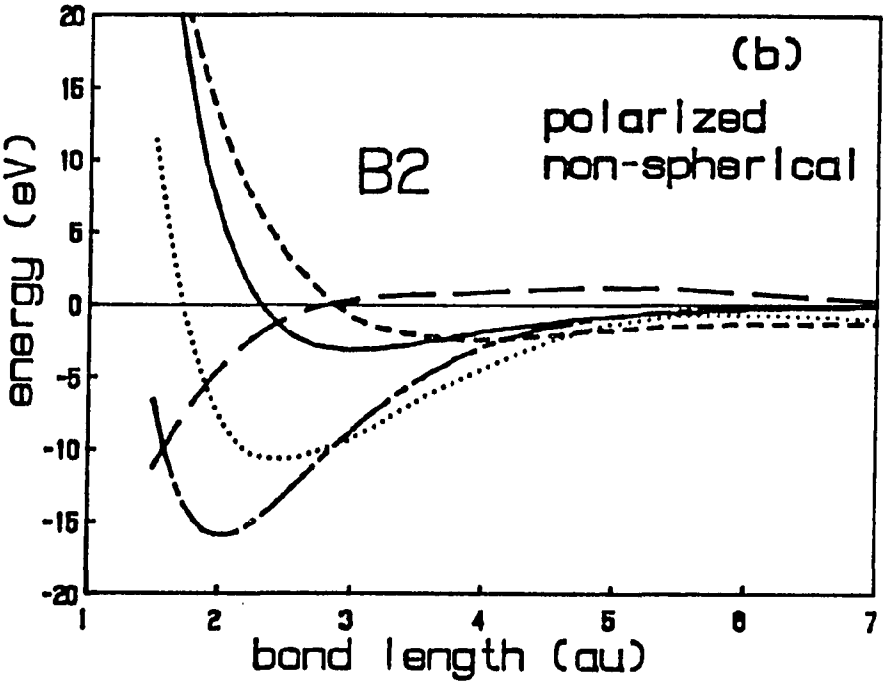
(b)
polarized
non-spherical
B2
energy (eV)
bond length (au)
20
15
10
5
0
-5
-10
-15
-20
1
2
3
4
5
6
7

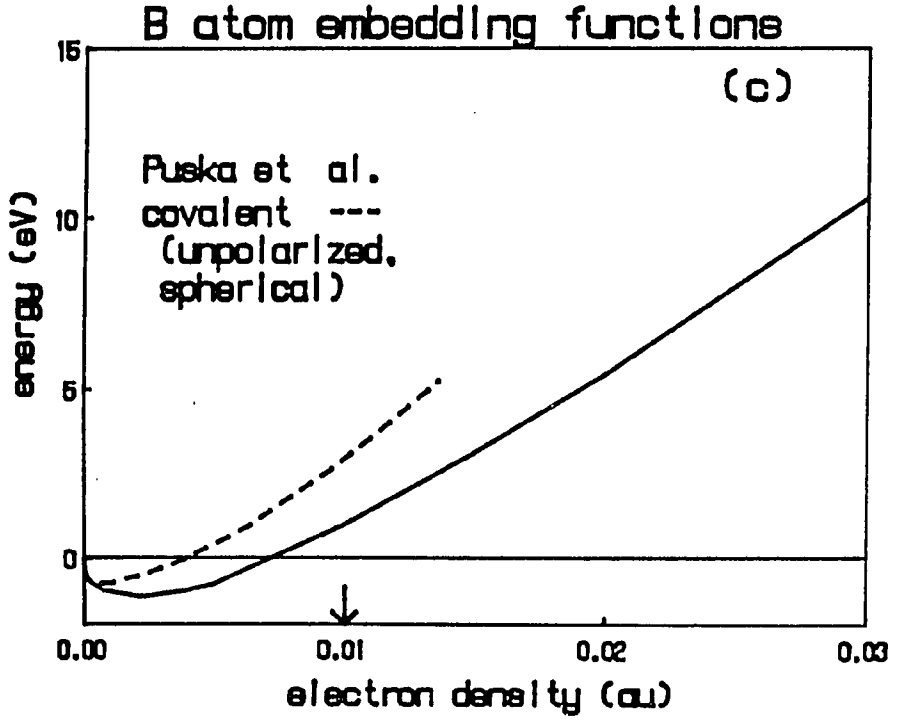


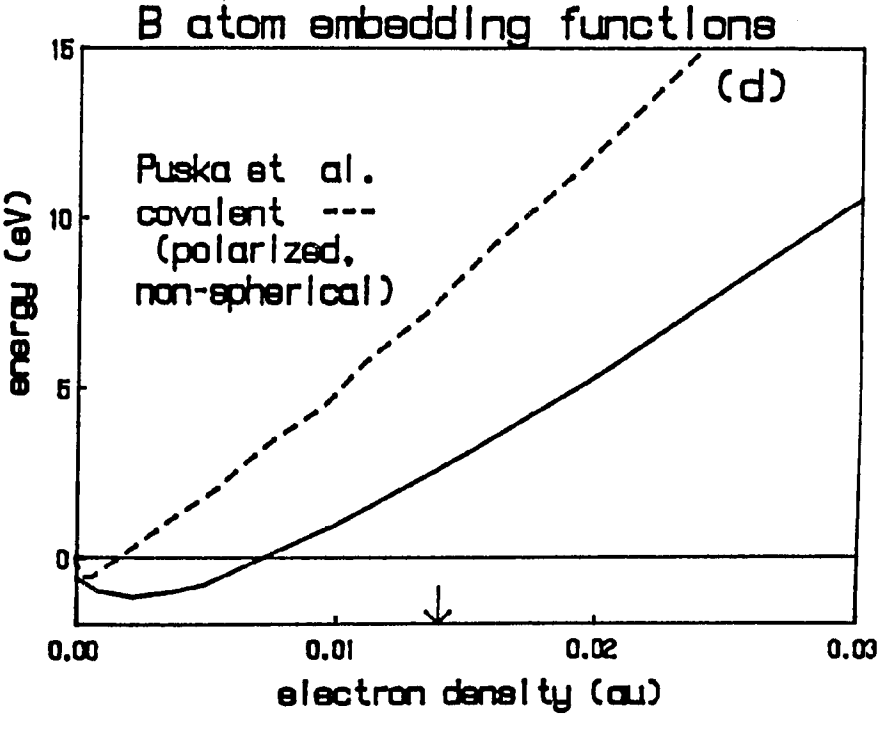


Figure 7 (Continued)

energy. The predicted potential minimizes at ~2.85 bohr with a value of -5.44 eV. When contrasted with the well depth of 0.81 eV from SCF calculations [29], the CEM-N value is quite good. Note that the bonding in $B_2$ is due to a strong Coulomb attraction. The minimum of $2\Delta E_p(B;n)$ does not determine the bond length; in fact the Puska et al. embedding energy is nearly zero at $r_e$. Such behavior is characteristic of bonding in small molecules described by the CEM-N theory. Note also that $\Delta G(B_2)$ is also rather small near $r_e$, and thus the overestimation of the binding energy is attributable to the underestimation of the embedding energy. This indicates the need for the covalent embedding functions discussed earlier. As for previous diatomics, the CEM-N potential is quite smooth, even though the three components sometimes vary rapidly in different directions.

In the next calculation, we modeled the electron density of the $B_2$ molecule as spin-polarized with the configuration in Table II. The CEM-N and Morse diatomic potentials are shown in Fig. 7(b) along with the components of the CEM-N energy. The predicted minimum of the potential is much too deep, 10.8 eV vs. 3.09 eV [28], and is at too short of a bond length, 2.65 bohr vs. 3.01 bohr [28]. These results are much worse than those in Fig. 7(a), exactly as was the case for the $Li_2$ molecule. This indicates that it is better to model the molecular density as a superposition of spherical, unpolarized atomic densities within CEM-N.

In Fig. 7(c), we show a comparison of the covalent (unpolarized, spherical) embedding function determined via Eq. (23) and the Puska et al. function. The down-arrow indicates the density corresponding to $\Delta E(B_2) = 0$. The covalent and Puska et al. functions are in disagreement as to the

position and depth of the minimum but agree better with respect to the rate of increase with density on the repulsive portion of the curve. The contrast with the previous Li-J system occurs because the reorganization energy due the formation of a negative anion in the B-J system extends to higher density than was the case in the Li-J system, which is in accord with the greater electronegativity of the B atom. It is difficult to see on Fig. 7(c) but the covalent function vanishes at n = 0 while the Puska et al. function equals -0.6 eV. The vanishing of the former eliminates the zero density electron transfer associated with $\Delta E_p$, a problem discussed in detail earlier.

For completeness, we show the covalent (polarized, non-spherical) embedding function in Fig. 7(d). It is in substantially worse agreement with $\Delta E_p$ than was the covalent (unpolarized, spherical) function in Fig. 7(c).

### $C_2$ Molecule and Embedding Functions

The experimental equilibrium well depth and bond length are 6.32 eV and 2.35 bohr, respectively [28]. In the first calculation, we modeled the electron density of the $C_2$ molecule with two spherical, unpolarized C atoms (i.e., the configuration in Table I). The CEM-N and Morse diatomic potentials are shown in Fig. 8(a) along with the components of the CEM-N energy. The predicted potential minimizes at ~2.5 bohr with a value of -9.8 eV. When contrasted with the well depth of 0.68 eV from SCF calculations [29], the CEM-N value is quite good. The bonding in $C_2$ is due again to a strong Coulomb attraction and the minimum of $2\Delta E_p(C;n)$ does not

Figure 8. $C_2$ molecule

The diatomic Morse potential (solid line), the predicted potential using CEM-N with the Puska et al. [19] embedding function (dotted line), and the three components of the latter: homogeneous embedding energy (short dashed line), Coulombic energy (long-short dashed line), kinetic-exchange-correlation difference energy (long dashed line). (a) Spin-unpolarized and spherical C atoms. (b) Spin-polarized and non-spherical C atoms. All are given as a function of bond length.

Also, the semi-empirical covalent and SCF-LD Puska et al. [19] embedding functions as a function of electron density. (c) Spin-unpolarized and spherical C atoms. (d) Spin-polarized and non-spherical C atoms. The density corresponding to the distance at which the Morse potential equals zero is denoted by the vertical down-arrow. The density corresponding to the equilibrium distance of the $C_2$ molecule is indicated by the up-arrow

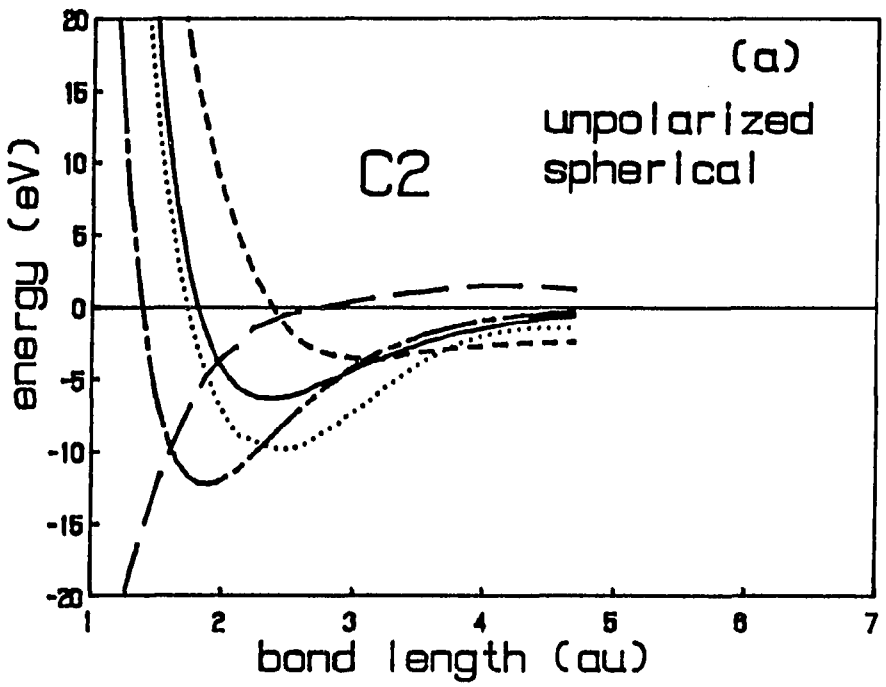
(a)
unpolarized
spherical
C2
energy (eV)
bond length (au)
20
15
10
5
0
-5
-10
-15
-20
1
2
3
4
5
6
7

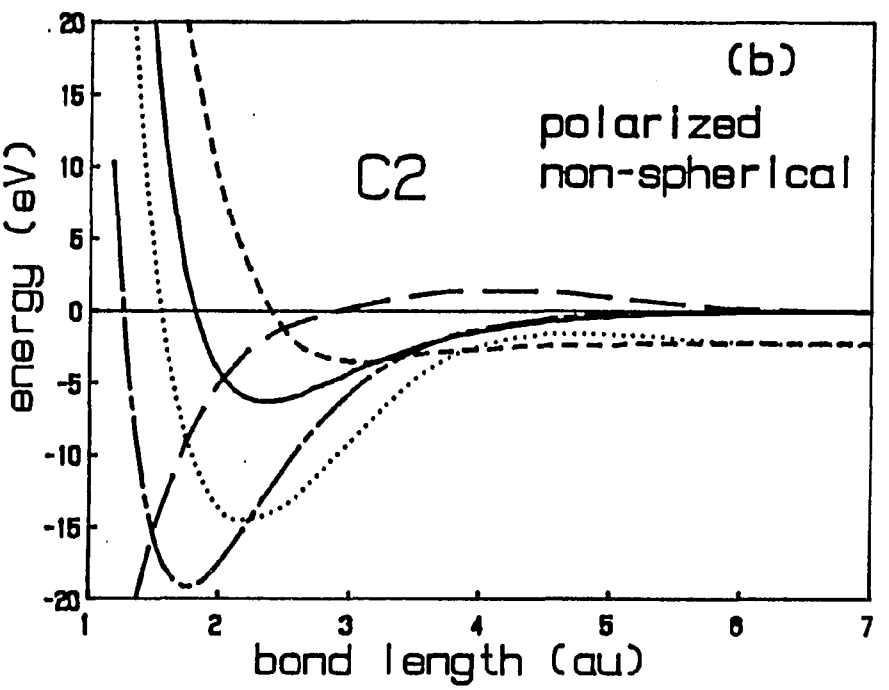
(b)
polarized
non-spherical
C2
energy (eV)
bond length (au)
20
15
10
5
0
-5
-10
-15
-20
1
2
3
4
5
6
7

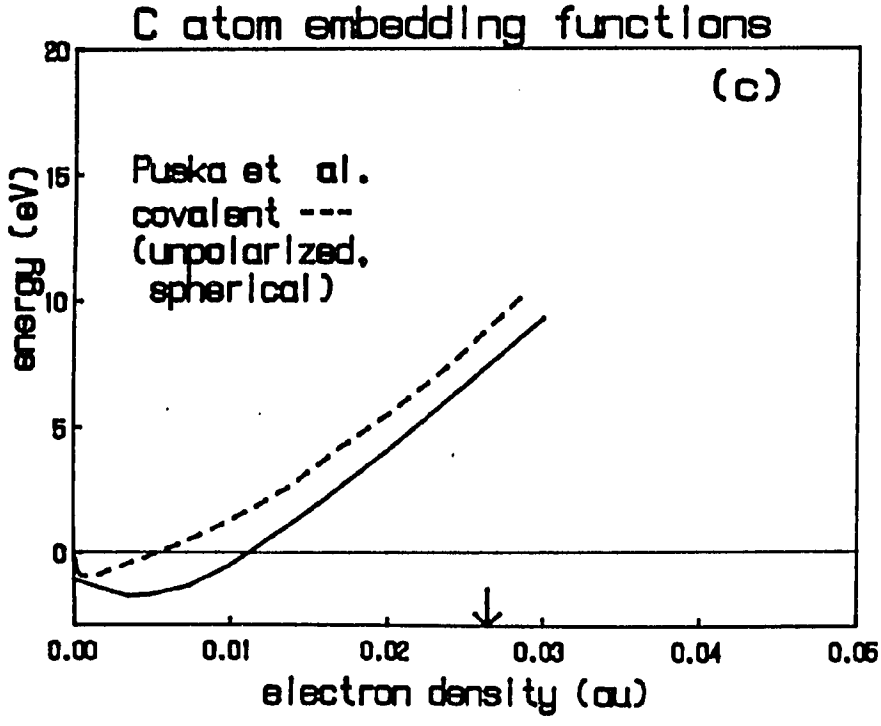


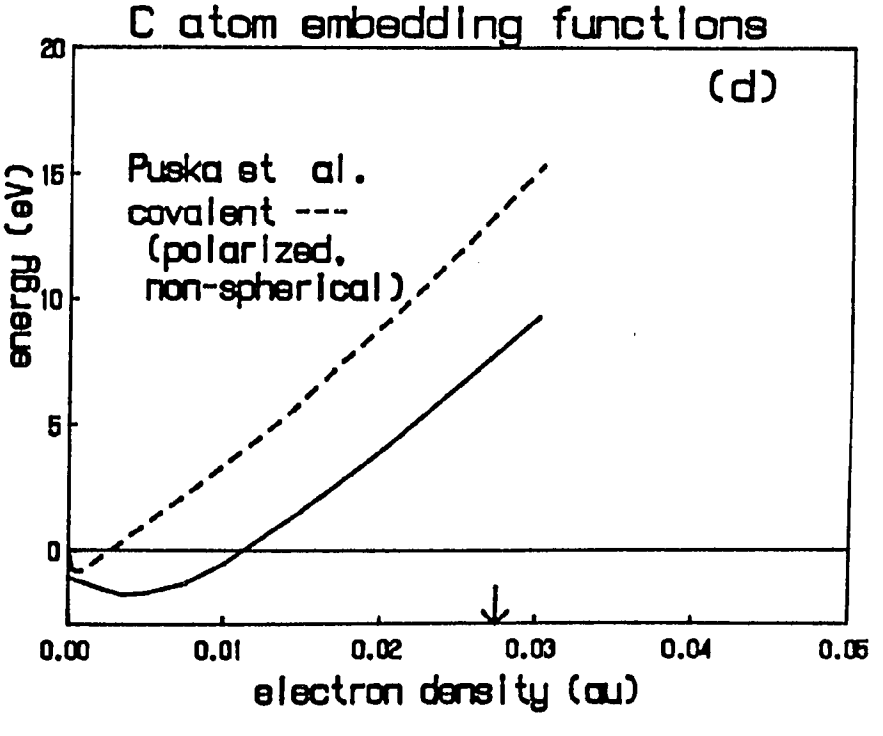


Figure 8 (Continued)

determine the bond length; in fact the Puska et al. embedding energy is nearly zero at $r_e$. Such behavior is characteristic of bonding in small molecules described by the CEM-N theory. Note also that $\Delta G(C_2)$ is also rather small near $r_e$, and thus the overestimation of the binding energy is attributable to the underestimation of the embedding energy. This indicates the need for the covalent embedding functions discussed earlier. As for previous diatomics, the CEM-N potential is quite smooth, even though the three components sometimes vary rapidly in different directions.

In the next calculation, we modeled the electron density of the $C_2$ molecule as spin-polarized with the configuration in Table II. The CEM-N and Morse diatomic potentials are shown in Fig. 8(b) along with the components of the CEM-N energy. The predicted minimum of the potential is much too deep, 14.6 eV vs. 6.32 eV [28], and is at too short of a bond length, 2.2 bohr vs. 2.35 bohr [28]. These results are much worse than those in Fig. 8(a), exactly as was the case for the $Li_2$ and $B_2$ molecules, again indicating that it is better to model the molecular density as a superposition of spherical, unpolarized atomic densities within CEM-N.

In Fig. 8(c), we show a comparison of the covalent (unpolarized, spherical) embedding function determined via Eq. (23) and the Puska et al. function. The down-arrow indicates the density corresponding to $\Delta E(C_2) = 0$. The covalent and Puska et al. functions are in disagreement as to the position and depth of the minimum but agree better with respect to the rate of increase with density on the repulsive portion of the curve. The contrast with the previous Li-J system (and similarity to the B-J system) occurs because the reorganization energy due the formation of a negative

anion in the C-J system extends to higher density. This is in accord with the greater electronegativity of the C atom. The covalent function vanishes at n = 0 while the Puska et al. function equals -1.12 eV. The vanishing of the former eliminates the zero density electron transfer associated with $\Delta E_p$, a problem discussed in detail earlier.

For completeness, we show the covalent (polarized, non-spherical) embedding function in Fig. 8(d). It is in substantially worse agreement with $\Delta E_p$ than was the covalent (unpolarized, spherical) function in Fig. 8(c).

Since the C atom can exhibit a number of valencies, we next considered an unpolarized C atom with the electronic configuration $1s^2$, $2s^1$, $2p^3$ divided equally between up- and down-spin electrons. The atomic electron density is spherical, with the two C atoms combined to form $C_2$. The CEM-N and Morse diatomic potentials are shown in Fig. 9(a) along with the components of the CEM-N energy, while the covalent embedding function is shown in Fig. 9(b). The agreement with the results in Figs. 8(a) and 8(c) is essentially perfect, demonstrating that the distinction between the $(2s^2,2p^2)$ and hybridized $(2s^1,2p^3)$ is negligible with respect to the binding in the $C_2$ molecule. This distinction will be shown in future work to be more significant for binding in graphite and diamond.

$N_2$ Molecule and Embedding Functions

The experimental equilibrium well depth and bond length are 9.91 eV and 2.07 bohr, respectively [28]. In the first calculation, we modeled the electron density of the $N_2$ molecule with two spherical, unpolarized N atoms

Figure 9. $C_2$ molecule

The diatomic Morse potential (solid line), the predicted potential using CEM-N with the Puska et al. [19] embedding function (dotted line), and the three components of the latter: homogeneous embedding energy (short dashed line), Coulombic energy (long-short dashed line), kinetic-exchange-correlation difference energy (long dashed line). (a) Spin-unpolarized, spherical and $sp^3$ hybridized C atoms. All are given as a function of bond length.

Also, the semi-empirical covalent and SCF-LD Puska et al. [19] embedding functions as a function of electron density. (b) Spin-unpolarized, spherical and $sp^3$ hybridized C atoms. The density corresponding to the distance at which the Morse potential equals zero is denoted by the vertical down-arrow. The density corresponding to the equilibrium distance of the $C_2$ molecule is indicated by the up-arrow

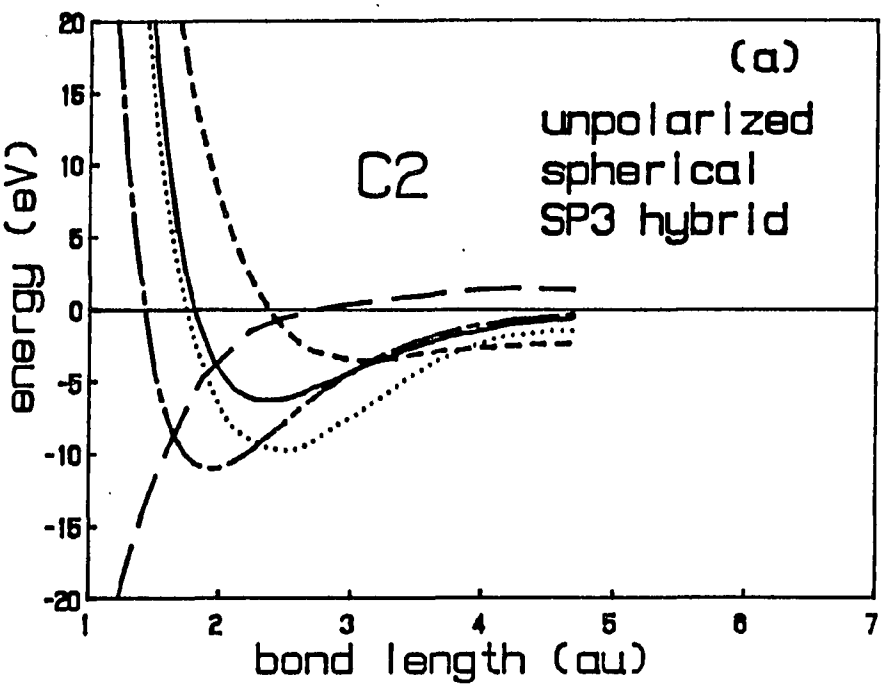


C atom embedding functions

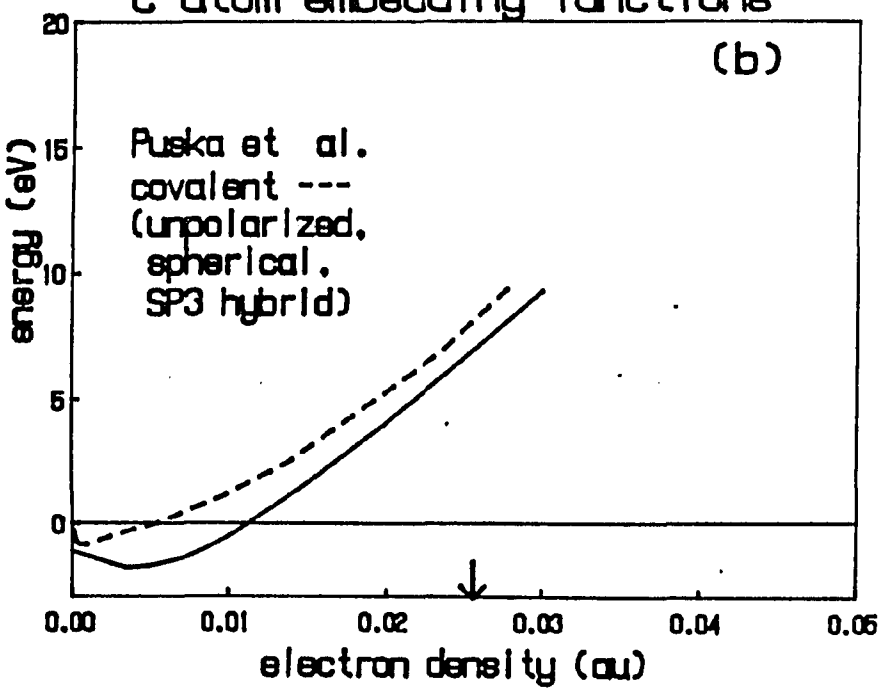

(i.e., the configuration in Table I). The CEM-N and Morse diatomic potentials are shown in Fig. 10(a) along with the components of the CEM-N energy. The predicted potential minimizes at ~2.28 bohr with a value of -9.88 eV. When contrasted with the well depth of 5.02 eV from SCF calculations [29], the CEM-N value is quite good. The bonding in $N_2$ is due to a strong Coulomb attraction, which is opposed by a repulsive $2\Delta E_p(N;n)$ and helped by $\Delta G(N_2)$. As for previous molecules, the embedding function does not determine the bond length and the CEM-N potential is quite smooth, even though the three components of the potential sometimes vary rapidly in different directions.

In the next calculation, we modeled the electron density of the $N_2$ molecule as spin-polarized with the configuration in Table II. The CEM-N and Morse diatomic potentials are shown in Fig. 10(b) along with the components of the CEM-N energy. The predicted minimum of the potential is much too deep, 14.0 eV vs. 9.91 eV [28], and is at slightly too short of a bond length, 2.02 bohr vs. 2.07 bohr [28]. These results are much worse than those in Fig. 10(a), exactly as was the case for the $Li_2$ molecule. Since there is no change in the coulomb energy between Figs. 10(a) and 10(b), the more accurate values in Fig. 10(a) provide unequivocal evidence that it is better to model the molecular density as a superposition of unpolarized atomic densities within CEM-N.

In Fig. 10(c), we show a comparison of the covalent (unpolarized) embedding function determined via Eq. (23) and the Puska et al. function. The down-arrow indicates the density corresponding to $\Delta E(N_2) = 0$. The covalent and Puska et al. functions are in excellent agreement except for

Figure 10. $N_2$ molecule

The diatomic Morse potential (solid line), the predicted potential using CEM-N with the Puska et al. [19] embedding function (dotted line), and the three components of the latter: homogeneous embedding energy (short dashed line), Coulombic energy (long-short dashed line), kinetic-exchange-correlation difference energy (long dashed line). (a) Spin-unpolarized N atoms. (b) Spin-polarized N atoms. All are given as a function of bond length.

Also, the semi-empirical covalent and SCF-LD Puska et al. [19] embedding functions as a function of electron density. (c) Spin-unpolarized N atoms. (d) Spin-polarized N atoms. The density corresponding to the distance at which the Morse potential equals zero is denoted by the vertical down-arrow. The density corresponding to the equilibrium distance of the $N_2$ molecule is indicated by the up-arrow

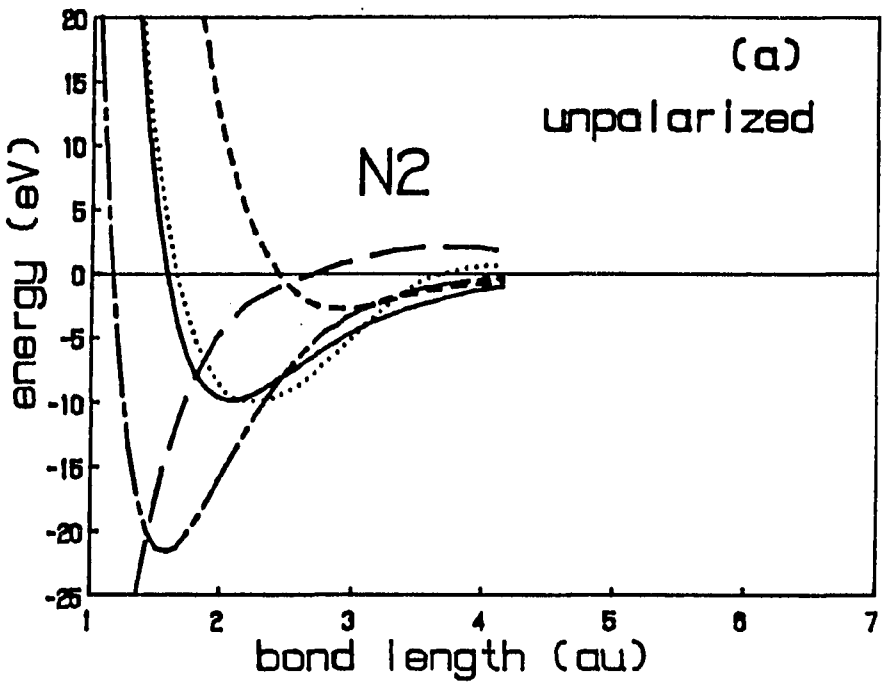
(a)
unpolarized
N2
energy (eV)
bond length (au)

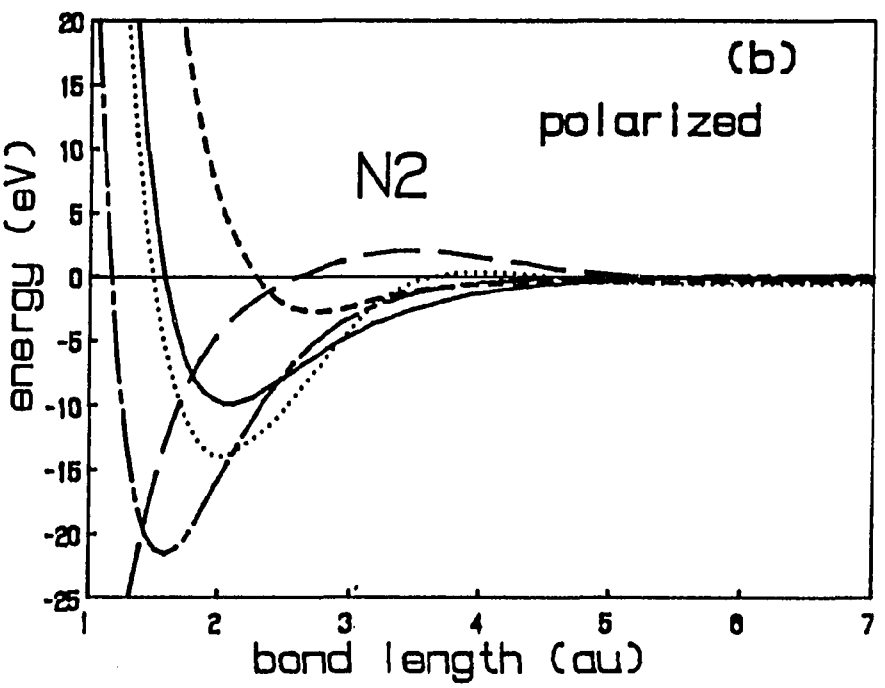
(b)
polarized
N2
energy (eV)
bond length (au)

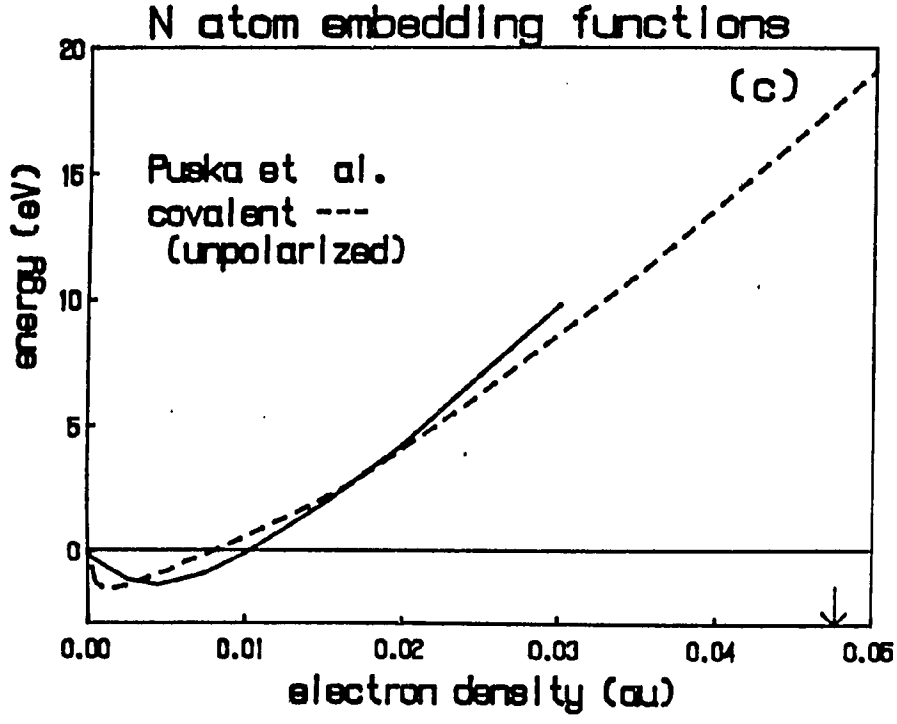


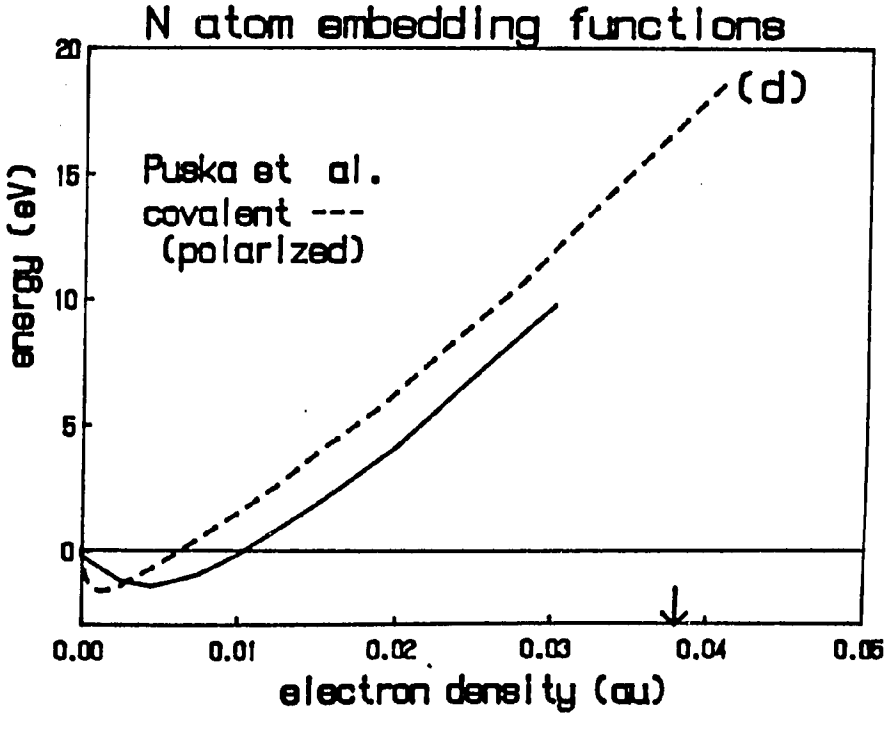


Figure 10 (Continued)

the position of the minimum. The contrast with the previous systems occurs because of the very small electron affinity of the N atom, 0.2 eV. Thus the reorganization energy due the formation of a negative anion in the N-J system is not particularly important. This system provides compelling evidence that the elimination of the zero density electron transfer problem in the $\Delta E_p$ function is central to describing bonding in small molecules; for N-J, the problem is not severe and the predicted $N_2$ binding potential is very good with the Puska et al. function.

For completeness, we show the covalent (polarized) embedding function in Fig. 10(d). It is in substantially worse agreement with $\Delta E_p$ than was the covalent (unpolarized) function in Fig. 10(c).

## $O_2$ Molecule and Embedding Functions

The experimental equilibrium well depth and bond length are 5.21 eV and 2.28 bohr, respectively [28]. In the first calculation, we modeled the electron density of the $O_2$ molecule with two spherical, unpolarized O atoms (i.e., the configuration in Table I). The CEM-N and Morse diatomic potentials are shown in Fig. 11(a) along with the components of the CEM-N energy. The predicted potential minimizes at ~2.16 bohr with a value of -14.2 eV. In the next calculation, we modeled the electron density of the $O_2$ molecule as spin-polarized with the configuration in Table II. The CEM-N and Morse diatomic potentials are shown in Fig. 11(b) along with the components of the CEM-N energy. The predicted potential minimizes at ~2.2 bohr with a value of -13.6 eV. For comparison, the SCF well depth is 1.12 eV [29].

Figure 11. $O_2$ molecule

The diatomic Morse potential (solid line), the predicted potential using CEM-N with the Puska et al. [19] embedding function (dotted line), and the three components of the latter: homogeneous embedding energy (short dashed line), Coulombic energy (long-short dashed line), kinetic-exchange-correlation difference energy (long dashed line). (a) Spin-unpolarized and spherical O atoms. (b) Spin-polarized and non-spherical O atoms. All are given as a function of bond length.

Also, the semi-empirical covalent and SCF-LD Puska et al. [19] embedding functions as a function of electron density. (c) Spin-unpolarized and spherical O atoms. (d) Spin-polarized and non-spherical O atoms. The density corresponding to the distance at which the Morse potential equals zero is denoted by the vertical down-arrow. The density corresponding to the equilibrium distance of the $O_2$ molecule is indicated by the up-arrow

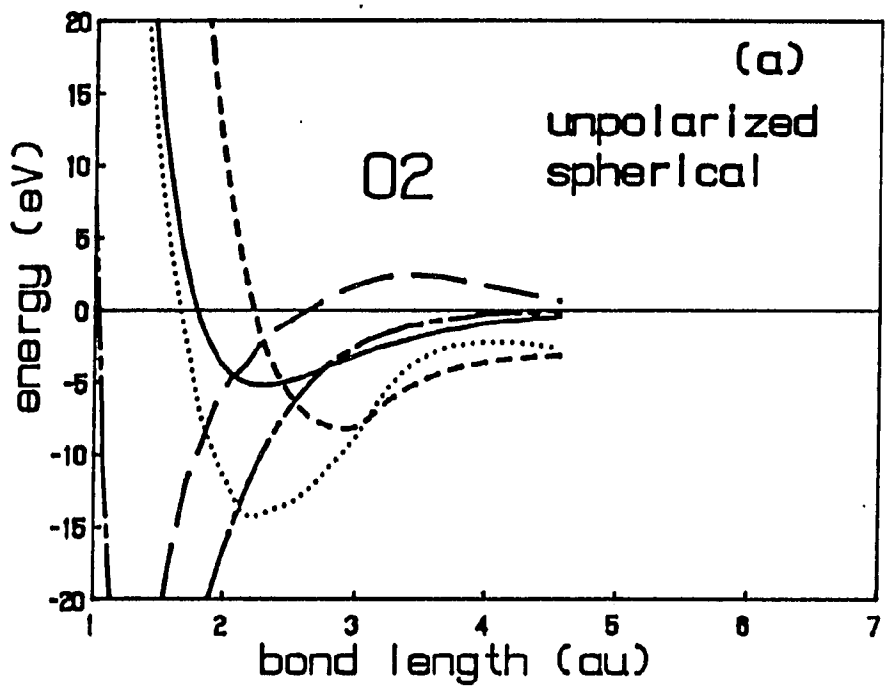
(a)
unpolarized
spherical
O2
energy (eV)
bond length (au)
20
15
10
5
0
-5
-10
-15
-20
1
2
3
4
5
6
7

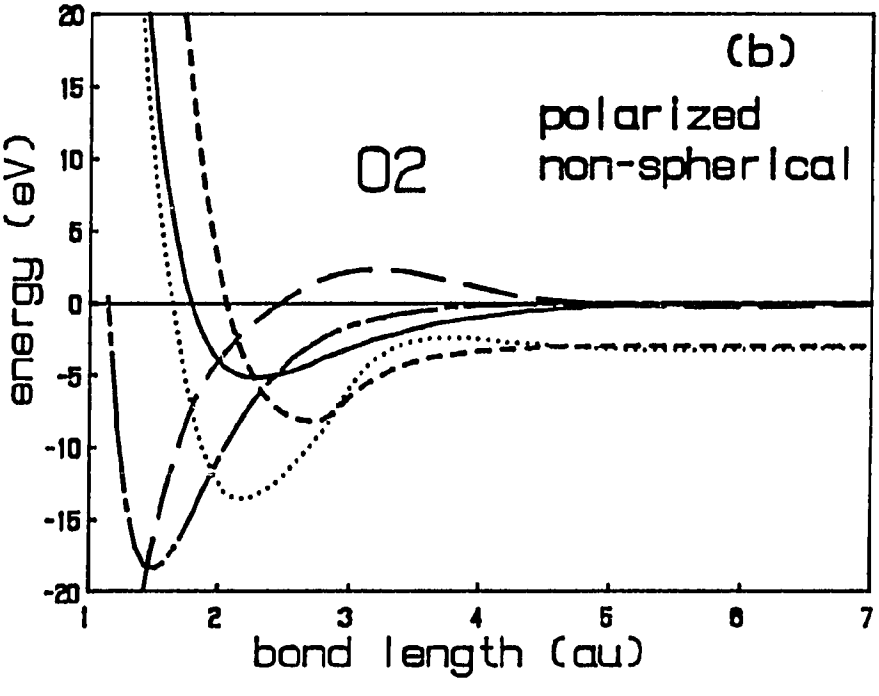
(b)
polarized
non-spherical
O2
energy (eV)
bond length (au)
20
15
10
5
0
-5
-10
-15
-20
1
2
3
4
5
6
7

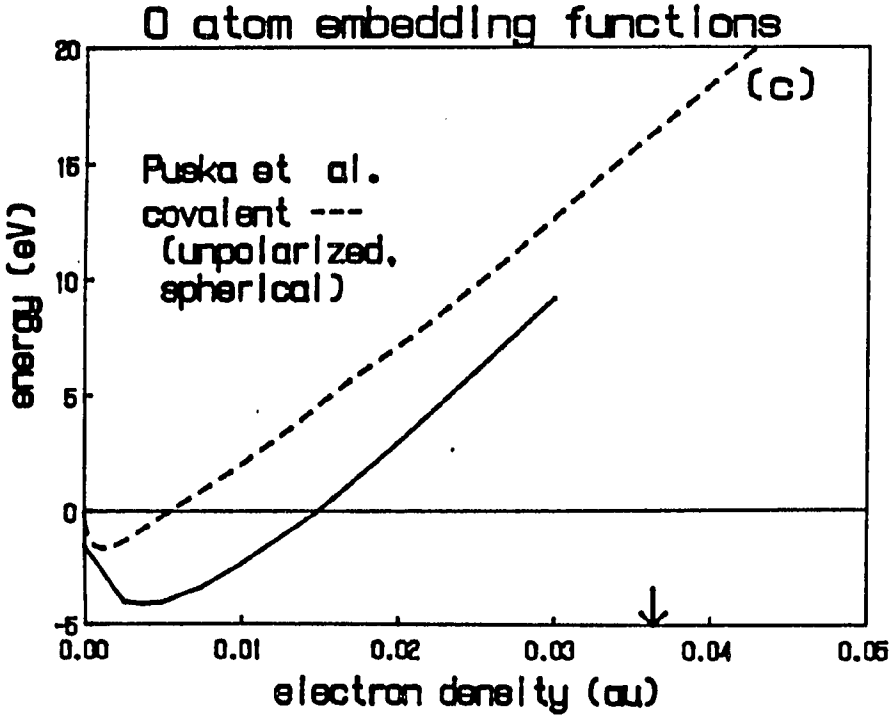


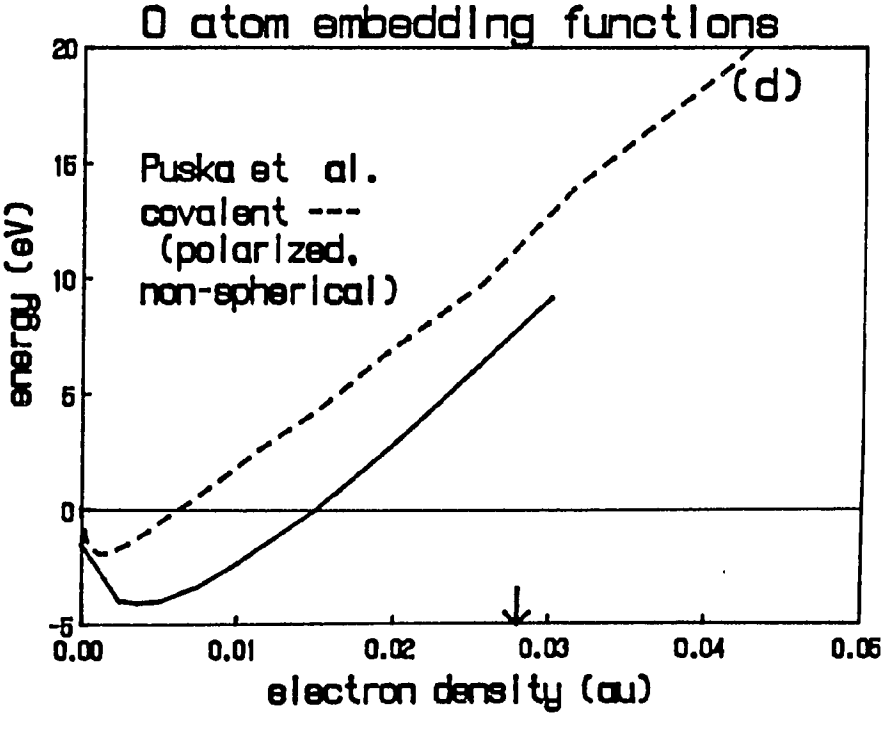


Figure 11 (Continued)

The minima predicted by both of these potentials are much too large. To see why $O_2$ is treated so poorly in contrast to the previous diatomics, consider the bonding in more detail. Note that the bonding in $O_2$ is due to about equal contributions from the Coulomb attraction and $2\Delta E_p(0;n)$, with only a small contribution due to $\Delta G(O_2)$. The spherical treatment yields a larger Coulomb contribution. The significant difference from $B_2$, $G_2$ and $N_2$ is the much larger effect of $\Delta E_p$, and this is a manifestation of the much larger reorganization energy of the O atom in jellium. The minimum of $2\Delta E_p(0;n)$ does not determine the bond length. Although the value of $\Delta G(O_2)$ at $r_e$ could be raised from about -2 eV to zero by reducing the homogeneous gas density, this would actually lower the minimum of the CEM-N potential since the value of $2\Delta E_p(0;n)$ would decrease more than this 2 eV.

The above discussion leads again to the problem with the low density electron transfer behavior for atoms in jellium. This is especially severe for the O atom due to a significant electron affinity of 1.47 eV and a propensity to form $O^{2-}$. The latter is the reason for the extremely large decrease of $\Delta E_p$ with increasing density at low density.

In Figs. 11(c) and 11(d), we show a comparison of the covalent (unpolarized, spherical) and covalent (polarized, non-spherical) embedding function determined via Eq. (23) and the Puska et al. function. The down-arrow indicates the density corresponding to $\Delta E(O_2) = 0$. The covalent and Puska et al. functions are in disagreement as to the position and depth of the minimum but agree better with respect to the rate of increase with density on the repulsive portion of the curve. Note that both embedding functions are essentially the same, reflecting the similarity of the

predicted potentials in Figs. 11(a) and 11(b). Both vanish at n = 0, thus eliminating the zero density electron transfer associated with $\Delta E_p$, a problem discussed earlier in detail.

## $F_2$ Molecule and Embedding Functions

The experimental equilibrium well depth and bond length are 1.66 eV and 2.67 bohr, respectively [28]. In the first calculation, we modeled the electron density of the $F_2$ molecule with two spherical, unpolarized F atoms (i.e., the configuration in Table I). The CEM-N and Morse diatomic potentials are shown in Fig. 12(a) along with the components of the CEM-N energy. The predicted potential minimizes at ~2.45 bohr with a value of -9.5 eV. In the next calculation, we modeled the electron density of the $F_2$ molecule as spin-polarized with the configuration in Table II. The CEM-N and Morse diatomic potentials are shown in Fig. 12(b) along with the components of the CEM-N energy. The predicted potential minimizes at ~2.53 bohr with a value of -10.9 eV. For comparison, the SCF well depth is -1.40 eV [29].

As for $O_2$, the minima predicted by both of these potentials are much too large. It is easy to see that the remnant of the zero density electron transfer, (i.e., $2\Delta E_p(F;n=0)$ = -7.02 eV), distorts the predicted potentials and makes them much too attractive. The distortion of the shape clearly precludes simple addition of the this value to the predicted potentials. The F molecule provides perhaps the most striking example of the need for a covalent embedding function.

Figure 12. $F_2$ molecule

The diatomic Morse potential (solid line), the predicted potential using CEM-N with the Puska et al. [19] embedding function (dotted line), and the three components of the latter: homogeneous embedding energy (short dashed line), Coulombic energy (long-short dashed line), kinetic-exchange-correlation difference energy (long dashed line). (a) Spin-unpolarized and spherical F atoms. (b) Spin-polarized and non-spherical F atoms. All are given as a function of bond length.

Also, the semi-empirical covalent and SCF-LD Puska et al. [19] embedding functions as a function of electron density. (c) Spin-unpolarized and spherical F atoms. (d) Spin-polarized and non-spherical F atoms. The density corresponding to the distance at which the Morse potential equals zero is denoted by the vertical down-arrow. The density corresponding to the equilibrium distance of the $F_2$ molecule is indicated by the up-arrow

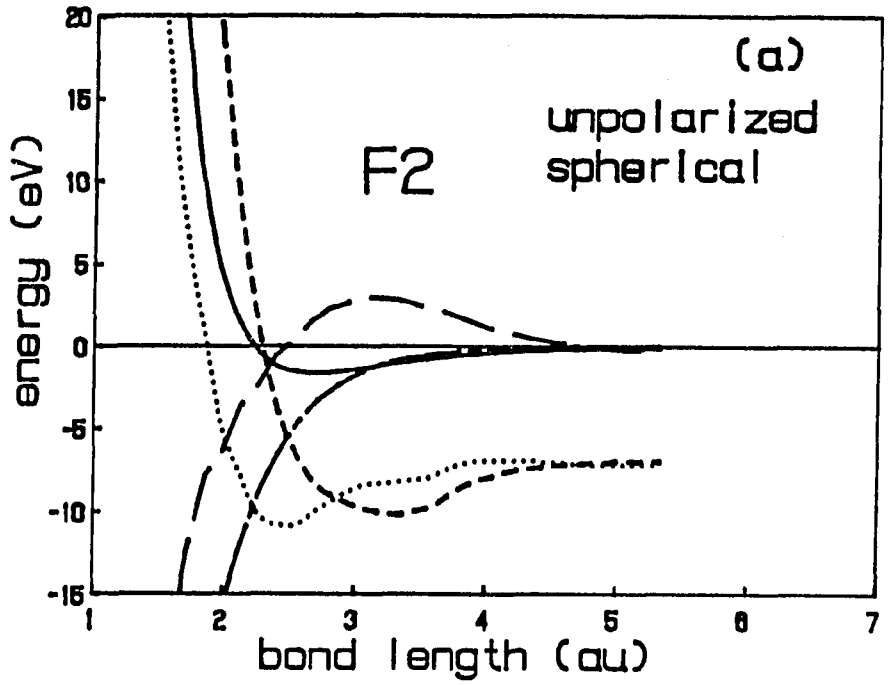
(a)
unpolarized
spherical
F2
energy (eV)
bond length (au)
20
15
10
5
0
-5
-10
-15
1
2
3
4
5
6
7

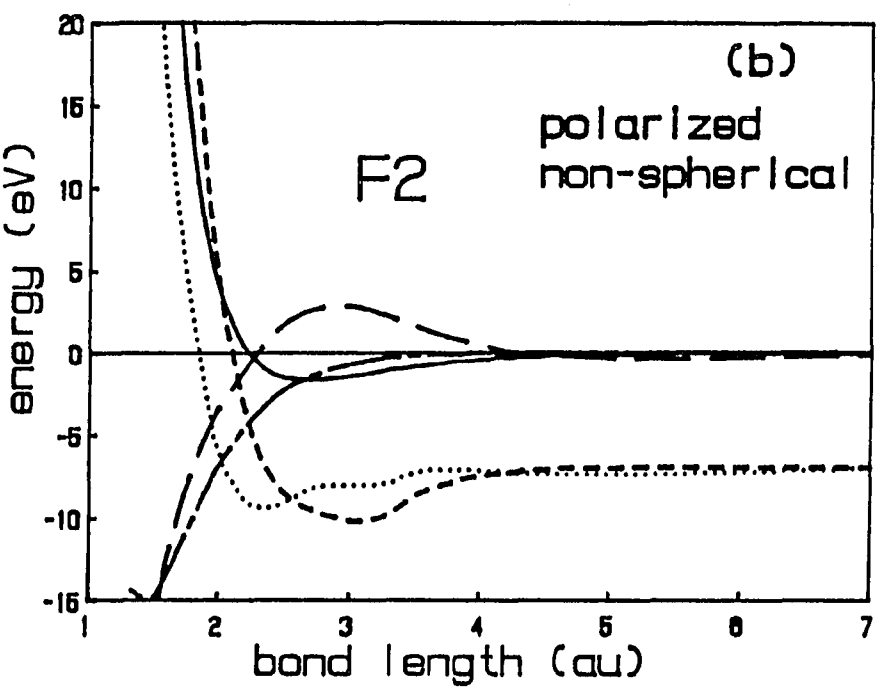
(b)
polarized
non-spherical
F2
energy (eV)
bond length (au)
20
15
10
5
0
-5
-10
-15
1
2
3
4
5
6
7

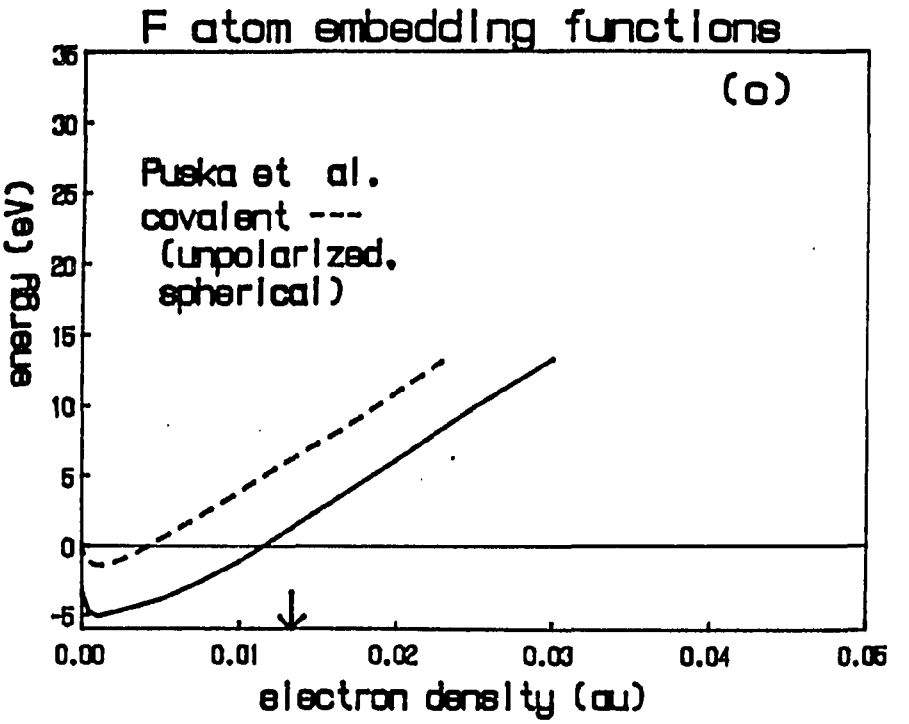


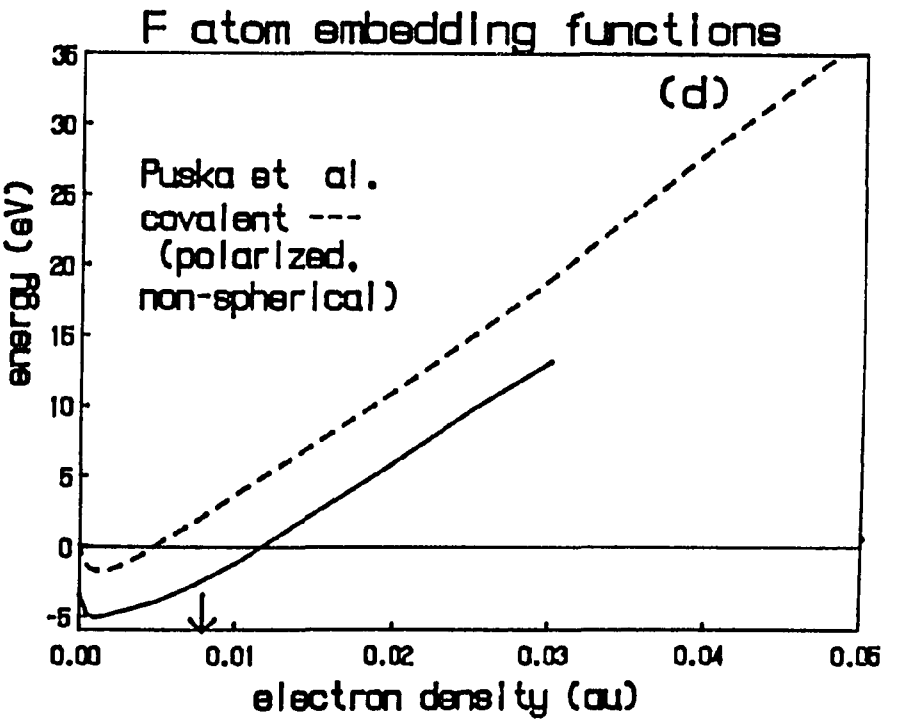


Figure 12 (Continued)

In Figs. 12(c) and 12(d), we show a comparison of the covalent (unpolarized, spherical) and covalent (polarized, non-spherical) embedding function determined via Eq. (23) and the Puska et al. function. The down-arrow indicates the density corresponding to $\Delta E(F_2) = 0$. The covalent and Puska et al. functions are in disagreement as to the position and depth of the minimum but agree better with respect to the rate of increase with density on the repulsive portion of the curve. Note that both embedding functions are essentially the same, reflecting the similarity of the predicted potentials in Figs. 12(a) and (b). Both vanish at $n = 0$, thus eliminating the zero density electron transfer associated with $\Delta E_p$, a problem discussed earlier in detail.

# SUMMARY AND CONCLUSIONS

We have presented a general corrected effective medium theory which yields the interaction energy of an N atom system. This is to be contrasted with a previous version of the CEM theory which provided the interaction energy for a single atom embedded into the other (N-1) atoms acting as a host. The CEM method presented in this paper treated all N atoms on an equal basis without identifying all but one as a host. The basis for this theory involved expressing the interaction energy for the real system in terms of the sum of the interaction energies for each atom embedded into jellium of appropriate density. With the energies provided by density functionals (evaluated within a superposition of atomic densities approximation), minimization of the difference in kinetic-exchange-correlation energy between the real and effective system yielded the prescription for choice of the electron densities of each jellium system. The full interaction energy then consisted of three terms: the embedding energy, Coulombic energy, and kinetic-exchange-correlation difference energy.

In an attempt to alleviate the troublesome behavior of the SCF-LD embedding functions of Puska et al. [19] which provide a residual interaction energy at zero jellium density, the difference between the jellium (A-J) and real (A-B) systems was interpreted using a charge transfer model. The main distinction was the donation of an electron from the Fermi level of the jellium at -WF(n) versus the donation of an electron from the HOAO of atom B at -IP(B) in the two cases, respectively. This

interpretation suggested the existence of a more complicated universal embedding energy function, which would be a function of both jellium density and Fermi level. The Puska et al. embedding functions corresponded to the case of $E_f = -WF(n)$. To determine the embedding energies for the case of $E_f = -IP(A)$, we constructed semi-empirical functions using the binding potentials for homonuclear ($A_2$) diatomic molecules. These covalent embedding functions are universal for homonuclear systems and thus have intrinsic utility in predicting the properties of homonuclear many-atom clusters.

Using the Puska et al. embedding functions, we predicted the CEM-N binding potentials for $H_2$, $Li_2$, $B_2$, $C_2$, $N_2$, $O_2$, and $F_2$ and compared the results with SCF and experimental potentials. A summary of the data is provided in Table IV where the atomic densities were set unpolarized and spherically symmetric. The modeling of the molecular density in this manner, which mimics a molecular orbital scheme, provided a better representation of the potentials than those generated with polarized and non-spherically symmetric atomic densities, which mimic a valence orbital scheme. All the CEM-N potentials exhibited a smooth behavior as a function of bond length even though the three components of the interaction energy all varied rapidly and often in different directions. Specifically, the $H_2$ CEM-N binding energy was of the same accuracy as the SCF value. The $Li_2$ CEM-N binding energy was better than the SCF result, although a metastable minimum occurs in the CEM-N potential due to the zero density limit of the Puska et al. embedding function. The $N_2$ CEM-N potential was very accurate when compared to experiment. The $B_2$, $C_2$, $O_2$, and $F_2$ CEM-N potentials were

Table IV. Experimental, SCF, and CEM-N binding potentials for selected homonuclear diatomic molecules

| | Expt. | | SCF[a] | | CEM-N[b] | |
|---|---|---|---|---|---|---|
| molecule | $D_e$ (eV) | $r_e$ (bohr) | $D_e$ (eV) | $r_e$ (bohr) | $D_e$ (eV) | $r_e$ (bohr) |
| $H_2$ | 4.7446 | 1.4100 | 3.63 | 1.38 | 3.45 | 2.0 |
| $Li_2$ | 1.07 | 5.051 | 0.16 | 5.051 | 1.00 | ~5.0[c] |
| $B_2$ | 3.085 | 3.005 | 0.81 | | 5.44 | ~2.85 |
| $C_2$ | 6.32 | 2.350 | 0.68 | | 9.8 | ~2.5 |
| $N_2$ | 9.906 | 2.074 | 5.02 | 2.068 | 9.88 | ~2.28 |
| $O_2$ | 5.214 | 2.282 | 1.12 | 2.282 | 14.2 | ~2.16 |
| $F_2$ | 1.66 | 2.668 | 1.40 | 2.68 | 9.5 | ~2.45 |

[a]Data from refs. [29] and [30].

[b]CEM-N values calculated with the Puska et al. embedding functions and with spin-unpolarized and spherically symmetric atomic densities.

[c]Metastable.

all too deep with respect to the experimental values. This overestimation of the binding energy was attributed to an underestimation of the embedding energy. The latter was mainly due to the zero density behavior of the Puska et al. embedding function which lead to an embedding energy too deep in the low density region. This problem indicated the need for the covalent embedding functions which were provided for the above mentioned diatomics. The covalent functions also provided the correct dissociation energy in the limit of infinite separation between the atoms.

We presented the formalism for constructing the jellium densities in the case where only M atoms out of the total N atom system were active with the remaining (N-M) atoms grouped together to form the host. One possible application of this division into active and host atoms is that of molecular chemisorption. Choosing the atoms of the adsorbing molecule as active, the atoms which make up the absorption surface could be chosen as the host. If backbinding of the surface into the adsorbate is desired, the system could also be studied using the full N-active atom formalism provided that the embedding energy function for the surface material exists. Investigations of this type are underway at the present time. Other future research will involve the determination of the equilibrium configurations of small atomic clusters and the effects which adsorbates have upon these configurations.

ACKNOWLEDGEMENT

This work was supported by NSF. We are pleased to note helpful conversations with Dr. S. Elbert and Prof. K. Ruedenberg. One of us (AED) benefited from discussions with Prof. J. Norskov.

REFERENCES


1. See, for example, P. Carsky and M. Urban, "Ab-initio Calculations, Lecture notes in Chemistry", Springer, Berlin, 1980, Vol. 16.
2. K. Raghavachari, J. Chem. Phys. 84, 5672 (1986).
3. R. P. Messmer, J. Vac. Sci. Tech. A 2, 899 (1984).
4. T. H. Upton and W. A. Goddard III, in "Chemistry and Physics of Solid Surfaces", edited by R. Vanselow and W. England, CRC Press, Boca Raton, Florida, 1985, Vol. III.
5. a) R. A. Chiles, C. E. Dykstra and K. D. Jordan, J. Chem. Phys. 75, 1044 (1981); b) W. C. Ermler, C. W. Kern, R. M. Pitzer and N. W. Winter, J. Chem. Phys. 84, 3937 (1986).
6. J. W. D. Connolly, "Modern Theoretical Chemistry, vol. 7", edited by G. A. Segal, Plenum, New York, 1977, Chapter 4.
7. N. A. Baykar, J. Andzelm, D. R. Salahub and S. Z. Baykara, Int. J. Quantum Chem. 29, 1025 (1986).
8. a) G. Kemister and S. Nordholm, J. Chem. Phys. 83, 5163 (1985); b) O. Gunnarsson and R. O. Jones, Phys. Rev. A 31, 7588 (1985).
9. For a survey, see U. von Barth and A. R. Williams, in "Theory of the Inhomogeneous Electron Gas", edited by S. Lundqvist and N. H. March, Plenum, New York, 1983.
10. E. Wimmer, C. L. Fu and A. J. Freeman, Phys. Rev. Lett. 55, 2618 (1985).
11. D. C. Langreth and M. J. Mehl, Phys. Rev. B 28, 1809 (1983).
12. a) A. E. DePristo and J. D. Kress, J. Chem. Phys. 86, 1425 (1987); b) J. P. Perdew, Phys. Rev. Lett. 55, 1665 (1985); c) A. D. Becke, J.

Chem. Phys. 84 4524 (1986); d) S. K. Ghosh and R. G. Parr, Phys. Rev. A 34, 785 (1986); e) O. Gunnarsson, M. Jonson and B. I. Lundqvist, Phys. Rev. B 20, 3136 (1979).

13. J. P. Perdew, Phys. Rev. B 33, 8822 (1986).
14. J. D. Kress and A. E. DePristo, "Corrected Effective Medium Method. I. One-body formulation with applications to atomic chemisorption and diatomic molecular potentials", J. Chem. Phys., accepted.
15. See, P. Nordlander, S. Holloway and J. K. Norskov, Surf. Sci. 136, 59 (1984), and references therein.
16. B. Chakraborty, S. Holloway and J. K. Norskov, Surf. Sci. 152, 660 (1985).
17. K. W. Jacobsen, J. K. Norskov and M. J. Puska, Phys. Rev. B 35, 7423 (1987).
18. M. J. Stott and E. Zaremba, Phys. Rev. B 22, 1564 (1980).
19. M. J. Puska, R. M. Nieminen and M. Manninen, Phys. Rev. B 24, 3037 (1981); supplemented by M. J. Puska, Helsinki University of Technology, Helsinki, Finland, private communication.
20. G. L. Oliver and J. P. Perdew, Phys. Rev. A 20, 397 (1979).
21. U. von Barth and L. Hedin, J. Phys. C 5 1629 (1972).
22. O. Gunnarsson and B. I. Lundqvist, Phys. Rev. B 13, 4274 (1976).
23. M. S. Daw and M. I. Baskes, Phys. Rev. B 29, 6443 (1984); for references to more recent work see, S. M. Foiles, M. I. Baskes and M. S. Daw, Phys. Rev. B 33, 7983 (1986).
24. W. Kohn and L. J. Sham, Phys. Rev. A 140, 1133 (1965).
25. S. Huzinaga, Prog. Theor. Physics Suppl. 40, 279 (1967).

26. A. E. DePristo and J. D. Kress, Phys. Rev A 35, 438 (1987).

27. E. Clementi, IBM J. Res. Develop. Suppl. 9 (1965); P. S. Bagus, T. L. Gilbert and C. J. Roothan, J. Chem. Phys. 56, 5159 (1972).

28. K. P. Huber and G. Herzberg, "Constants of Diatomic Molecules", Von Nostrand, New York, 1979.

29. M. W. Schmidt, M. T. B. Lam, S. T. Elbert and K. Ruedenberg, Theor. Chim. Acta 68, 69 (1985).

30. R. S. Mulliken and W. C. Ermler, "Diatomic Molecules", Academic Press. New York, 1977.

31. J. N. Murrell, S. Carter, S. C. Farantos, P. Huxley and A. J. C. Varandas, "Molecular Potential Energy Functions", John Wiley, New York, 1984.

32. See B. I. Dunlap and M. Cook, Int. J. Quantum Chem. 23, 767 (1986) for a discussion of integration methods.

33. M. Abramowitz and I. A. Stegun, "Handbook of Mathematical Functions", Dover. New York, 1972.

# APPENDIX: MULTICENTER THREE-DIMENSIONAL INTEGRATION

The major numerical problem which must be addressed in the implementation of the CEM-N theory is the efficient calculation of the integrals over the kinetic, exchange, and correlation energy functionals. We denote the generic integral by

$$F = \int f(n)\, d\underline{r} \,, \tag{A1}$$

where f(n) is a function of the total electron density due to all the atoms. This function will peak around each center $\underline{r}_i$, and therefore any attempt to perform the three-dimensional quadrature with a fixed spatial origin is destined to be extremely inefficient. Hence we must move the origin around each of the centers. The standard way to do this integral [32] involves setting up a radial Herman-Skillman based grid around each center along with an angular grid chosen as pointing to the centers, sides or vertices of a cube. The quadrature weights are then the volumes around each point. The weakness in this approach is that each quadrature is not optimal. In particular, the radial integration would perhaps be more optimal if one could use Gauss-Laguerre (or Gauss-Hermite) quadrature while the angular integrations would certainly be most efficient over $\theta$ and $\phi$ using Gauss-Legendre and Gauss-Chybyshev quadrature. This would also allow considerable flexibility in the choice of the number of quadrature points.

Since a three-dimensional Gaussian quadrature is defined on an infinite range already, implementation of this scheme for a multicenter

integrand is not apparent. The 'trick' is to define new integrands in the following manner:

$$f_i(n) = f(n) \qquad |\underline{r}-\underline{r}_i| < |\underline{r}-\underline{r}_j| \quad \text{for all } j \neq i \tag{A2}$$

$$= 0 \qquad \text{otherwise .}$$

This has the effect of dividing the integrand into N pieces, defined simply by whether any point in space is closer to center $\underline{r}_i$ than any other center. Eq. (A1) can be rewritten exactly as

$$F = \sum \int f_i(n)\, d\underline{r}_i \ . \tag{A3}$$

Integration of Eq. (A3) can be accomplished with high accuracy using Gaussian quadrature schemes at each center, especially in the angular variables. Within a computer program, one centers the origin at $\underline{r}_i$ and performs a three-dimensional quadrature with the additional but trivial work of checking whether each point in space is closer to the center at $\underline{r}_i$. If a point is closer, then the integrand f(n) is evaluated. If not, then the point is skipped, since multiplication by zero is unnecessary. Indeed, since f(n) is rather complex and time consuming to evaluate, the work of evaluating all the distances is a small part of the integration effort. The reader should note that as the centers coalesce, discontinuity of the functions $f_i(n)$ render the Gaussian radial quadrature scheme impractical. In practice, when this occurs we have found that the radial quadrature can be performed to high accuracy using a quartic polynomial rule [33].

# SUMMARIES, CONCLUSIONS, AND EXTENSIONS

## Interaction Picture Gaussian Wavepacket Dynamics

In Paper I, a scheme to treat the atom-diatom collinear exchange reaction using the semiclassical propagation of Gaussian wavepackets (GWPs) has been presented. Two extensions to the present technology of Gaussian wavepacket dynamics (GWD) were needed to adequately describe the scattered wavefunction which bifurcates into both the reactant's and product's channel. First, the interaction picture representation in each channel of the scattering wavefunction was explicitly evaluated by integrating the GWP equations of motion forward in time using the full interaction Hamiltonian followed by a subsequent integration backwards in time using a channel Hamiltonian. Second, to provide more flexibility in the GWP basis, the initial translational wavefunction was linear least squares fit to a plane wave using GWPs, thus providing an expansion in both the translational and vibrational degrees of freedom. The use of these two extensions provided a propagation scheme, (denoted IPGWD-M), which was independent of: 1) the choice of the stopping time for the integration of the GWP equations of motion in the asymptotic region of the interaction potential; and 2) the initial representation of the initial wavefunction. Within the IPGWD-M approach, two desirable properties present in the standard GWD method still remain: 1) each GWP in the wavefunction expansion remains Gaussian throughout the entire propagation; and 2) each GWP propagates

independently, yielding trajectories for the phase space parameters which adhere strictly to Hamilton's equations.

The IPGWD-M procedure was applied to the H + $H_2$ collinear exchange reaction using the Porter-Karplus potential energy surface. Satisfactory results for the reaction probabilities, in comparison to the quantum results, were obtained for total system energies between the "practical" classical threshold of 0.51 eV, and 0.58 eV.

In the only previous treatment of a collinear exchange reaction using the standard GWD method, application to the F + $H_2$ reaction [17] yielded a final scattering wavefunction $|\psi_{out}>$ which failed to conserve norm. The failure of this study, as well as the failure of the author's attempt to treat the H + $H_2$ reaction using the standard GWD method, was due mainly to two reasons. First, only a forward propagation in time was used, thus creating an uncertainty in $|\psi_{out}>$. Second, and more importantly, the use of a single GWP representation for the initial translational state X(x) in a two arrangement channel problem biased $|\psi_{out}>$ due to the non-invariance of the initial wavefunction with respect to a choice of the initial translational coordinate parameter $x_0$. The IPGWD-M procedure eliminated these two inaccuracies and provided a significant improvement in the application of GWP dynamics formalism to the collinear reactive scattering problem.

Still, the IPGWD-M method as applied to collinear exchange reactions can be improved and extended in many ways. One such adjustment is to remove the proportionality between the values of the translational ($\beta^x$) and vibrational ($\beta^y$) widths. (See Eq. (34) in Paper I.) This modification,

which is simple to implement within the current IPGWD-M computer code, provides an extra variational freedom when attempting to construct a normed $|\psi_{out}>$, since both $\beta^x$ and $\beta^y$ can be varied. By allowing both $\beta^x$ and $\beta^y$ to vary, a crossterm parameter multiplying $(x'-x_j')\cdot(y-y_j')$ appears in the argument of the GWPs, given by Eq. (32c) in Paper I, for any classical trajectory which ends in the product's channel. As pointed out in Paper I, the integration of the coupled differential equations of motion, which arise for the crossterm and width parameters in the product's channel (see Eq. (33) in Paper I), can be accomplished by integrating the equations of motion to and from time = 0 for all the GWP parameters in the reactant's channel. Then, the parameters which reside in the product's channel asymptotically can be transformed to the appropriate values. This yields a $|\psi_{out}>$ in the product's channel which is non-separable in x' and y' due to the crossterms. But, these crossterms may provide a better description of the dynamics with the only increase in effort being a two parameter non-linear search to determine $\beta^x$ and $\beta^y$.

Another extension to the IPGWD-M method would be to allow the GWPs to propagate coupled to each other. Propagating the IPGWD-M wavefunction using the MEM formalism [9] may incorporate more quantum effects into the scattering wavefunction, since the GWPs are allowed to communicate with each other through the coupled MEM equations of motion for the phase space parameters. However, the MEM approach does require a large increase in computational effort since the coupled trajectories for the phase space parameters must be run for every choice of $\beta^x$ and $\beta^y$ when constructing a normed $|\psi_{out}>$. This should be contrasted with the IPGWD-M method outlined

in Paper I, where more than one $|\psi_{out}>$ for a given total classical energy can be constructed from a single run of classical trajectories. Both $\beta^x$ and $\beta^y$ can be varied independently of the classical trajectories since the width parameter equations of motion are decoupled from the equations of motion for the phase space parameters.

Quantum mechanical tunneling through a barrier by a semiclassically propagated GWP is a desirable feature which is not possible using the present approaches. Since the center of a propagated GWP obeys classical mechanics and since the GWP retains its shape, the GWP cannot tunnel. Attempts to model a single GWP tunneling event, such as using a "ghost" GWP in product's space [34], have failed. A fundamental method to allow a semiclassically propagated GWP to tunnel would greatly improve the IPGWD-M description of quantum dynamics in the tunneling region. (See Fig. (3) in Paper I.)

## The Corrected Effective Medium Theory

In Paper II, a corrected effective medium theory (CEM) has been derived which describes the binding between a single atom and an inhomogeneous host. This one-active-body approach was denoted CEM-1. The zeroth order term of the CEM-1 interaction was represented by the embedding energy of the atom into a spin-unpolarized homogeneous electron gas with compensating positive background (i.e., the effective medium was jellium). The Coulomb interactions between the atom and the host were accounted for by an explicit evaluation of the electrostatic interactions between the charge densities on the atom and host. The difference in kinetic-exchange-

correlation energies between the atom/inhomogeneous host system and the atom/jellium system was provided by a spin-polarized density functional evaluation. Both the coulomb and difference energy terms were calculated using a superposition of atomic charge densities approximation. The contribution from the difference energy was minimized by constructing the appropriate jellium density using the averaged sampling procedure. This minimization ensured that the non-self-consistent terms which depend on the jellium density were as small as possible. The embedding energy provided the many-electron energy, which is difficult to calculate for a real inhomogeneous host, via a self-consistent treatment of the atom embedded in jellium. It is worthwhile to note that the CEM formalism can be interpreted as a spin-polarized generalization of the Gordon-Kim electron gas model where a self-consistent reference system, the atom in jellium, is used instead of the original reference system, vacuum.

The CEM-1 method was applied to the description of an H atom embedded into spin-polarized jellium, yielding results in good agreement with the SCF-LD values. The CEM-1 method was also used to calculate the binding potentials for a set of hydrogen containing diatomic molecules. The use of spin-polarized atomic densities and an averaged homogeneous electron density sample provided the best CEM-1 potentials both in terms of binding energy and equilibrium binding length.

Next, the CEM-1 method was applied to H atom chemisorption on the transition metal surfaces, Ni(100), Cu(100) and Fe(110). By representing the metal surface as a finite cluster of spin-unpolarized metal atoms, chemisorption potentials were examined as a function of: 1) the symmetry

site within the surface unit cell; 2) homogeneous electron density sampling procedure; 3) spin polarization of the H atom; and, 4) occupation of the valence 4s electron density of the metal. The options implemented within the CEM-1 method which generated potentials most consistent with experiment were the use of the averaged sampling procedure and a polarized H atom spin density. It also was found that the H atom preferred the symmetry site which provided the largest number of metal atom nearest neighbors on the surface and that the ground state valence configurations for Cu and Ni provided a stronger chemisorption bond than did the promoted but unrelaxed configurations.

In Paper III, an extension to the CEM-1 method has been presented which yields the interaction energy of an N atom system. In contrast to the CEM-1 theory, which provided the interaction energy for a single atom embedded into the other (N-1) atoms acting as a host, the CEM method presented in Paper III treated all N atoms on an equal basis without identifying all but one as a host. This N-active-body formalism was denoted CEM-N. The basis for this theory involved expressing the interaction energy for the real system in terms of the sum of the interaction energies for each atom embedded into jellium of appropriate density. With the energies provided by density functionals, (evaluated within a superposition of atomic charge density approximation), minimization of the difference in kinetic-exchange-correlation energy between the real and effective system yielded the prescription for choice of the electron densities of each jellium system. The full interaction energy then consisted of three terms: the embedding energy, Coulombic

energy, and kinetic-exchange-correlation difference energy.

In an attempt to alleviate the troublesome behavior of the SCF-LD embedding functions of Puska et al. [23] which have residual interaction energy at zero jellium density, the difference between the jellium (A-J) and real (A-B) systems was interpreted using a charge transfer model. This suggested the existence of a universal embedding energy function which was a function of both jellium density and Fermi level, where the Puska et al. embedding functions corresponded to the case of $E_f$ = -WF(n). Embedding energies were constructed semi-empirically for the case of $E_f$ = -IP(A) using the binding potentials for homonuclear ($A_2$) diatomic molecules.

Using the Puska et al. embedding functions, the CEM-N binding potentials for $H_2$, $Li_2$, $B_2$, $G_2$, $N_2$, $O_2$, and $F_2$ were predicted and compared with Hartree-Fock-SCF and experimental potentials. A summary of the data is provided in Table IV in Paper III. All the CEM-N potentials exhibited a smooth behavior as a function of bond length even though the three components of the interaction energy all varied rapidly and often in different directions. The CEM-N potentials for $B_2$, $C_2$, $O_2$, and $F_2$ were all too deep with respect to the experimental values. This overestimation of the binding energy was attributed to an underestimation of the embedding energy. The latter was mainly due to the zero density behavior of the Puska et al. embedding function which leads to an embedding energy that is too negative in the low density region. This problem indicated the need for the covalent embedding functions which were provided for the diatomics investigate above.

Since the CEM theory is still in a developmental stage, possible

applications to other systems beyond the those examined in this dissertation far out-number the envisioned extensions to the theory. But, the approximation of superposed atomic densities approximation could be improved, thus allowing the system electron density to redistribute as the bodies begin to interact. One strategy would be to use a superposition of diatomic molecular electron densities in a "diatomics-in-molecules" type of approach. For each pair of atoms in the many-atom system, electron densities obtained from molecular Hartree-Fock-SCF calculations could be used to construct the system electron density. Alternatively, the CEM-N interaction energy could be solved self-consistently with respect to a variation in the electron density. If a solution of this accuracy is desired, then the direct minimization of the formal energy expression, Eq. (1) in Paper III, would be easier to implement. Two arguments can be made against such a procedure. First, such a first principles method is much more time consuming than the CEM-N theory. Second, the CEM-N theory does include electron redistribution in the atom/jellium systems via the self-consistently (or semi-empirically) determined embedding functions. Only the corrections within the CEM-N theory are evaluated non-self-consistently. Also, the appeal of all EM theories is lost in such an approach, that of providing accurate interaction energies without performing a self-consistent calculation.

The original impetus for deriving the CEM theory was to provide interaction potentials for dissociative molecular chemisorption processes. Even though the evolution from a one- to an N-active-body theory has improved the description of the binding in these cases, still the CEM-N

method provides only a qualitative picture of the PES. To see the reason why, consider the $H_2$/Ni(surface) system. The CEM-N method allows for a symmetric treatment of both the light (H) atoms and the surface (Ni) atoms, as well as providing a backbinding mechanism which allows the $H_2$ molecule to perturb the bonding between the Ni atoms. When the $H_2$ molecule is separated from the Ni(surface), the interaction between the two H atoms is correctly described by the covalent embedding function. At the other extreme when the two chemisorbed H atoms are separated on the Ni(surface), the H atoms interacting with the Ni are correctly described by the Puska et al. embedding function, if the electron transfer arguments in Paper III are valid. In the intermediate region, such as when the $H_2$ molecule is physisorbed on the Ni(surface), both the covalent binding present in $H_2$ and the ionic binding present in the H-Ni(surface) bond must be considered. Thus, to provide a quantitative description of the binding in this system, a procedure is needed which would construct a "general" embedding function by interpolating between the Puska et al. and covalent embedding functions. This is one avenue for future research.

A promising application of the CEM-N method which is underway [31] involves the calculation of interaction energies for homogeneous clusters of metal atoms. With the advances of modern technology, such as supersonic jet expansion techniques, experimentalists have been able to generate a wealth of data [35] concerning metal clusters in the gas phase. For these systems, the above mentioned problem of interpolating the embedding functions is removed, since homogeneous clusters bind covalently by definition, within the CEM-N theory. Semi-empirical embedding functions

have been constructed [31] which incorporate the experimental binding potentials for both the diatomic molecule (N=2) and the bulk solid (N=∞). Using these embedding functions, which are assumed universal for all N, the CEM-N method could answer many questions such as: 1) at what value of N does an N-atom cluster exhibit binding energies and structures similar to that of the periodic infinite solid; 2) what is the significance of the observed "magic number" patterns of stability, where either N = odd or N = even tends to dominate; and 3) for a given metal and value of N, which geometrical arrangement is most stable? In most cases the calculation of cluster binding energies is outside of the realm of Hartree-Fock and Local-Density methods, since each atom in the cluster contains many electrons. The calculations which are available [36] generally incorporate little or no electron correlation and are usually limited to clusters of N < 5. The calculation of such potentials using the CEM-N method is more efficient in terms of computational requirements, and is, in this author's opinion, as accurate or even more accurate than the calculated potentials which presently exist.

# REFERENCES


1. E. J. Heller, J. Chem. Phys. 62, 1544 (1975).
2. W. H. Miller, Adv. Chem. Phys. 25, 69 (1974).
3. E. J. Heller, J. Chem. Phys. 68, 3891 (1978); S. Y. Lee and E. J. Heller, J. Chem. Phys. 76, 3035 (1982).
4. S. Y. Lee and E. J. Heller, J. Chem. Phys. 71, 4777 (1979); D. Tannor and E. J. Heller, J. Chem. Phys. 77, 202 (1982).
5. G. Drohlshagen and E. J. Heller, J. Chem. Phys. 79, 2072 (1983); G. Drohlshagen and E. J. Heller, Surface Sci. 139, 260 (1984).
6. R. D. Coalson and M. Karplus, Chem. Phys. Lett. 90, 301 (1982).
7. A. D. McLachlan, Mol. Phys. 8, 39 (1964); E. J. Heller, J. Chem. Phys. 64, 63 (1976).
8. R. T. Skodje and D. G. Truhlar, J. Chem. Phys. 80, 3123 (1984).
9. S. Sawada, R. Heather, B. Jackson and H. Metiu, J. Chem. Phys. 83, 3009 (1985).
10. B. Jackson and H. Metiu, J. Chem. Phys. 82, 5707 (1985); J. Chem. Phys. 83, 1952 (1985).
11. B. Jackson and H. Metiu, J. Chem. Phys. 84, 3535 (1986); J. Chem. Phys. 85, 4129 (1986).
12. S. Sawada and H. Metiu, J. Chem. Phys. 84, 227 (1986); J. Chem. Phys. 84, 6293 (1986).
13. a) S. Mukamel, J. Phys. Chem. 88, 3185 (1984); b) J. T. Muckerman, S. Kanfer, R. D. Gilbert, and G. D. Billing, Brookhaven National Laboratory, Brookhaven, New York, preprint.

14. R. B. Gerber. R. Kosloff, and M. Berman, Comp. Phys. Reports 5, 61 (1986).

15. Z. H. Zhang and D. J. Kouri, Phys. Rev. A 34, 2687 (1986).

16. C. Zuhrt, Mol. Phys. 51, 241 (1984).

17. R. T. Skodje, thesis, "Topics in the Theory of Chemical Reactions", U. of Minnesota, Minneapolis, 1984, Chapter 7.

18. For an overview see, Adv. Chem. Phys. 69, (1984), Part I.

19. W. Kohn and L. J. Sham, Phys. Rev. A 140, 1133 (1965).

20. J. K. Norskov and N. D. Lang, Phys. Rev. B 21, 2131 (1980).

21. M. Stott and E. Zaremba, Phys. Rev. B 22, 1564 (1980).

22. For a survey, see U. von Barth and A. R. Williams, in "Theory of the Inhomogeneous Electron Gas", edited by S. Lundqvist and N. H. March, Plenum, New York. 1983.

23. M. J. Puska, R. M. Nieminen and M. Manninen, Phys. Rev. B 24, 3037 (1981).

24. J. K Norskov, Phys. Rev. B 24, 2875 (1982).

25. R. G. Gordon and Y. S. Kim, J. Chem. Phys. 56, 3122 (1972).

26. M. S. Daw and M. I. Baskes, Phys. Rev. B 29, 6443 (1984); for references to more recent work see, S. M. Foiles, M. I. Baskes and M. S. Daw, Phys. Rev. B 33, 7983 (1986).

27. K. Ruedenberg, in "Localization and Delocalization in Quantum Chemistry, Vol. I", edited by O. Chalvet et al., D. Reidel, Dordrect, Holland, 1975.

28. T. Raeker, J. D. Kress and A. E. DePristo, manuscript in preparation.

29. M. Manninen, Phys. Rev. B 34, 8486 (1986).

30. K. W. Jacobsen, J. K. Norskov and M. J. Puska, Phys. Rev. B 35, 7423 (1987).

31. J. D. Kress, M. Stave and A. E. DePristo, "Corrected effected medium method. III. Applications to metal clusters", manuscript in preparation.

32. P. E. M. Siegbahn, M. R. A. Blomberg, and C. W. Bauschlicher, Jr., J. Chem. Phys. 81, 2103 (1984).

33. J. K. Norskov, A. Houmoller, P. K. Johansson, and B. I. Lundqvist, Phys. Rev. Lett. 46, 257 (1981).

34. W. A. Kraus and A. E. DePristo, unpublished results.

35. For a review see, M. D. Morse, Chem. Rev. 86, 1049 (1986); A. W. Castleman and R. G. Keesee, Acc. Chem. Res. 19, 413 (1986).

36. For a review see, J. Koutecky and P. Fantucci, Chem. Rev. 86, 539 (1986).

# ACKNOWLEDGEMENTS

First, I would like to thank my high school chemistry teachers, whom I remember only as Mr. Costigan and Mr. McDougall, for introducing me to the fascinating subject of chemistry. My thanks are also due to Prof. Mark Gordon who introduced me to theoretical chemical research and who encouraged me to pursue graduate studies at Iowa State. I also would like to thank my major professor, Dr. Andrew E. DePristo, for his patience and guidance over the last five years. I hope to retain his enthusiastic attitude towards scientific research and pass it on to my future colleagues and students. Next, I would like to thank my parents who have always supported me and my pursuit of higher education, and who encouraged me to put forth my best effort no matter what the task. Most importantly, I wish to thank my wife, Barbara, for her love, support and infinite patience throughout all of my years of graduate studies.